Neutron capture on ^{76}Ge

Dissertation

der Mathematisch-Naturwissenschaftlichen Fakultät
der Eberhard Karls Universität Tübingen
zur Erlangung des Grades eines
Doktors der Naturwissenschaften
(Dr. rer. nat.)

vorgelegt von
Dipl. Ing. Georg Meierhofer
aus Salzburg

Tübingen
2010

Zusammenfassung

Für Experimente zur Suche nach dem neutrinolosen Doppelbetazerfall ($0\nu\beta\beta$) ist aufgrund der langen Halbwertszeiten ein sehr geringer, gut verstandener Untergrund unerlässlich. Im GERDA-Experiment, das den $0\nu\beta\beta$-Zerfall von ^{76}Ge untersucht, wird ein relevanter Anteil des Untergrundes durch den Einfang von myoninduzierten Neutronen an den ^{76}Ge Kernen in den Detektoren erzeugt. Dadurch werden radioaktive ^{77}Ge Kerne gebildet, deren Zerfall fälschlicherweise als $0\nu\beta\beta$ Signal interpretiert werden kann. Ist der Zeitpunkt des Einfangs bekannt, kann ein Veto initialisiert werden, das den folgenden ^{77}Ge-Zerfall unterdrückt. Dies kann durch die Detektion der prompten γ-Strahlung geschehen, durch welche die gewonnene Bindungsenergie abgestrahlt wird. Die prompte γ-Strahlung trägt ihrerseits auch zum Untergrund bei. Die prompte Kaskade in ^{77}Ge war jedoch bisher weitgehend unbekannt. Das Spektrum der ^{76}Ge(n,γ)-Reaktion wurde am Instrument für "Prompte Gamma Aktivierungsanalyse" (PGAA) an der Forschungs-Neutronenquelle Heinz Maier-Leibnitz (FRM II) in Garching vermessen und die Energien sowie die Intensitäten der Übergänge in ^{77}Ge bestimmt. In einer zweiten Messung wurden Koinzidenzen zwischen den einzelnen Linien gesucht. Dadurch konnte ein beträchtlicher Teil des Zerfallsschemas rekonstruiert werden. Zur quantitativen Abschätzung des Untergrundes in GERDA wurden die Wahrscheinlichkeiten, d.h. die Wirkungsquerschnitte für den Neutroneneinfang von ^{76}Ge mit der Aktivierungsmethode bestimmt. Äquivalente Messungen wurden auch für das ebenfalls in den GERDA-Detektoren vorhandene Isotop ^{74}Ge durchgeführt.

Abstract

Experiments searching for the neutrinoless double beta ($0\nu\beta\beta$) decay require a very low and well understood background because of the expected long half-lives. GERDA investigates the $0\nu\beta\beta$-decay, a part of this background is due to the capture of muon induced neutrons on the ^{76}Ge nuclei within the germanium diodes. The decay of the created ^{77}Ge nuclei could be misinterpreted as $0\nu\beta\beta$-signal. If the moment of the neutron capture is known, the decay can be suppressed by introducing a sufficiently long dead time. The capture is revealed by the prompt γ-cascade that releases the binding energy gained. The prompt radiation itself contributes to the overall background in the GERDA experiment as well. So far the prompt cascade was not well known. The spectrum of the ^{76}Ge(n,γ) reaction was measured using the instrument for "Prompt Gamma Activation Analysis" (PGAA) at the Forschungs-Neutronenquelle Heinz Maier-Leibnitz (FRM II) in Garching to obtain the energies and intensities of the prompt transitions in ^{77}Ge. In a second measurement coincidences between these lines were determined to reconstruct the decay scheme. For a quantitative estimation of the background in GERDA the neutron capture propability for ^{76}Ge, *i.e.* its cross section, was determined by the activation method. Similar measurements were carried out for the ^{74}Ge isotop, present in the GERDA diodes as well.

Contents

Chapter 1

Introduction: The GERDA experiment

1.1 Neutrinoless double beta decay

Double beta decay is a second order process in which two neutrons are converted into two protons. While two neutrino double beta decay ($2\nu\beta\beta$) with the emission of two electrons and two anti-neutrinos was observed in several isotopes with half-lives of 7.0×10^{18} y - 7.2×10^{24} y [6], neutrinoless double beta decay ($0\nu\beta\beta$) is only a theoretically predicted process extending the standard model of particle physics. So far the decay was not observed and only lower limits on the half-life could be set. The experimentally obtained limits show that $0\nu\beta\beta$, if it exists, has the longest half-life of all known decays. The best limit on the half life of $0\nu\beta\beta$ decay in ^{76}Ge is currently $T_{1/2} = 1.9 \times 10^{25}$ y (90 % C.L.) set by the Heidelberg-Moscow (HdM) experiment [29]. Part of this collaboration claims the observation of the $0\nu\beta\beta$ with a half-life of $T_{1/2} = 1.19^{+2.99}_{-0.50} \times 10^{25}$ y (3σ range) [30].

The observation of $0\nu\beta\beta$ would prove that the neutrino is a Majorana particle, *i.e.* the neutrino is its own anti-particle. This implies a lepton number violation by 2, leading to physics beyond the standard model. A necessary condition for the experimental observation is that the neutrino is not massless, in contradiction to the standard model. By several neutrino oscillation experiments it was shown that at least two mass eigenstates are non-zero. The best limit on the neutrino mass results from cosmic observations including the cosmic microwave background, supernova neutrinos, baryon acoustic oscillations and photometric redshift survey data. Making several assumptions the sum of the neutrino mass $\Sigma m_\nu = 0.28$ eV (95 % C.L.) was obtained [55]. From the position of the end point in the β-spectrum of tritium the mass of the electron neutrino can be determined directly. The current mass limit by such experiments is $m(\nu_e) < 2$ eV [47]. The new KATRIN experiment will use the same approach, reaching a sensitivity of about $m(\nu_e) = 0.2$ eV [22].
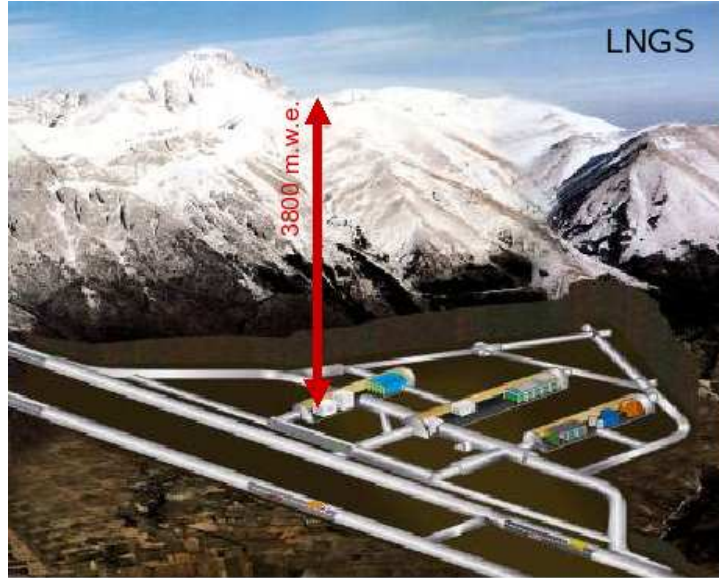
Figure 1.1: Underground laboratory LNGS of the INFN.

Assuming that only light Majorana neutrino exchange contributes, the observation of neutrinoless double beta decay would allow to derive the effective neutrino mass m_{ee} from the measured half-life by

$$m_{ee}^2 = \frac{1}{G^{0\nu}(E_0, Z)\,|\mathcal{M}^{0\nu}|^2\,T_{1/2}^{0\nu}}. \tag{1.1}$$

$G^{0\nu}$ is the integral over the phase space of the two electrons and $|\mathcal{M}^{0\nu}|$ the matrix element supplied by theory. The experimental half-life limit of $T_{1/2} = 1.9 \times 10^{25}$ y corresponds to an effective neutrino mass of $m_{ee} = 0.35$ eV [29] depending on the matrix element used. In the near future $0\nu\beta\beta$ experiments will probe effective neutrino masses down to 100 meV.

1.2   GERDA experiment

In summer 2010 the GERmanium Detector Array (GERDA) experiment [14] started its operation. GERDA searches for $0\nu\beta\beta$ decay in the underground laboratory LNGS of the INFN in Italy (fig. 1.1). The overburden of 3800 m.w.e. of rock reduces the flux of cosmic muons by six orders of magnitude compared to the surface of the earth. Like the IGEX [5] and the HdM experiments germanium detectors, isotopically enriched in ^{76}Ge are employed, actually the same detectors are being used after refurbishment. However, the shielding concept is contrary to this two experiments that used lead and very clean

scintillator

clean   room

PMT

cryostat/
LAr

HPGe
diodes

9,4m   10m

water tank/Cherenkov muon veto
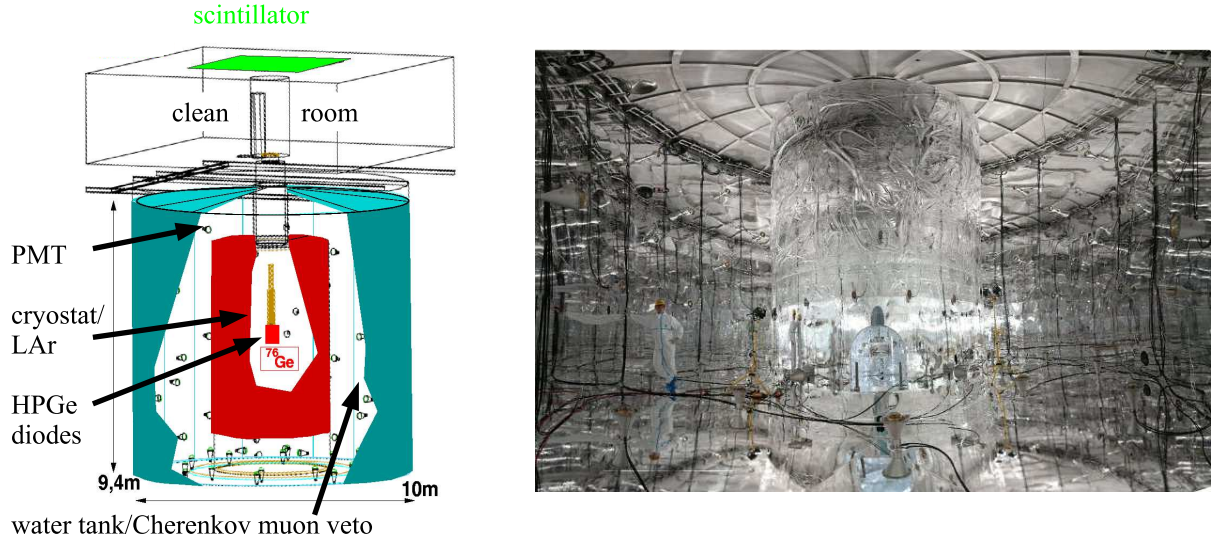
Figure 1.2: Left: Setup of GERDA. Right: Water tank, the walls and the floor are covered with reflective foil for the active muon veto.

copper to reach a sufficiently low background. The background data of the HdM experiment suggested that most of the residual background is due to neutrons produced by cosmic radiation. Therefore, in the GERDA experiment high Z-materials that are source of fast neutrons are avoided in the vicinity of the detectors. The germanium diodes are submerged directly into liquid argon ($T = 87.3\,K$) that acts as coolant and shielding against external radiation. The stainless steel dewar in which the detectors are operated has a diameter of 4 m and is lined with a 6 cm thick copper inlet. The copper serves as shield against radiation from impurities contained in the steel. The cryostat is surrounded by a water tank with 10 m in diameter and 9 m in height. The water is passive shielding and acts also as Cherenkov medium for the active muon veto (fig. 1.2). The Cherenkov light is detected by 66 photomultipliers mounted on the wall and the bottom of the water tank. The germanium diodes are lowered from a cleanroom on the top of the water tank through the neck of the cryostat into the liquid argon.

GERDA uses the calorimetric approach, measuring the kinetic energy of the two electrons emitted. The signature of the $0\nu\beta\beta$-decay in the energy spectrum of the electrons is a discrete peak at $E = Q_{\beta\beta} = 2039\,keV$ [17] because the two electrons carry the whole reaction energy (neglecting nuclear recoil) and are absorbed in a very small volume inside the germanium crystal (few mm^3). $2\nu\beta\beta$ decay on the other hand causes a continuous spectrum since the energy is divided between the electrons and anti-neutrinos (fig. 1.3). The measured signal of $2\nu\beta\beta$ can not be distinguishedfrom $0\nu\beta\beta$ and therefore represents an unavoidable background in the search for $0\nu\beta\beta$-decay.

In the first phase of the experiment isotopically enriched germanium detectors previ-

3
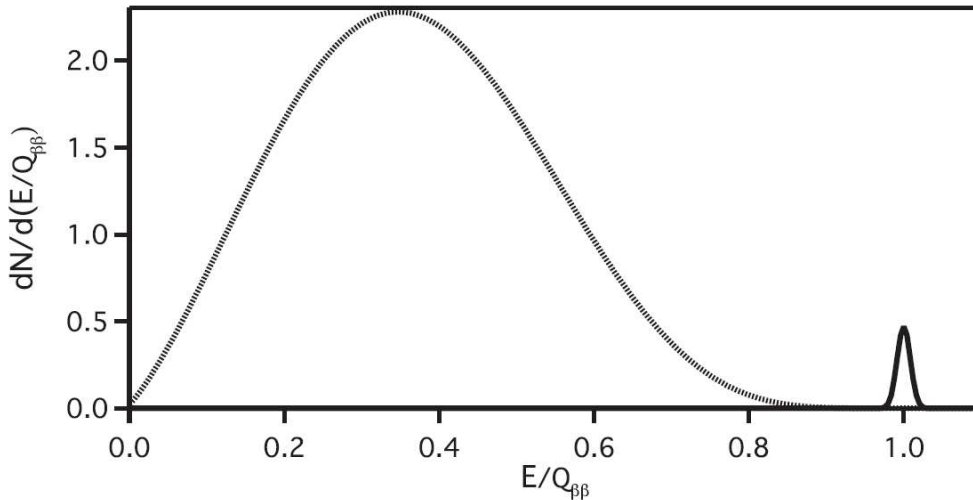
Figure 1.3: Spectrum of the sum of electron energies in $2\nu\beta\beta$ decay (dashed line) and $0\nu\beta\beta$-decay (full line) [7]

ously employed by IGEX and HdM are used ($m = 17.66\,\text{kg}$). With an exposure of $15\,\text{kg y}$ and a background index of 10^{-2} counts/(keV kg y) the claim of observation can be checked.

In phase II new detectors will be added to the detector array, increasing the total mass to $\sim 40\,\text{kg}$. The additional diodes will be broad energy germanium detectors (BEGe) that feature very good pulse shape analysis (PSA) properties due to the strong gradient in the electric field. The electrons emitted in double beta decay are stopped in a very small volume inside the germanium crystal resulting in so called single-site events (SSE). The SSE signature can be distinguished by PSA from multi-site events produced for example by multiple Compton scattering of a γ-ray in the detector (fig. 1.4). The background of γ-rays in the region of interest ($Q_{\beta\beta} = 2039\,\text{keV}$) can be reduced by a up to factor ten applying PSA [9]. The second phase will collect an exposure of about $100\,\text{kg y}$ with a background level of 10^{-3} counts/(keV kg y) aiming for a limit on the half-life of 1.5×10^{26} y, if no event is observed around $2039\,\text{keV}$. This half life corresponds to an effective neutrino mass between $0.09\,\text{eV}$ and $0.15\,\text{eV}$ [53].

1.3 Neutron capture on ^{76}Ge

The present work was motivated by a technical report written to the GERDA collaboration (GSTR-06-012 [50]) by L. Pandola aiming at the delayed decay of ^{77m}Ge contributing to the background in the GERDA experiment. In this section the problem and the solutions proposed in this technical report are presented.
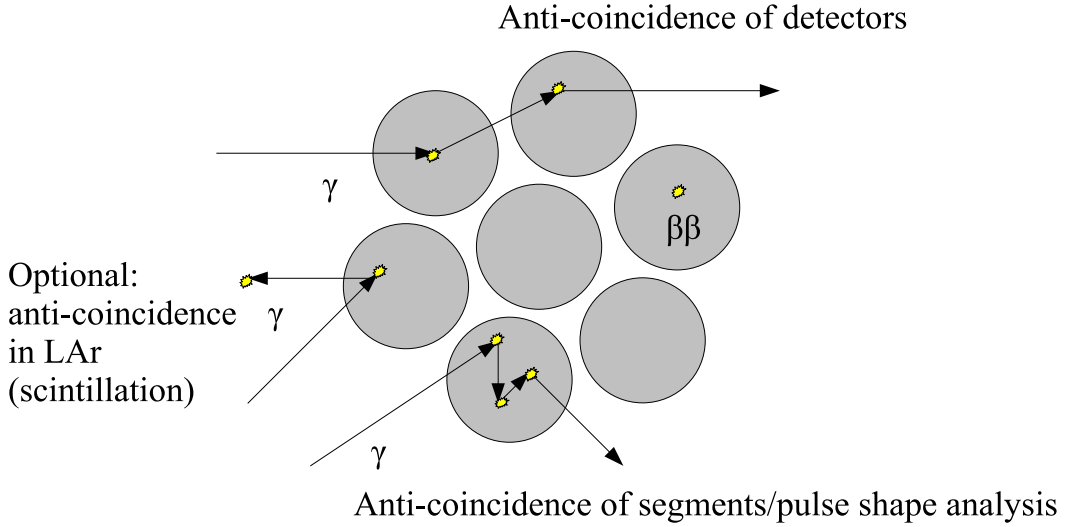
Figure 1.4: Hypothetical detector array for GERDA. While double beta decay has a single-site signature, high energetic γ-rays cause mostly multi-site events that can be rejected by pulse shape analysis.

In the LNGS underground laboratory the neutron flux originates from natural radioactivity (fission, (α,n) reactions) in the surrounding materials and from spallation by muons. The first component is produced mainly outside the experiment and contributes at rather low energies ($< 10\,\mathrm{MeV}$). These neutrons are stopped and absorbed in the water shield or the liquid argon. Muon induced neutrons carry a much higher energy and can be produced close to the germanium diodes as well. Neutrons that were thermalized by elastic and inelastic scattering can be captured in the detectors on $^{76}\mathrm{Ge}$ or $^{74}\mathrm{Ge}$.

The neutron flux in one kilogram of detector mass was estimated for the GERDA setup by a Monte-Carlo simulation. For energies below $1\,\mathrm{keV}$ a flux of $39\,\mathrm{neutrons/(kg\,y)}$ was calculated [48]. The dismissed setup with a copper cryostat filled with liquid nitrogen would have allowed only $1.7\,\mathrm{neutrons/(kg\,y)}$ to penetrate the crystals. The large difference is due to the increased amount of material acting as additional neutron source and the enhanced stopping power of nitrogen compared to argon. The setup including the copper cryostat was not realized due to safety arguments and explosion of copper prices.

The neutron capture on $^{76}\mathrm{Ge}$ leads to $^{77}\mathrm{Ge}$ in an excited state with an excess energy of $6072\,\mathrm{keV}$ (fig. 1.5). This state decays under emission of prompt γ-rays to an isomeric level ($E = 159\,\mathrm{keV}$, $T_{1/2} = 52.9\,\mathrm{s}$) or to the also unstable ground state ($T_{1/2} = 11.3\,\mathrm{h}$). These two states decay further via β-decay to $^{77}\mathrm{As}$. The isomeric state also undergoes isomeric transition to the ground state (branching: $19\,\%$). While the β-decay of the ground state is accompanied by γ-emission (I_β to $^{77}\mathrm{As}$ g.s. $< 10\,\%$, ref. [19]), the decay of $^{77m}\mathrm{Ge}$ is almost
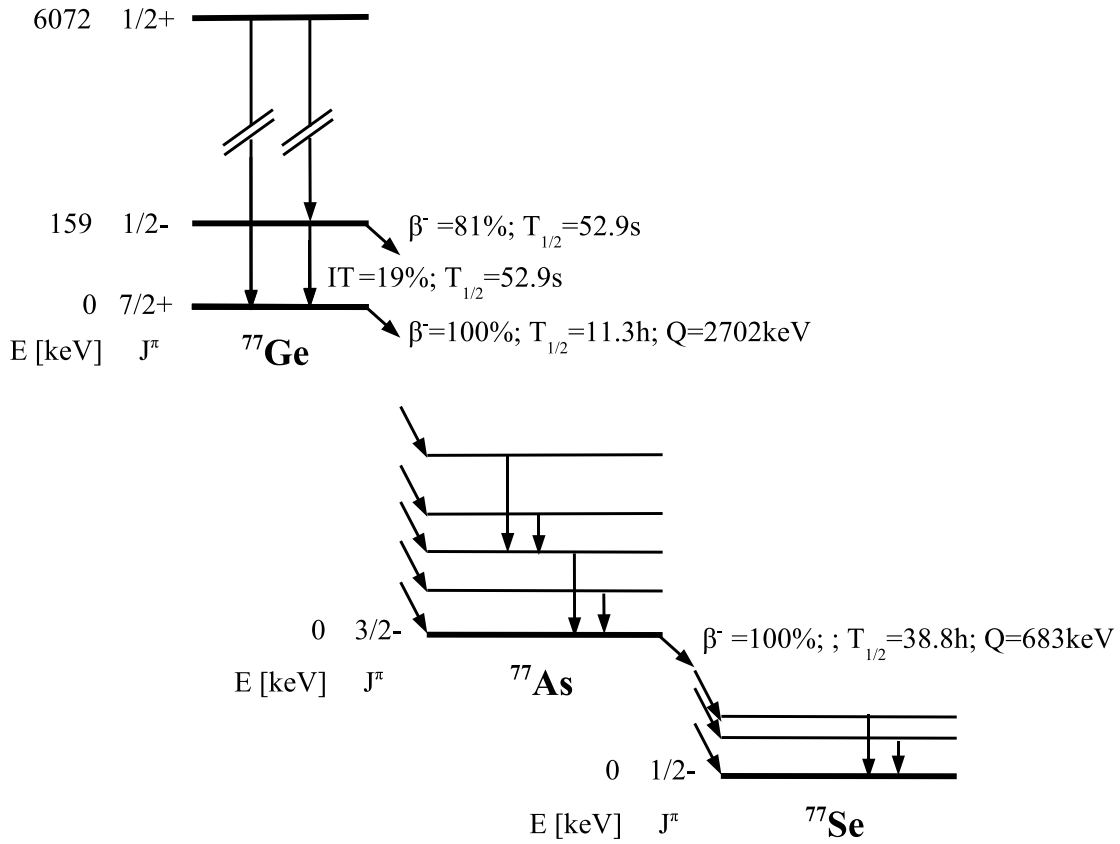
Figure 1.5: Decay chain after neutron capture on ^{76}Ge.

of pure β^- emission with a maximum energy of $E_{max} = 2862\,\text{keV}$. An electron without coincident γ-radiation has the same signature as neutrinoless double beta decay and since $E_{max} > Q_{\beta\beta}$, such events may be misidentified as $0\nu\beta\beta$-decay. If the β-decay populates excited states in ^{77}As there is coincident γ-emission and the event is likely identified by PSA.

Using the capture cross sections of ref. [37] (to isomeric state: $\sigma^m = 137\,\text{mb}$, to ground state: $\sigma^d = 6\,\text{mb}$) a production rate of 0.5 - 1 nuclei/(kg y) in the isomeric state was simulated [50]. This results in the case of an array of 21 18-fold segmented detectors (phase II[1]) in a background index for the region of interest of 2.1×10^{-4} counts/(keV decay). Applying PSA, this value is reduced to 1.8×10^{-4} counts/(keV decay)[2], still a non-negligible

---

[1] Instead of segmented detectors BEGe detectors will be used in phase II.

[2] The number of captures and subsequent of decays per (kg year) is about 1, hence the background index is equivalent to the one usually used by the GERDA experiment: counts/(keV kg y).

contribution. From the ground state decay a background of 8×10^{-5} counts/(keV decay) is expected that can be reduced by a factor of three by anti-coincidences [50]. The background due to the delayed decay of ^{77}Ge after neutron capture amounts to $20\,\%$ of the goal of $1\,\text{count}/(\text{keV kg y})$ for phase II.

1.3.1 Rejection strategy

To veto the decay of ^{77m}Ge a dead time has to be introduced, starting with the capture of the neutron. A time span of four minutes was proposed, resulting in a suppression efficiency of $96\,\%$ considering the half-life time of $T_{1/2} = 52.9\,\text{s}$. An option to start the dead time could be the detection of a muon passing the water tank. This results in a trigger rate of 2.5 counts/minute, *i.e.* no life time remains for the measurement. A more reasonable rate of only 9 events/day was obtained by simulation if a coincident energy deposition in the muon veto and at least one germanium detector is required. The total dead time is then about $3\,\%$ [48].

The efficiency of the latter approach can be calculated as

$$\epsilon = \epsilon_{mv} \times \epsilon_{Ge} \times \epsilon_{dec} \tag{1.2}$$

with ϵ_{mv} the muon veto efficiency ($> 95\,\%$) and ϵ_{dec} the probability of the decay of ^{77m}Ge within the dead time. ϵ_{Ge} is the efficiency of the germanium diodes to detect at least one of the prompt γ-rays that indicate the capture of a neutron. Since the prompt decay scheme in ^{77}Ge is poorly known ϵ_{Ge} can not be evaluated precisely. Due to the selection rule the direct transition from the capture state to the ground state is strongly suppressed (fig. 1.5), so the most conservative case is the emission of one photon carring the total energy difference from the capture to the isomeric state ($E_\gamma = 5912\,\text{keV}$). If two or more photons are emitted the detection probability will be higher, additionally the location of the starting point in the detector array (central or peripheric crystal) is of importance. Table 1.1 shows the results of Monte-Carlo simulations for different assumptions for the splitting of the emitted energy.

For a homogeneous distribution of the nuclei in the crystals and a single photon emission with $E_\gamma = 6\,\text{MeV}$ a detection probability of $56\,\%$ is reached and therefore the overall efficiency is

$$\epsilon = 0.95 \times 0.56 \times 0.96 = 0.51. \tag{1.3}$$

$\epsilon_{Ge} = 0.56$ represents the lower limit, depending on the actual decay scheme it will be higher.

Alternatively the dead time could be triggered only by the germanium detectors. This approach allows to suppress neutrons from (n,α) events from natural radioactivity which do not deposit energy in the muon veto. Applying a threshold of $4\,\text{MeV}$ (above natural radioactivity, but $< S_n = 6\,\text{MeV}$) the event rate and with it the total dead time is decreased by a factor of three. On the other hand due to the high threshold the efficiency is

Table 1.1: Detection probability of prompt γ-rays after neutron capture on ^{76}Ge by at least one detector/segment . Different decay schemes and starting points of the photon were tested [50].

Detector scheme	γ-rays	events > thr.	events > 4 MeV
1 no seg.	1 γ 6 MeV	37.7 %	25.9 %
1 no seg.	2 γ 3 MeV	64.7 %	9.6 %
1 no seg.	3 γ 2 MeV	82.3 %	7.1 %
21 seg.	1 γ 6 MeV	56.3 %	38.7 %
21 seg.	2 γ 2 + 4 MeV	84.8 %	27.2 %
21 seg.	3 γ 2 MeV	94.5 %	18.9 %
21 seg. - central detector	1 γ 6 MeV	66.2 %	46.4 %
21 seg. - central detector	2 γ 3 MeV	92.0 %	36.6 %
21 seg. - central detector	3 γ 2 MeV	98.2 %	29.2 %
21 seg. - peripheric detector	1 γ 6 MeV	53.9 %	36.9 %
21 seg. - peripheric detector	2 γ 2 + 4 MeV	82.8 %	25.1 %
21 seg. - peripheric detector	3 γ 2 MeV	93.4 %	16.7 %

significantly lower. The most favorable case would be a single photon emission with a detection probability $\epsilon_{Ge} = 38.7\,\%$.

1.3.2 Prompt γ-rays

Another background source are the prompt γ-rays itself. No line in the region of interest (ROI) around 2039 keV is reported in the literature, but since the spectrum is not well known the existence of prompt peaks in the ROI can not be excluded. For sure a contribution has to be expected from Compton scattering of high energetic transitions. To calculate this amount by a Monte-Carlo-simulation the energies and intensities of these lines have to be known. In addition to the ^{76}Ge(n,γ) reaction the ^{74}Ge(n,γ) reaction will contribute as well. The delayed decay of ^{75}Ge on the other hand has not to be taken into account because of its low reaction energy of $Q = 682.9\,$keV ($< Q_{\beta\beta}$).

With

$$v = \frac{\sum E_i \sigma_i}{S_n \sigma_{tot}} = \frac{\sum E_i I_i}{S_n}. \tag{1.4}$$

the fraction of emitted energy can be calculated inserting the γ-ray energy for E_i and the emission probability per 100 neutron captures for I_i or the partial γ-ray production cross section σ_i. S_n is the binding energy gained by the neutron capture and σ_{tot} the total cross

section for ^{76}Ge(n,γ). Using the intensities and energies given in ref. [19] a fraction of $v = 10.6\,\%$ is determined for the transitions in ^{77}Ge. For ^{75}Ge a higher value of $v = 30.3\,\%$ was derived using the numbers in ref. [20]. As discussed in ref. [27] and sect. 5.1.5 the realistic value for ^{75}Ge might be even by a factor of about 2 higher, resulting in $v \sim 60\,\%$.

The contribution by prompt γ-rays were discussed already in ref. [16] for the HdM experiment and found to be negligible. Indeed, no evidence for prompt γ-lines obtained in our work could be found in the spectra published in ref. [16]. But since the goal of the GERDA experiment is an increase of sensitivity by a factor of 100 these processes have to be considered carefully.

The limited information available about the prompt γ-rays in ^{77}Ge originate from measurements in the early 1970s. The sensitivity needed in the present and future neutrinoless double beta decay experiments using ^{76}Ge requires a more elaborate knowledge of the decay scheme in ^{77}Ge and the background to be expected from the neutron capture reaction. Therefore new measurements of the prompt γ-ray spectra were carried out. From the same spectra also the prompt radiation in ^{75}Ge, abundant in the enriched germanium diodes as well, was determined.

Comparing the different cross sections for the capture reactions on these two germanium isotopes given in the literature, it was found that their agreement is relatively poor. To determine the production rate of ^{77}Ge and ^{75}Ge more precisely the cross sections for ^{76}Ge(n,γ) and ^{74}Ge(n,γ) were measured relative to a gold reference.

Chapter 2

Prompt Gamma Activation Analysis

Prompt **G**amma **A**ctivation **A**nalysis (PGAA) is a non-destructive method to determine the isotopic composition of samples. The sample to be analyzed is irradiated with neutrons and simultaneously the emitted prompt γ-radiation is detected. From the peaks in the spectra obtained the isotopic abundance can be derived. This method is applied in various fields of material science, archaeology, medicine et cetera. In the present work in contrast, PGAA was used to determine the characteristic prompt γ-radiation in ^{77}Ge and ^{75}Ge from a sample of known isotopic composition.

In this chapter neutron reactions and the PGAA method are discussed briefly, moreover the PGAA instrument at the research reactor "Forschungs-Neutronenquelle" Heinz Maier-Leibnitz (FRM II) in Garching bei München is characterized.

2.1 Neutron reactions

The atomic nucleus consists of nucleons, that is protons and neutrons. Both particles are fermions, *i.e.* have a spin 1/2. Neutrons are electrical neutral particles with a finite life time of (885.7 ± 0.8) s [18] if not bound in a baryonic system (atomic nucleus). The mass is $939.565346(23)$ MeV/c^2 [43] and thermalized $(293.15\,\mathrm{K})$ the neutron carries a kinetic energy of 25.26 meV, corresponding to a velocity of $v_0 = 2200$ m/s or a wavelength of $\lambda = 1.80$ Å. The parameters for neutrons, like the capture cross sections used in PGAA, are commonly given for the thermal energy, denoted with an index "0" (σ_0).

For many applications it is useful to classify neutrons by their energy. Energies below 100 meV are called "thermal" and below room temperature "cold". Fast neutrons have energies above 1 MeV, the region in between is called "epithermal". This graduation is rather rough, but in this context precise enough.

The most imortant neutron-atom interaction is the strong interaction with the nucleus. Because of the missing net charge, neutrons interact with the electrons of an atom by
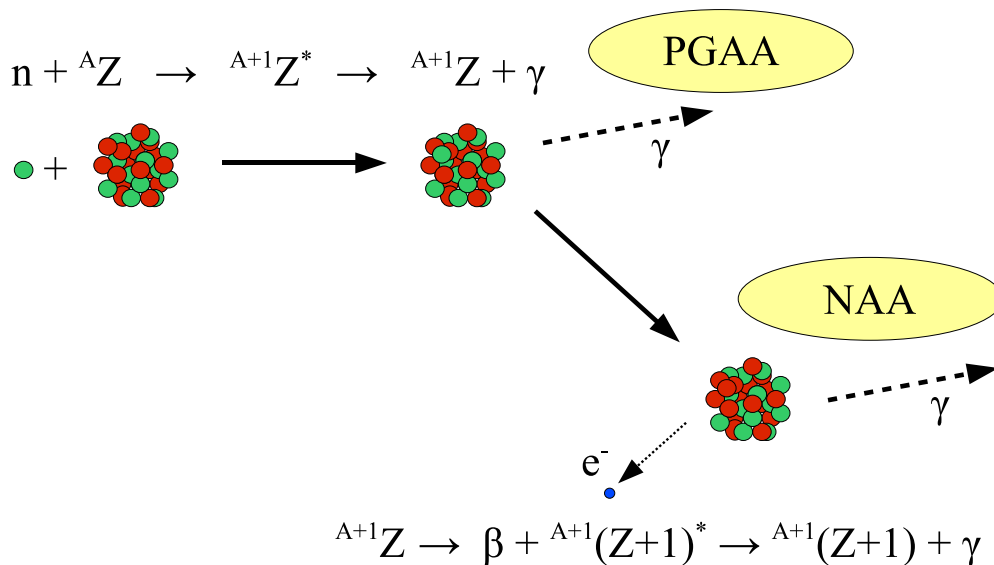
Figure 2.1: PGAA principle.

magnetic coupling of the spins only. Therefore the penetration depth into materials is much higher than for charged particles and neutrons can be used to explore the bulk of a sample.

PGAA is based on the radiative capture of cold or thermal neutrons. The kinetic energy transferred to the nucleus can be neglected. Hence the gained energy is equal to the binding energy S_n of the neutron, which is characteristic for each isotope. The excited state of the compound nucleus decays within about 10^{-16} s and after the emission of one or several subsequent γ-rays the nucleus reaches its ground state. Typically the emission of the γ-cascade takes up to 10^{-9} s if no isomeric states are populated.

All isotopes, except ^{4}He, are able to undergo a (n,γ)-reaction. In general the complexity of the prompt γ-cascade increases with the mass of the nucleus, since the number of nucleons affects the number of possible transitions. Spectra of light nuclei show only a few lines, while ^{77}Ge investigated in this work includes several hundred transitions. A sketch of a typical PGAA spectrum is presented in fig. 2.2. The primary γ-rays from the capture state with an excitation energy of S_n are mostly high energetic because the transition probability scales with E^3 for dipole and with E^5 for quadrupole radiation. For the low energetic states populated by these transitions only few decay cascades are available. Hence the lower and upper end of the energy spectrum few strong lines are observed. In the mid energy range on the contrary the level density is very high and the emission probability low at the same time. The resulting forest of overlapping peaks is hard to analyse and usually not used for PGAA purposes. Besides the energy difference the spins of the initial and final state are determinant for the branching of the decay of a level.
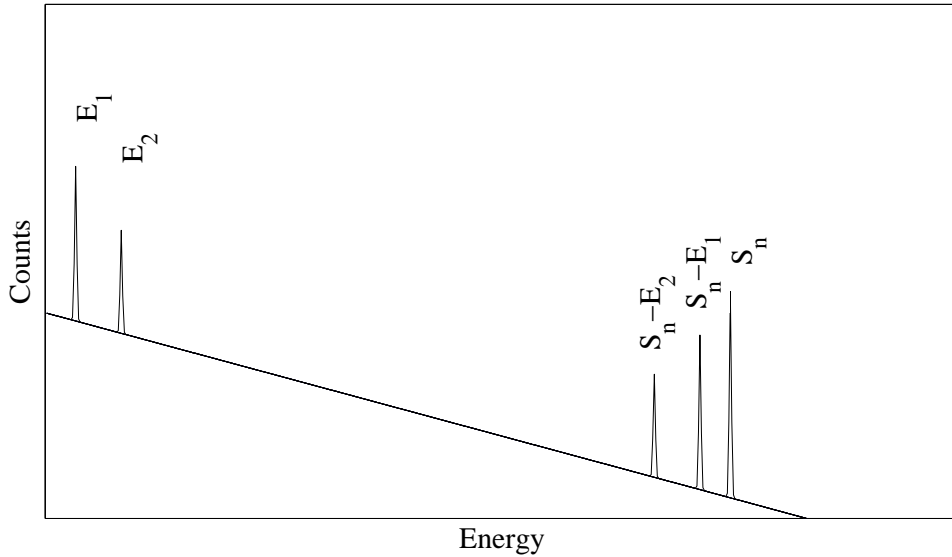
Figure 2.2: Sketch of a typical PGAA spectrum.

If the ground state is unstable, the nucleus undergoes a further decay. In most cases this is a β^--decay, but electron capture is observed as well for several nuclei. This delayed radiation is used in the neutron activation analysis (NAA). NAA is more sensitive because the prompt background disturbing in PGAA does not contribute to the spectrum. But not all isotopes can be observed as not all isotopes are unstable after neutron capture. In addition the time needed for NAA exceeds the time for PGAA because of the partially long half-lives.

Neutron capture can be followed by charged particle emission as well. The emitted particles have a very short mean free path and do not affect the measurement. At the same time there is no or a rather low energetic γ-emission. Such reactions are used for shielding, like the ^{6}Li(n,t)^{4}He (no γ) or the ^{10}B(n,α)^{7}Li ($E_\gamma = 478\,\text{keV}$[1]) reactions. Another application is the neutron detection utilizing the ^{3}He(n,p)^{3}H-reaction.

Neutrons can be elastically scattered by a nucleus, loosing energy due to the recoil. This effect is used for the thermalization of initially fast neutrons to thermal or cold energies. Neutrons with energies above the first excited state of the nucleus can also scatter inelastically, changing the population of states. If the transferred energy is below the threshold for particle emission the excess energy is given away by γ-radiation.

Secondary reactions can lead to the production of fast neutrons, even though initially only slow neutrons were present. If tritium or alpha particles are emitted in (n,t)- or (n,α)-reactions they can react with ^{6}Li, ^{7}Li or other light nuclei producing neutrons with

---

[1] The ^{10}B(n,γ)^{11}B reaction emits γ-rays up to 11 MeV, but its cross section is smaller by a factor of 10^4 than for (n,α).

energies up to $15\,\mathrm{MeV}$ [35]. Fast neutrons can also be created by (γ,n) reactions if the incoming γ-ray energy exceeds the binding energy of the target nucleus. Again, this γ-ray might result from a (n,γ)-reaction of a cold neutron.

The cross section for neutron capture σ can be described for resonances with the Breit-Wigner formula

$$\sigma_{n,\gamma}(E) = \pi \bar{\lambda}^2 \frac{\Gamma_n \Gamma_\gamma}{(E - E_R)^2 + (\Gamma/2)^2} \tag{2.1}$$

where $\bar{\lambda} = \frac{\hbar}{mv}$ denotes the de Broglie wavelength of the neutrons and E_R the energy of a resonance. Γ is the sum of the individual decay widths for neutrons Γ_n and photons Γ_γ. For neutron energies much smaller than E_R one obtains after short derivation [8]

$$\sigma_{n,\gamma}(E) \approx \pi \bar{\lambda}^2 \frac{\Gamma_{n0}\Gamma_\gamma}{E_R^2} \sqrt{E} = \pi \bar{\lambda}_R^2 \frac{\Gamma_{n0}\Gamma_\gamma}{E_R} \frac{1}{\sqrt{E}} \tag{2.2}$$

with the reduced neutron width $\Gamma_{n0} = \Gamma_n \sqrt{E}$ and λ_R the neutron wavelength at the resonance energy. The Breit-Wigner formula follows a $1/v$ law for neutron capture at energies much lower than the first resonance. For most isotopes this law is valid for the complete cold and thermal energy region. Only cadmium, samarium, europium and gadolinium are exceptions showing strong resonances for thermal neutrons.

2.2 PGAA analysis

The reaction rate R in a sample irradiated in a neutron flux $\Phi(\lambda_n,\mathbf{r})$ is given by

$$R = \int_V \int_0^\infty \frac{\mu(\mathbf{r})}{M} N_A \sigma(\lambda_n) \Phi(\lambda_n, \mathbf{r}) \, \mathrm{d}\lambda_n \, \mathrm{d}\mathbf{r}. \tag{2.3}$$

$\mu(\mathbf{r})$ is the mass density in the sample, M its relative atomic weight, N_A the Avogadro constant and $\sigma(\lambda_n)$ the wavelength dependent cross section. If only cold or thermal neutrons are present the average energy of the beam can be used because of the $1/v$ law. For a sample of mass m and a homogeneous neutron beam follows

$$R = \frac{m}{M} N_A \sigma \Phi. \tag{2.4}$$

To obtain the partial count rate ρ_γ for a certain line in a measurement σ has to be replaced by the partial γ-ray production cross section σ_γ and also the detector efficiency $\epsilon(E_\gamma)$ has to be considered. The cross sections are usually given for thermal neutrons, therefore Φ has to be converted into the thermal equivalent flux Φ_0.

$$\rho_\gamma = \varepsilon(E_\gamma) \frac{m}{M} N_A \sigma_{\gamma 0} \Phi_0 \tag{2.5}$$

with

$$\Phi_0 = \frac{\langle\lambda\rangle}{\lambda_0}\,\Phi \tag{2.6}$$

where $\langle\lambda\rangle$ is the average neutron wave length and $\sigma_{\gamma 0}$ the thermal partial γ-ray production cross section. These equations are valid only for very thin targets with small cross sections, otherwise corrections have to be applied.

Neutron self-shielding

In a thick target the rear layers are shielded by absorption of neutrons in the front layers of the sample. The average flux $\langle\Phi\rangle$ seen by the target is

$$\langle\Phi\rangle = f\Phi_i \tag{2.7}$$

where Φ_i denotes the flux before entering the target and f the shielding factor given by

$$f = \frac{1 - e^{-d\sigma_a}}{d\,\sigma_a}. \tag{2.8}$$

d is the thickness of the target and σ_a the total absorption cross section.

For certain geometries scattering in the target can cause a change of the length of the path the neutron propagates in the material. By elastic scattering of cold neutrons on a target with room temperature their energy increases, affecting the energy dependent cross section. Both effects lead to small deviations in the rates measured. The latter two effects were neglected in this work, while neutron self shielding was included in the analysis to determine the neutron capture cross sections.

γ-ray self absorption

γ-rays are attenuated when propagating through a layer of matter. The attenuation k is calculated by

$$k = 1 - e^{-\mu t} \tag{2.9}$$

where μ is the energy and material dependent attenuation factor and t the thickness of the layer. For self absorption in the target eq. 2.9 has to be integrated over t, resulting in

$$k_{self} = 1 - \frac{1 - e^{-\mu t}}{\mu t}. \tag{2.10}$$

2.3 PGAA FRM II

In 2007 the PGAA instrument at the FRM II was connected to the neutron guide and first measurements were carried out to characterize the beam [33]. The following year, regular user operation was started. Presently this instrument has the strongest cold neutron beam in the world available for PGAA.
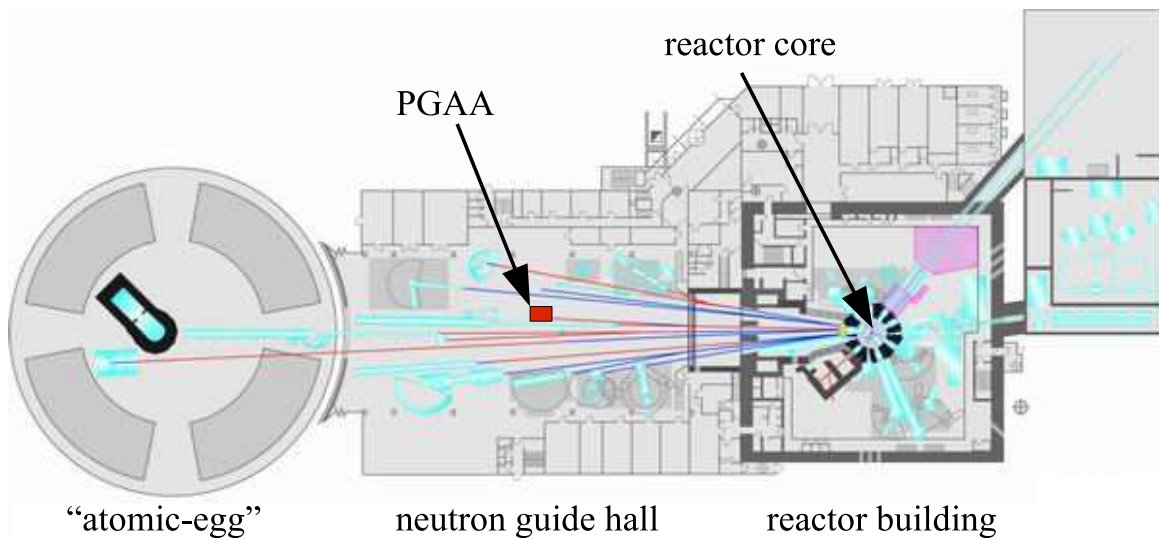
Figure 2.3: Neutron guide hall at the FRM II [2]. The PGAA instrument is located at the end of neutron guide NL 4b.

2.3.1 Setup

The instrument is situated in a concrete bunker at the end of the neutron guide NL4b in a distance of about 52 m from the reactor core (fig. 2.3).

The neutrons are moderated in liquid deuterium (24 K) before entering the neutron guide. The curvature of the guide ($r = 390$ m) prohibits γ-radiation from the core to reach the experiment. Only cold neutrons with long wavelengths are scattered in the neutron guide while faster neutrons leave the beam, this results in a further cooling of the neutron spectrum. The energy distribution of the neutrons was measured by time of flight, the resulting spectrum is shown in fig. 2.5. The calibration of the spectrum relies on the small dip at 4.05 Å, caused by Bragg reflection in the aluminum exit window of the beam guide. An average neutron energy of 1.83 meV was found, corresponding to a wavelength of 6.7 Å.

The last 7 m of the super mirror guide are straight and elliptically tapered. The target position is situated in the focus of the neutrons about 30 cm behind the exit window of the guide. The neutron beam illuminates an area of 34 mm × 50 mm with a maximum cold neutron flux of $\Phi = 6.54 \times 10^9$ n/(cm s). This value corresponds to a thermal equivalent neutron flux of $\Phi_0 = 2.42 \times 10^{10}$ n/(cm s). The neutron guide can be extended by an additional elliptical focusing device ("nose") of 1.1 m length, reducing the dimensions of the neutron beam to 17 mm × 19 mm. At the same time the flux increases to $\Phi = 1.64 \times 10^{10}$ n/(cm^2 s) and $\Phi_0 = 6.07 \times 10^{10}$ n/(cm^2 s) respectively. These intensities can be reduced by three retractable boral attenuators (A1, A2 and A3), transmitting between about 18 % (A1 and A2) and 6 % (A3) of intensity. A high count rate in the detectors reduces the
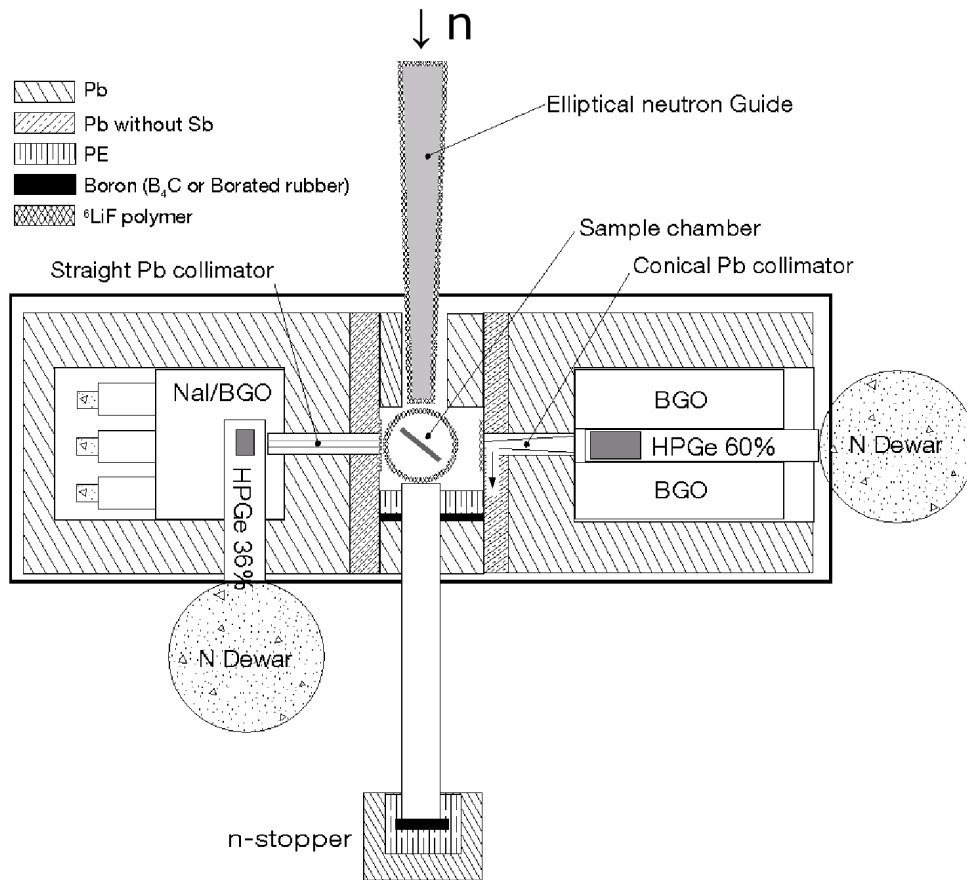
Figure 2.4: Setup of the PGAA-instruments at the FRM II [11].

energy resolution, therefore in this work lower intensities than the maximum values were used. For each measurement the flux is given individually in the corresponding chapter.

The beam enters the target chamber through a thin zirconium window. The targets are mounted on a ladder made of fluorinated ethylene propylene (FEP) with six target positions. To ensure direct sight on the target for the neutrons and both detectors the ladder is tilted by 45° to the beam axis.

For the γ-ray detection two HPGe detectors are provided with efficiencies of 60 % (detector I) and 36 % (detector II) relative to a 3 in. × 3 in. NaI detector. The smaller detector has a distance of 30 cm to the target and is shielded by 10 cm of lead. The γ-rays reach the detector through a straight collimator (length: 10 cm, diameter: 10 mm). The larger detector is protected by 15 cm of lead with a conical collimator (length: 15 cm, diameter: 10 - 40 mm). Its distance from the target is about 35 cm (fig. 2.4). The first 5 cm of the lead shielding are Sb-free because activated Sb has a long half life ($T_{1/2} = 60.3$ d) and should not be used close to the neutron beam. The lead is additionally protected

17
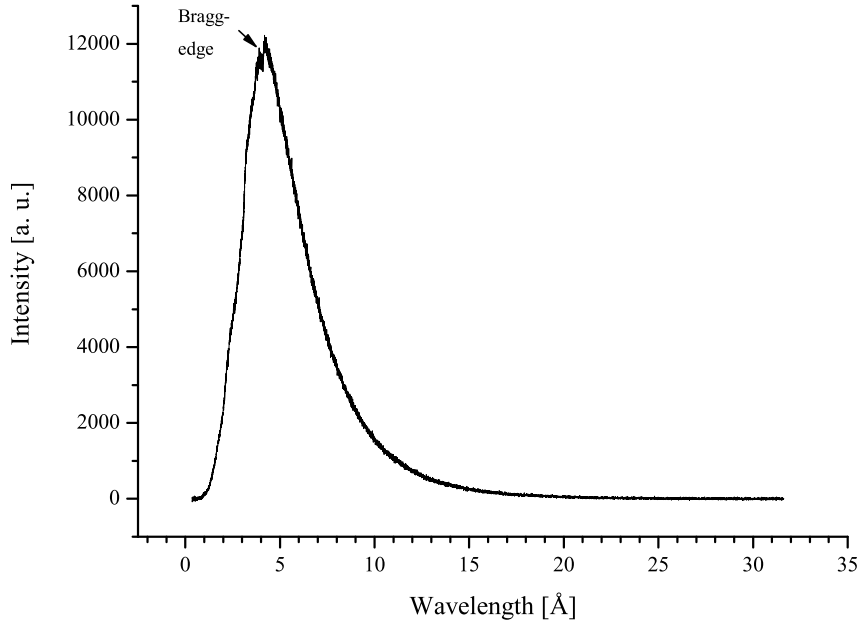
Figure 2.5: Measured wave length spectrum at the target position. At $\lambda = 4{,}05\,\text{Å}$ the Bragg edge used for calibration is visible.

from neutrons by a thin sheet of ^{113}Cd. Close to the target chamber a combination of ^{6}LiF polymer and ceramic, boron and PE is used. The larger of the two detectors is equipped with a Compton suppression made of BGO, the smaller one with a combination of BGO and NaI [11].

2.3.2 Data acquisition

The signals of the preamplifiers are further amplified and shaped by two Ortec 572A modules. To digitize the analog signal different systems were used. The cross section measurements were done using the two self-made MCAs (by IKP, Universität zu Köln) provided by the standard setup (16k channels). The prompt γ-ray spectra were taken in one measurement campaign with a Multiport II MCA (Canberra), all other runs were also recorded with the self-made MCA. For the coincidence measurement a FADC was utilized recording the trace of each event. The data acquisition system used for this purpose will be discussed in more detail in sect. 6.2.2.

18
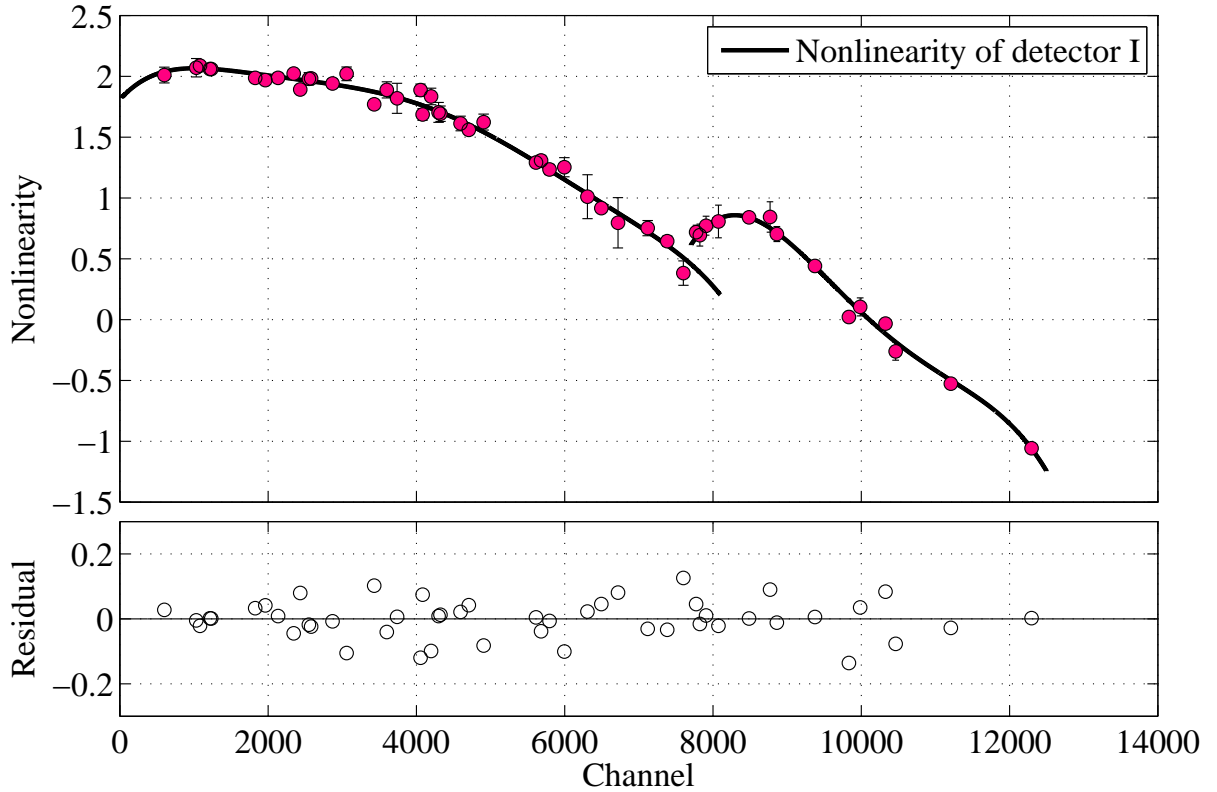
Figure 2.6: Nonlinearity of detector I in channels fitted with a polynomial of 6th degree (lower energy region) and 4th degree (upper energy region). The lower diagram shows the deviation of the data from the fit. Multiply with 0.5365 to obtain the nonlinearity in keV for the prompt γ-ray measurement in chapter 6.

2.3.3 Detector characterization

Energy calibration

The energy calibration was done using the prompt background lines of ^{19}F(n,γ). Fluorine is contained in the FEP foil utilized to pack the targets and is therefore part of all spectra.

Firstly, the spectrum was calibrated preliminary with a linear function. For many applications, especially if the energy range is not very broad, a linear calibration is sufficient. Due to uncertainties in the comperator of the ADC the calibration function is not perfectly linear but has a small nonlinearity. The nonlinearity was determined from the empty target measurement (chapter 6) using again fluorine in the FEP foil. The spectrum was calibrated with the linear function and then the measured peak positions were compared to the values given in literature [1]. The difference of these values in channels shows the nonlinearity. The use of channels rather than energy makes the calibration
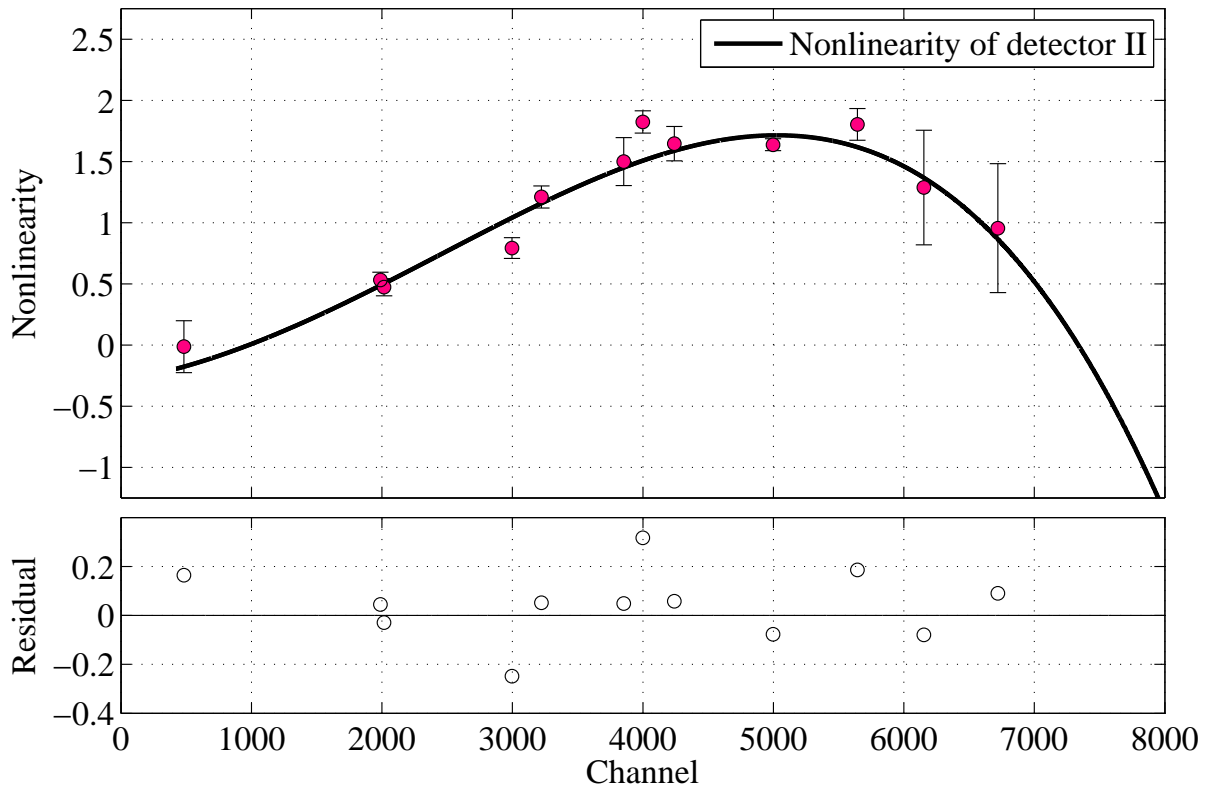
Figure 2.7: Nonlinearity of detector II in channels fitted with a polynomial of 4th degree. The lower diagram shows the deviation of the data from the fit. Multiply with 0.325 to obtain the nonlinearity in keV for the prompt γ-ray measurement in chapter 6.

less dependent of the actual gain of the amplifier used. The nonlinearity of detector I and the deviations of the measured energies from the polynomial fit are shown in fig. 2.6. The nonlinearity for detector II was determined only for the energy region below 1800 keV (fig. 2.7), correspondingly only detector I was used for higher energies in this work. The errors in the plot result from the uncertainties of the experimental peak positions and the errors of the values given in the literature for the transition energy. For the evaluation of the spectra an additional systematic uncertainty of 0.10 keV was added quadratically.

The nonlinearity of detector I shows an unexpected behavior around channel 8000. After a continuous decrease the nonlinearity suddenly rises and then prolongs the decrease again. Although the origin of this behavior is unclear, using this calibration the levels in the decay scheme of ^{77}Ge can be calculated consistently (chapter 6). Between different measurements small jumps in the energy spectra were observed ($\Delta E \sim 0.1$ keV), *i.e.* for

the analysis this deviation had to be corrected. During a running measurement no jumps occurred, otherwise it would have effected the resolution of the peaks.

Efficiency calibration

The efficiency of a detector depends mainly on its volume and the geometry of the experimental setup. The efficiency calibration is usually done with standard radioactive sources of known intensity. Since the energies observed in PGAA exceed the range of radioactive sources available, one has to use prompt γ-rays for calibration as well. Detector I was calibrated using ^{133}Ba and ^{152}Eu, for high energies N, Cl and Cr were irradiated with neutrons. For detector II ^{60}Co, ^{133}Ba and ^{152}Eu respectively N and Cr were utilized. During the period the measurements for this thesis were carried out the efficiency of the detectors changed because of some modifications in the setup. The curves in figs. 2.8 and 2.9 are those valid for the measurement of prompt γ-rays in ^{75}Ge and ^{77}Ge.

Energy resolution

A good energy resolution is important to distinguish peaks from each other even in very complex spectra. The resolution is usually specified by the full-width-half-maximum (FWHM) of a peak. This value increases with energy, but is also affected by the count rate of the detector. For all measurements the rate was therefore kept below 5 kHz. For the measurement of the prompt γ-rays, detector I had a FWHM of 2.14 keV and detector II of 2.27 keV at 1.3 MeV.

2.3.4 Background

Neutrons are easily scattered in the target chamber and can be captured also by other material than the target. The radiation produced by the capture of these neutrons creates background in the spectra. The most severe background is the prompt radiation from ^{19}F(n,γ) in the FEP foil containing the target. Other elements are H, C, Na, Al, Si, Fe, Ge, Zr, Cd and Pb. Nitrogen is suppressed completely if the target chamber is evacuated ($p < 1$ mb). Fast neutron can be scattered inelastically on the target or the germanium detectors, this reaction is the origin of the typical "germanium triangles" at 596 keV and 692 keV.
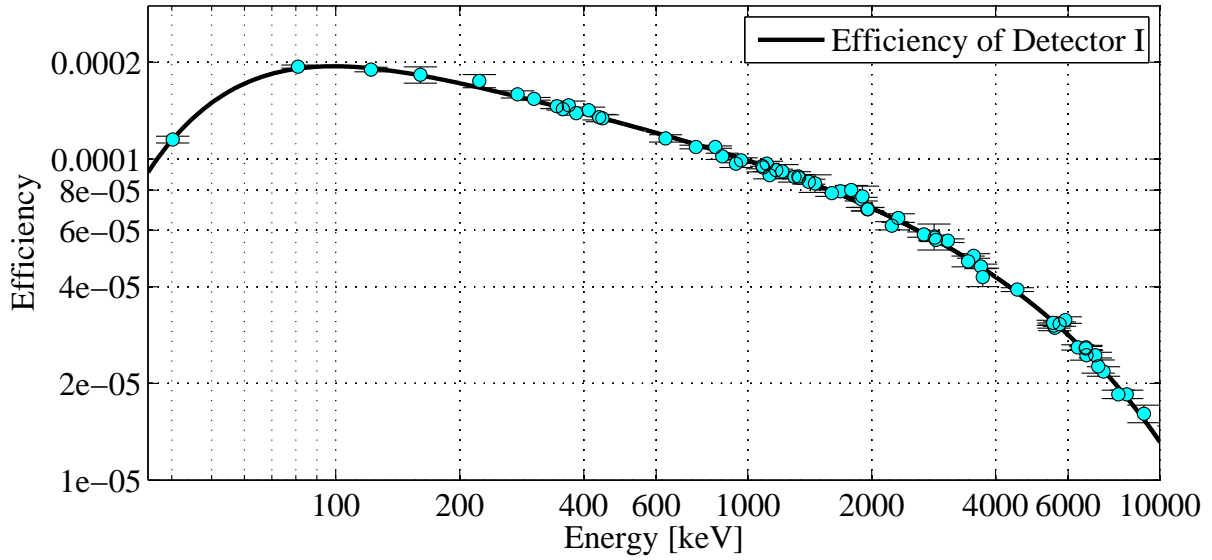
Figure 2.8: Efficiency of Detector I [10].
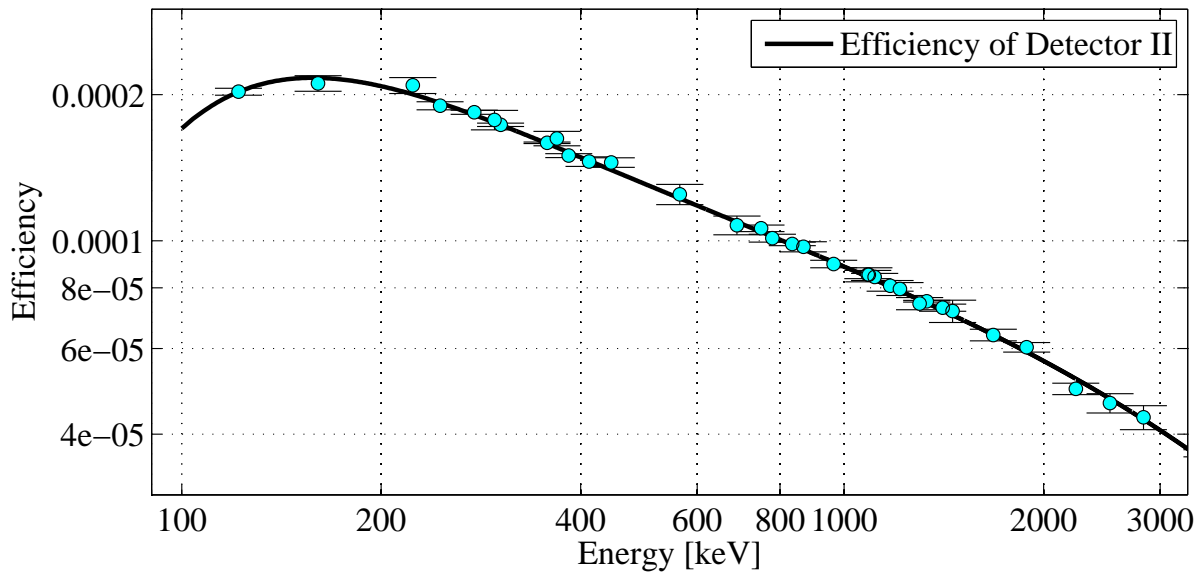
Figure 2.9: Efficiency of Detector II [10].

Chapter 3

Thermal neutron capture cross sections

The cross sections for the ^{76}Ge(n,γ) and ^{74}Ge(n,γ) reactions are important for a quantitative estimation of the background contribution by neutron capture in the GERDA experiment. The values given by different references have a broad spread and do not match well. Most of the values available for ^{76}Ge were obtained by the activation method using Geiger counters [37,52] and anthracene crystals [15] to observe the β-radiation rate or NaI detectors for the γ-ray detection [37,40,57]. Pile oscillation was used in ref. [51]. If the neutron spectrum is not limited to thermal energies [15,40] the cadmium ratio has to be determined to correct for epithermal and fast neutrons. This introduces an additional systematic error. Similar methods were applied for the ^{74}Ge(n,γ)-reaction [15,36,40,51,57]. Moreover the transmission technique through a target was used here [32].

Cross section measurements applying the activation method using HPGe detectors were carried out, delivering new thermal neutron capture cross section values for the ^{76}Ge(n,γ) and ^{74}Ge(n,γ) reactions. The GeO$_2$ targets used in this measurements were taken from the raw material that will be utilized to produce the GERDA phase II detectors.

The main outcomes discussed in this chapter have been published already in [41,42].

3.1 Activation method

The activation method measures the samples radioactivity induced by neutron capture. Detecting the emitted decay radiation after the exposure to the neutron beam the amount of activated nuclei *i.e.* the number of neutrons captured during the irradiation can be derived considering the γ-ray emission probabilities. It has to be stressed that the cross section of ^{76}Ge(n,γ) is determined by measuring the intensities of the transitions in ^{77}As after the decay of ^{77}Ge (fig. 3.1).
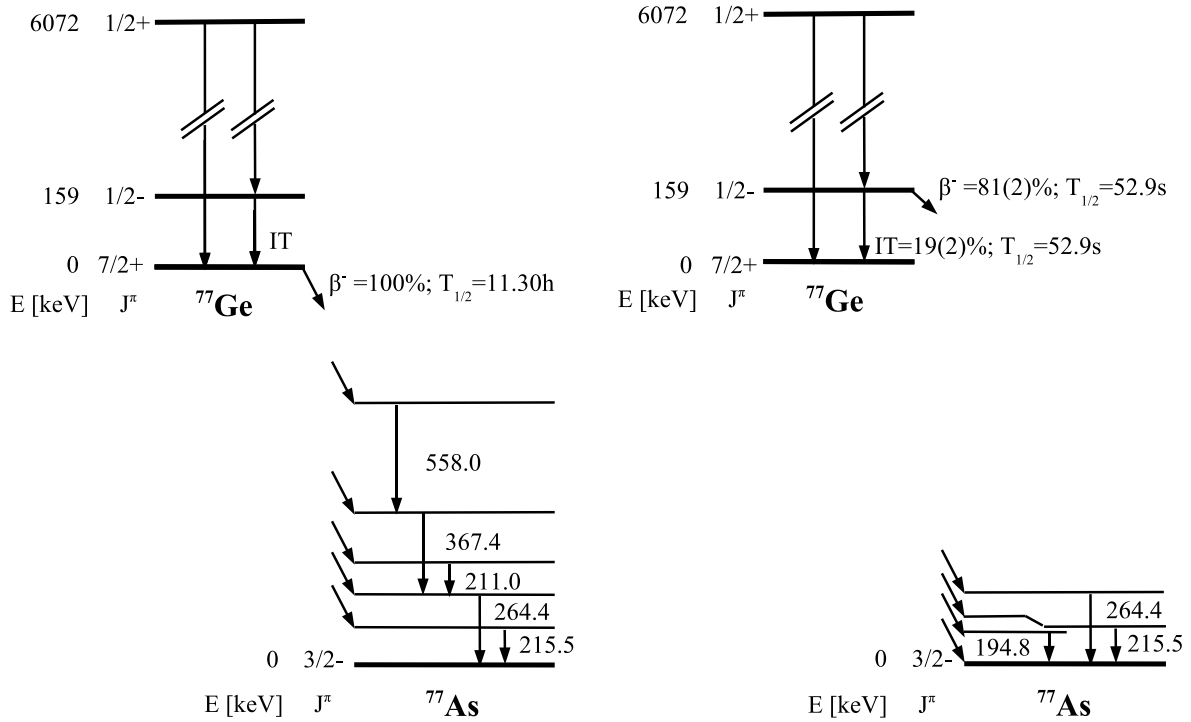
Figure 3.1: Decay scheme of the ground state (left) and the isomeric state (right).

Usually the exact flux penetrating the sample is not known precisely enough for small uncertainties. So in most cases the cross section is derived relative to a well known reference isotope that is irradiated together with the sample, exposed to the same neutron flux.

In our experiment we evaluated the γ-radiation accompanying the β-decay of ^{77}Ge and ^{75}Ge respectively relative to a gold standard ($\sigma_{\mathrm{Au}} = (98.65 \pm 0.09)\,\mathrm{b}$ [44]). A spectrum containing the ^{77}Ge decay lines and the $411\,\mathrm{keV}$ peak of the gold reference is shown in fig. 3.2.

3.2 Method

The cross sections were derived from the recorded spectra using the number of counts in a certain peak C_γ. C_γ allows to calculate the number of activated nuclei A at the end of the activation process by

$$A = \frac{C_\gamma}{I_\gamma\,\epsilon_\gamma\,f\,K_\gamma\,(1 - e^{-\lambda t_m})\,e^{-\lambda t_w}}, \tag{3.1}$$
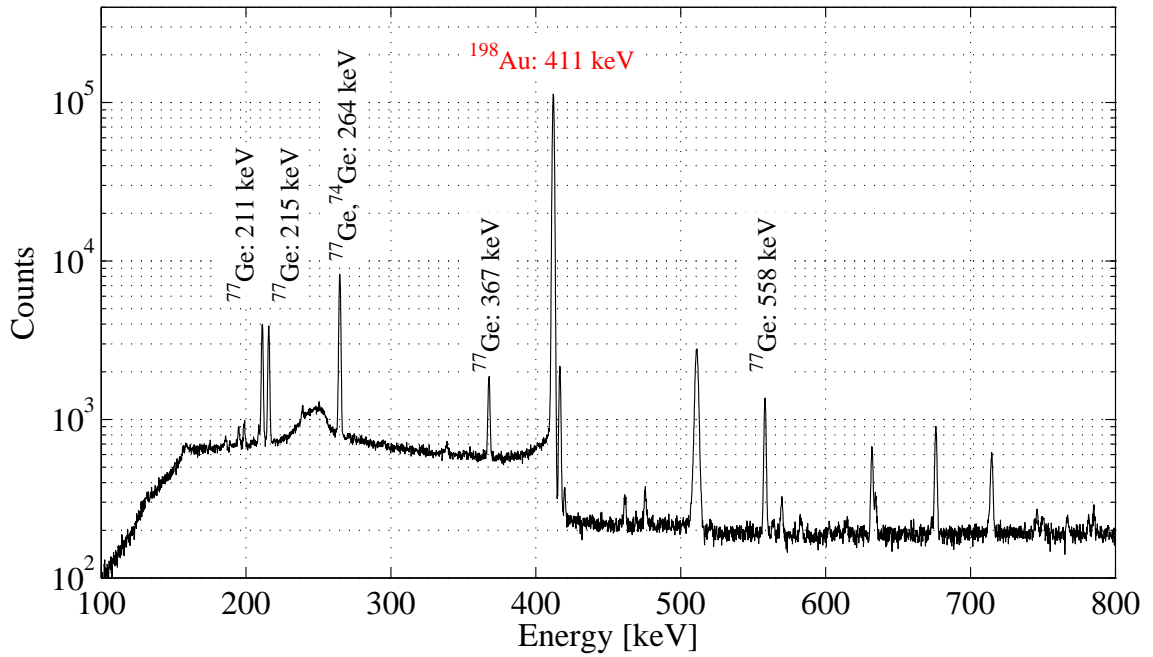
Figure 3.2: Spectrum with ^{77}Ge and ^{198}Au decay lines used to evaluate the cross section.
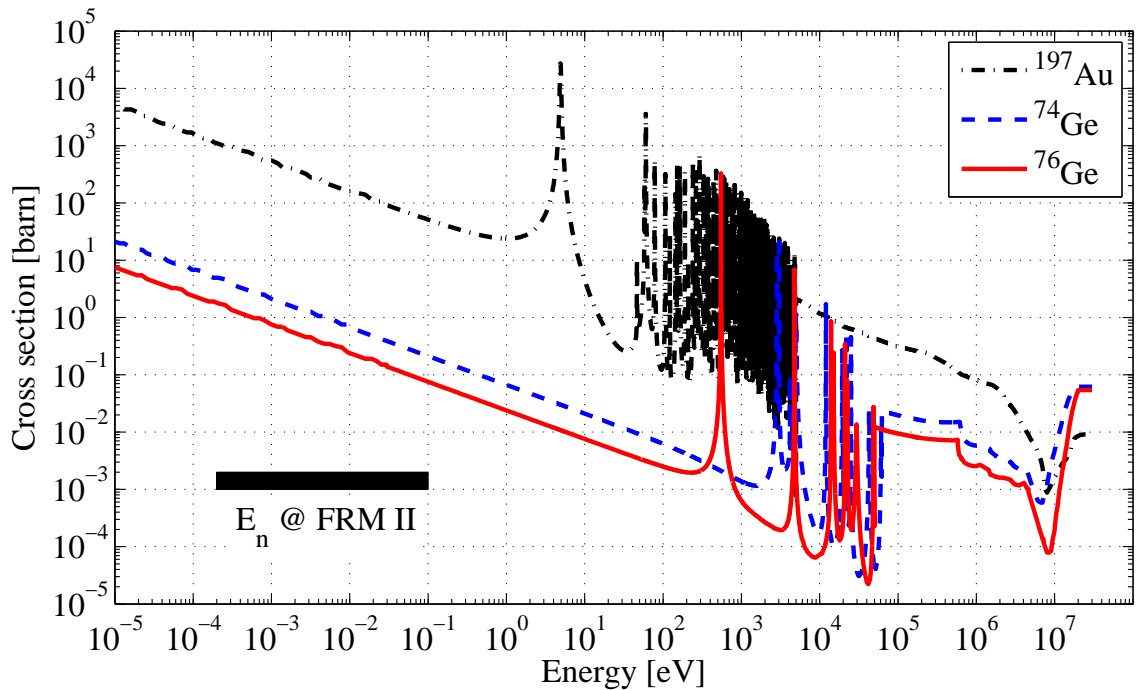
Figure 3.3: Neutron capture cross sections of ^{74}Ge, ^{76}Ge and ^{197}Au [3]. The black bar represents the energy range of the neutron beam available at the PGAA instrument.

25

Table 3.1: Target properties and the times used for activation t_a, waiting t_w and measurement t_m in the ^{76}Ge(n,γ)^{77}Ge and ^{74}Ge(n,γ)^{75}Ge cross section experiments.

Target	Composition	Mass [mg]	t_a [s]	t_w [s]	t_m [s]
A	enriched	468.7	1 200	480	55 200
B	enriched	503.9	1 800	720	55 076
C	depleted	435.7	1 200	300	14 100
D	depleted	401.5	1 500	660	10 800

where I_γ denotes the emission probability per neutron capture, ϵ_γ the detector efficiency, f the neutron self shielding of the target [21] and K_γ the correction factor for γ-ray attenuation in the target [26] for the specific γ-ray energy. t_m denotes the time of measurement, t_w the time waited between activation and measurement and λ the decay constant of the isotope. The number of all activated nuclei during activation is given by $A_{all} = \Phi \, n \, \sigma \, t_a$, where Φ is the constant neutron flux per cm^2 and per s, n the number of nuclei in the target and σ the neutron capture cross section. Correcting A_{all} for those nuclei which decayed during the time of activation, again the number of activated nuclei A at the end of irradiation is obtained

$$A = A_{all} - \int_0^{t_a} \Phi \, n \, \sigma \, (1 - e^{-\lambda t}) \, \mathrm{d}t \tag{3.2}$$

$$= \Phi \, n \, \sigma \, t_a - \Phi \, n \, \sigma \, \left(t_a - \frac{1 - e^{-\lambda t}}{\lambda} \right) \tag{3.3}$$

$$= \Phi \, n \, \sigma \, \frac{1 - e^{-\lambda t_a}}{\lambda}. \tag{3.4}$$

Since the neutron flux seen by the germanium target and the gold foil is the same eq. 3.4 can be written as

$$\sigma_{\mathrm{Ge}} = \frac{A_{\mathrm{Ge}}}{A_{\mathrm{Au}}} \frac{n_{\mathrm{Au}}}{n_{\mathrm{Ge}}} \frac{1 - e^{-\lambda_{\mathrm{Au}} t_a}}{1 - e^{-\lambda_{\mathrm{Ge}} t_a}} \frac{\lambda_{\mathrm{Ge}}}{\lambda_{\mathrm{Au}}} \sigma_{\mathrm{Au}}. \tag{3.5}$$

A_{Ge} and A_{Au} are the experimental values obtained from eq. 3.1. These values include also the factor f, accounting for the slightly different flux in germanium and gold due to neutron self absorption.

Altough σ_{Ge} and σ_{Au} are energy dependent, eq. 3.5 is correct for cold and thermal neutrons. Both isotopes follow the $1/v$ law (sect. 2.1) in this energy region, *i.e.* the change in σ with energy is the same for germanium and gold and therefore cancels out (fig. 3.3). If the well known thermal neutron capture cross section of gold $\sigma_{0,\mathrm{Au}}$ at $v_0 = 2200 \, \mathrm{m/s}$ is inserted into eq. 3.5, the thermal cross section of germanium $\sigma_{0,\mathrm{Ge}}$ is obtained.

Table 3.2: Decay properties of ^{75}Ge [20], ^{77}Ge [19] and ^{198}Au [13].

Nucleus	$T_{1/2}$	E_γ [keV]	I_γ [%]
^{75}Ge	82.78 ± 0.04 m	198.6	1.19 ± 0.12
		264.6	11.4 ± 1.1
^{75m}Ge	47.7 ± 0.5 s	139.68 (IT)	39.4 ± 0.8
^{77}Ge	11.30 ± 0.01 h	211.0	53.9 ± 0.5
		215.5	14.0 ± 0.3
		264.4	53.9 ± 0.5
		367.4	14.0 ± 0.3
		558.0	16.1 ± 0.4
		714.4	7.17 ± 0.17
		1193.3	2.57 ± 0.06
^{77m}Ge	52.9 ± 0.6 s	159.7 (IT)	10.3 ± 1.1
		215.5	21.6 ± 3.3
		264.7	0.022 ± 0.004
^{198}Au	2.69517 ± 0.00021 d	411.8	95.58 ± 0.12

In principle prompt γ-radiation can be used to determine the cross section as well. If the γ-ray intensity per 100 neutron captures I_γ for the isotope that is examined is known for at least one transition, the total cross sections σ_0 can be evaluated relative to the partial γ-ray production cross sections σ_γ^p of the reference isotope. In the case of ^{74}Ge these absolute intensities in [27] were normalized using the cross section of the ^{74}Ge(n,γ) reaction [45]. Accordingly the cross section used for normalization is reproduced in the analysis. Reference [25] normalizes the I_γ to the primary prompt transitions, but this is not reliable because the decay scheme is poorly known. Here this alternative method can be applied here only to check for consistency. The same holds for ^{76}Ge, where Groshev *et al.* [24] used also cross sections for normalization.

3.3 Cross sections of ^{76}Ge

After neutron capture by ^{76}Ge the created ^{77}Ge nucleus is in a highly excited state at $S_n = 6072$ keV ($J^\pi = +1/2$). This energy is released via a prompt γ-cascade to the ground state or an isomeric state at 159 keV ($J^\pi = -1/2$). The isomeric state undergoes an isomeric transition (IT) to the ground state ($J^\pi = +7/2$) with a branching of (19 ± 2) % or with (81 ± 2) % a β-decay and reaches ^{77}As. The ground state β-decays to ^{77}As as well (fig. 3.1). The half-lives are 52.9 s for the IT and 11.30 h for the ground state. Due to the disadvantageous spin quantum numbers no direct β decay of ^{77}Ge (g.s.) to ^{77}As (g.s.) was

observed experimentally, the limit is $I_\beta < 10\,\%$. The emission probabilities of the γ-rays used to calculate the cross sections were derived assuming no direct β-transition to the ground state [19].

The γ-rays used for the analysis are those shown in fig. 3.1. The 264 keV peak was not used, although it is the most intense line, because it overlaps with a line of ^{75}Ge decay and is therefore more difficult to analyze. Some peaks at other energies were used to check for consistency.

3.3.1   Experiment

The GeO$_2$ powder was pressed into pill shaped targets ($\varnothing = 12$ mm) using a hydraulic press with 600 bar pressure. For the ^{76}Ge(n,γ)-reaction enriched GeO$_2$ ($87.1 \pm 1.2\,\%$) was used. The masses of the targets can be found in table 3.1. As reference material a piece of thin gold foil ($m_{\mathrm{Au}} = 28.7 \pm 0.6$ mg) of same diameter was irradiated together with the germanium pills to monitor the neutron flux.

The thermal equivalent neutron flux used was $\Phi_0 = 2.28 \times 10^9\,\mathrm{n}_{th}/(\mathrm{cm}^2\,\mathrm{s})$ for sample "A" and $\Phi_0 = 1.48 \times 10^9\,\mathrm{n}_{th}/(\mathrm{cm}^2\,\mathrm{s})$ for sample "B".

The cross section for the ^{76}Ge(n,γ)^{77m}Ge reaction was measured using target "A". A series of measurements with different time spans for the activation, waiting and measurement was carried out. The time of activation and measurement was kept short (< 3 half-lives) to reduce the contribution to the 215 keV peak by the decay of the ground state.

To measure the population of the ground state the waiting time was chosen to be ~ 10 half-lives of the isomeric state to prevent any significant contribution from the decay of the isomeric state to appear in the 215 keV peak. Target "A" and "B" were used, their masses and the times used in this part of the measurement are given in table 3.1.

3.3.2   Results

For the evaluation of the thermal neutron capture cross section to the isomeric state the IT with an energy of 159.7 keV and the strongest γ-line in the β-decay with 215.5 keV (fig 3.1 right) were used. The γ-ray attenuation in the target was considered with 0.936 and 0.953 respectively. The correction factor used for neutron self shielding for the germanium target was 0.999 and 0.978 for the gold foil. The distribution of the results following the method described in sect. 3.2 show, that there is no systematic dependence on the times used for activation, waiting or measurement. The mean value of the cross section achieved over all runs is $\sigma^m = (115 \pm 16)$ mb. The uncertainties entering into the total error of $14\,\%$ are given in table 3.5. The dominating contribution comes from the uncertainty of the emission probabilities ($10.7\,\%$ and $15.3\,\%$). If the values of the two emission probabilities are assumed to be independent the uncertainty for σ^m can be reduced from 16 mb to 11 mb.

Table 3.3: Results of the thermal cross section measurement for ^{76}Ge(n,γ)^{77m}Ge performed with target "A". For all runs the corresponding time intervals used for activation t_a, waiting t_w and measurement t_w are given.

t_a [s]	t_w [s]	t_m [s]	E_γ [kev]	Cross section [mb]
60	4	175	159.7	113 ± 14
			215.5	113 ± 18
120	4	175	159.7	115 ± 14
			215.5	113 ± 18
180	4	175	159.7	114 ± 14
			215.5	112 ± 18
180	9	110	159.7	119 ± 14
			215.5	114 ± 18
180	9	175	159.7	117 ± 14
			215.5	112 ± 18
180	14	175	159.7	114 ± 14
			215.5	117 ± 19
180	19	175	159.7	118 ± 14
			215.5	114 ± 18
Mean value				115 ± 16

Table 3.4: Results of thermal cross section measurement of the ^{76}Ge(n,γ)^{77}Ge reaction.

Target	Detector	E_γ [kev]	Attenuation correction	Total cross section [mb]	Direct cross section [mb]
A	I	367.4	0.9730	66.3 ± 3.3	44.4 ± 4.5
		558.0	0.9784	67.1 ± 3.4	45.2 ± 4.7
	II	367.4	0.9660	67.8 ± 3.4	45.9 ± 4.6
		558.0	0.9714	68.8 ± 3.5	46.9 ± 4.7
B	I	367.4	0.9710	68.0 ± 3.3	46.1 ± 4.6
		558.0	0.9768	70.0 ± 3.5	48.2 ± 4.8
	II	367.4	0.9640	70.7 ± 3.4	48.8 ± 4.7
		558.0	0.9698	71.5 ± 3.6	49.6 ± 4.8
Mean value				68.8 ± 3.4	46.9 ± 4.7

Table 3.5: Relative uncertainties for the ^{76}Ge(n,γ)^{77}Ge measurement. The uncertainty of the branching of the IT was used only to calculate the direct cross section to ^{77}Ge (g.s.).

| | Relative uncertainty [%] | |
	^{77m}Ge	^{77}Ge
Emission probability	10.7 / 15.3	2.1 - 2.5
Peak area	1.8 - 3.4	0.7 - 1.7
Detector efficiency	2.4 - 3.2	1.8 - 2.1
Correction for decay during activation	0.7 - 1.0	≤ 0.2
Correction for decay during waiting and measurement	1.3 - 1.4	≤ 0.2
Target inhomogeneity	2	2
γ-ray attenuation	≤ 0.1	≤ 0.1
Neutron self shielding	≤ 0.1	≤ 0.1
Number of ^{76}Ge nuclei	1.4	1.4
Gold reference	2.8	2.8
Branching of IT		10.5

To obtain the thermal capture cross section of ^{76}Ge(n,γ)^{77}Ge the transitions with energies of 367.4 keV and 558.0 keV were used (fig. 3.1 left). These transitions are intense and the energies are close to the reference peak of ^{198}Au at 411 keV, reducing the influence of the efficiency calibration on the result. The correction factors for the γ-ray attenuation used are given in table 3.4, those for the neutron self shielding are the same as in the measurement of σ^m. Experimentally a total cross section of $\sigma^t = (68.8 \pm 3.4)$ mb was obtained. This value includes the feeding from the shorter-lived isomeric state with a branching of (19 ± 2) %. Correcting for this contribution the direct cross section to the ground state σ^d can be determined. The very small influence of the delay of the feeding due to the short half-life of the isomeric state ($T_{1/2} = 52.9$ s) during activation was considered in the evaluation as well. The value derived for the direct cross section is $\sigma^d = (46.9 \pm 4.7)$ mb. Due to the large difference of the half lives between the two states the correction could also be approximated by $\sigma^d = \sigma^t - 0.19 \times \sigma^m$. Since the uncertainty of σ^m is dominated only by the emission probabilities of ^{77m}Ge, it can be treated as independent from the uncertainty of σ^t when calculating the error of σ^d. The correction for IT was applied to the number of activated nuclei A_{Ge} in eq. 3.5 rather than to the cross section as suggested by the approximation. This avoids double counting of uncertainties. Consequently the

Table 3.6: Results obtained in this work for the thermal cross sections of ^{76}Ge(n,γ)^{77m}Ge and ^{76}Ge(n,γ)^{77}Ge compared with previous publications.

Cross section [mb]			Year	Reference
^{77m}Ge	^{77}Ge			
	Total	Direct		
	85 ± 17		1947	[52]
	350 ± 70		1952	[51]
137 ± 15	43 ± 2	6 ± 5	1957	[37]
87 ± 15	76 ± 15		1957	[15]
120 ± 30			1962	[57]
86 ± 9			1968	[40]
115 ± 16	68.8 ± 3.4	46.9 ± 4.7	2009	this work
	61.7 ± 3.7	39.6 ± 4.9	2009	this work, new intensities

approximation can be used only to estimate the cross section but should not be used to calculate the uncertainty of σ^d.

If the more intense transitions with energies of 211.0 keV and 215.5 keV are used to derive the cross section to the ground state, significantly lower values are obtained $\sigma^t(211) = (57.9 \pm 3.3)$ mb and $\sigma^t(215) = (58.5 \pm 3.3)$ mb respectively. The transitions at higher energies are in good agreement with the values calculated from the 367 keV and 558 keV lines. The 714.4 keV transition yields $\sigma^t = (69.4 \pm 3.8)$ mb and the 1193.3 keV transition $\sigma^t = (66.7 \pm 4.3)$ mb. This discrepancy of about 18 % results from the emission probabilities given in the literature (chapter 4).

The thermal cross section for the ^{76}Ge(n,γ)^{77m}Ge reaction obtained in our measurement $\sigma_m = (115 \pm 16)$ mb is consistent with the values from other publications [15, 37, 40, 57] within the error bars (table 3.6). The large uncertainties of the emission probabilities prohibit a significant improvement of the size of the error bars. The detailed list of uncertainties contributing to the overall error (table 3.5) allows to recalculate the cross sections if in future more precise data will be available. The capture cross sections to the ground state σ_t and σ_d are lower than those published by [15, 51, 52], but higher than the value in ref [37]. A significant improvement of the uncertainty was achieved in this measurement.

3.3.3 Recalculation of the cross section with new emission probabilities

The discrepancies observed in the cross section measurement were confirmed by another cross section measurement for ^{76}Ge(n,γ) at higher energies in Karlsruhe [38]. Similar problems occurred determining the k_0 values of ^{77}Ge for INAA in ref. [56]. A remeasurement of the emission probabilities of the γ-rays in the ^{77}Ge-decay was carried out (chapter 4). After a reanalysis of the data discussed in sect. 3.3.2 consistent values for the thermal neutron capture cross sections were derived, if the new emission probabilities were used. The new value for the total cross section is $\sigma^t = (61.7 \pm 3.7)$ mb and for the direct cross section $\sigma^d = (39.9 \pm 4.9)$ mb (table 3.7).

Table 3.7: Cross section of the ^{76}Ge(n,γ)^{77}Ge-reaction applying the new emission probabilities from chapter 4.

Target	Detector	E_γ [kev]	Attenuation correction	Total cross section [mb]	Direct cross section [mb]
A	I	211.5	0.9590	59.5 ± 3.5	37.6 ± 4.8
		215.0	0.9598	59.6 ± 3.5	37.8 ± 4.8
		367.4	0.9730	61.1 ± 3.6	39.2 ± 4.9
		558.0	0.9784	60.0 ± 3.6	38.1 ± 4.8
A	II	211.5	0.9521	59.7 ± 3.5	37.8 ± 4.8
		215.0	0.9529	60.0 ± 3.5	38.1 ± 4.8
		367.4	0.9660	62.4 ± 3.7	40.5 ± 4.9
		558.0	0.9714	64.5 ± 3.6	42.6 ± 5.0
B	I	367.4	0.9710	62.7 ± 3.7	40.8 ± 4.9
		558.0	0.9768	62.7 ± 3.8	40.8 ± 5.0
B	II	211.5	0.9491	61.5 ± 3.6	39.7 ± 4.9
		215.0	0.9500	61.7 ± 3.6	39.8 ± 4.9
		367.4	0.9640	65.1 ± 3.8	43.2 ± 5.0
		558.0	0.9698	63.9 ± 3.8	42.0 ± 5.0
Mean value				61.7 ± 3.7	39.9 ± 4.9

3.3.4 Consequences for the GERDA experiment

The cross sections of the ^{76}Ge(n,γ)-reaction were the main ingredient to calculate the neutron capture rate of about 1 capture/(kg y) in the germanium detectors of GERDA. The
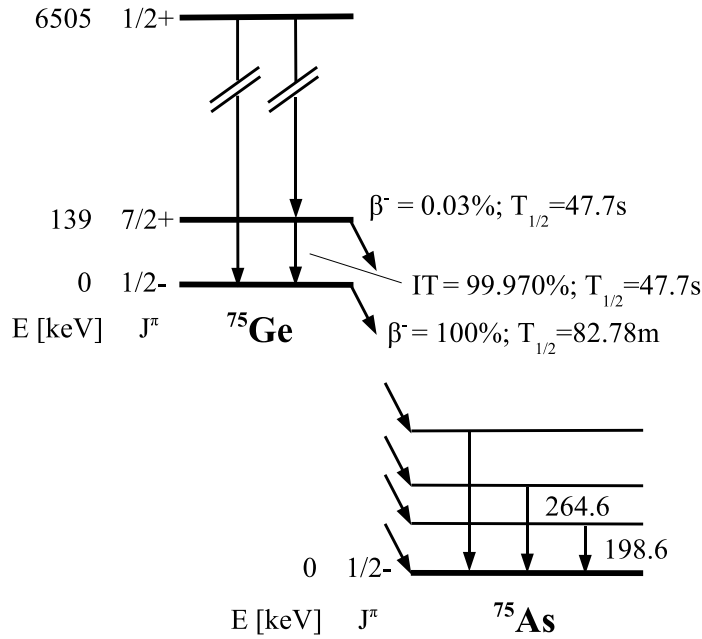
Figure 3.4: Decay scheme of ^{75}Ge.

cross sections of $\sigma^m = (137 \pm 15)$ mb to the isomeric state used in the simulations was found to decrease only slightly to $\sigma^m = (115 \pm 16)$ mb. Hence no significant changes in rate are expected. The cross section to the ground state $\sigma^t = (43 \pm 2)$ mb used to calculate the ^{77}Ge has to be replaced by $\sigma^t = (61.7 \pm 3.7)$ mb. Thus, the simulated background by the decay of ^{77}Ge of 8×10^{-5} counts/(keV decay) [50] increases to 1.1×10^{-4} counts/(keV decay), considering not only the direct capture but also the feeding by from the isomeric state with a branching of 19 %.

3.4 Cross sections of ^{74}Ge

Similar to ^{76}Ge, neutron capture by ^{74}Ge results in one of two states of the produced ^{75}Ge nucleus. An isomeric state in ^{75}Ge with $E_m = 139.68$ keV ($J^\pi = +7/2$) is populated as well as the ground state ($J^\pi = -1/2$). The isomeric state decays via IT to the ground state (99.970 %) or via β-decay to ^{75}As (0.03 %) with a half-life of $T_{1/2} = 47.7$ s. The ground state decays with $T_{1/2} = 82.78$ m by β-decay directly to the ground state of ^{75}As without the emission of γ-rays (87.1 %) or to excited levels, followed by γ-transitions (fig. 3.4).

33

3.4.1 Experiment

The γ-rays emitted by the decay of ^{75}Ge are dominated by the 264 keV transition in ^{75}As ($I_\gamma = 11.4\,\%$). Since in the decay of ^{77}Ge a transition occurs with similar energy, GeO_2 pills, isotopically depleted in ^{76}Ge (0.58 % [23]) were used in this measurements to reduce the corrections to be done for the 264 keV peak.

For the activation of the germanium pills attenuator $\#3$ was moved into the beam and the elliptical "nose" was used. The thermal equivalent neutron flux was measured with a Ti foil to be $\Phi_0 = 2.9 \times 10^9\,n_{th}/(cm^2\,s)$.

For the determination of the cross section to the isomeric state several runs with target "C" and "D" (table 3.1) were carried out, varying the times for activation and measurement (table 3.8). The masses and the times used in two runs with target "C" and "D" to determine the cross section to the ground state can be found in table 3.9.

The settings of the Compton suppression system of detector I did not allow to measure energies below 220 keV, hence no data for the isomeric state were gained by detector I and the 198 keV transition in the ground state decay could not be evaluated as well.

Table 3.8: Results of the thermal cross section measurement for ^{74}Ge(n,γ)^{75m}Ge using detector II. For all runs the corresponding time intervals used for activation t_a, waiting t_w and measurement t_w are given.

Target	t_a [s]	t_w [s]	t_m [s]	Cross section [mb]
C	1200	5	180	132.8 ± 7.3
	60	5	120	132.2 ± 9.7
	60	5	120	129.8 ± 8.2
	180	5	180	129.4 ± 7.2
	180	30	240	132.0 ± 7.7
	120	5	120	131.0 ± 7.6
	120	5	120	134.2 ± 7.8
	120	5	120	132.0 ± 7.7
D	1500	5	180	125.1 ± 6.9
	120	5	120	130.2 ± 7.5
	120	5	120	130.0 ± 7.5
	120	5	120	128.7 ± 7.5
Weighted mean				130.5 ± 5.6

34

Table 3.9: Results for the thermal cross section measurement of the ^{74}Ge(n,γ)^{75}Ge reaction.

Target	Detector	E_γ [kev]	Attenuation correction	Cross section [mb] Total	Cross section [mb] Direct
C	I	264.6	0.9685	507 ± 52	375 ± 51
	II	198.6	0.9525	516 ± 57	384 ± 56
		264.6	0.9615	494 ± 51	362 ± 50
D	I	264.6	0.9709	492 ± 51	360 ± 50
	II	198.6	0.9556	498 ± 56	366 ± 55
		264.6	0.9639	480 ± 50	348 ± 49
Weighted mean				497 ± 52	365 ± 51

3.4.2 Results

The energy of the decay of the isomeric state is released almost exclusively by the 139.68 keV γ-rays in ^{75}Ge. Using this line the weighted mean for the thermal neutron capture cross section to the isomeric state results in $\sigma^m = (130.5 \pm 5.6)$ mb. All statistical and systematic errors can be found in table 3.10. Since the uncertainties of the number of nuclei in the two targets as well as their inhomogeneities are not correlated to each other, they were treated independently. The same is true for the uncertainties induced by the opening/closing beam shutter and the peak areas in the measured spectra.

For the cross section of the ^{74}Ge(n,γ)^{75}Ge-reaction the 198.6 keV (only detector II) and the 264.6 keV transition were used. The small contribution from the decay of ^{77}Ge ($\sim 0.2\,\%$) to the 264.6 keV peak was considered in the evaluation. A correction for the line at the same energy from the decay of ^{77m}Ge was not necessary because of the sufficient waiting time before starting the measurement and its small emission probability. The cross sections obtained are $\sigma^t = (497 \pm 52)$ mb for the experimentally measured total cross section and $\sigma^d = (365 \pm 51)$ mb for the cross section corrected for the feeding by IT, *i.e.* the cross section direct to the ground state. Like for ^{76}Ge the correction considers the delayed feeding from the isomeric state ($T_{1/2} = 47.7$ s) and the decay of the ground state during activation. Since the difference in the half-lives between the isomeric and the ground state is large, the correction turns out to be very small. The values are weighted means and the uncertainties were treated as in the case of the isomeric state. To avoid double counting of errors the correction for the feeding was applied in eq. 3.5 to the number of activated nuclei A_{Ge} and not to the derived cross section, resulting in a smaller uncertainty for σ^d.

The cross section for ^{74}Ge(n,γ)^{75}Ge is consistent to previous works within error bars (table 3.11). Again, similar to ^{76}Ge the large uncertainties are dominated by the emission

Table 3.10: Relative uncertainties for the ^{74}Ge(n,γ)^{75}Ge measurement.

	Relative uncertainty [%]	
	^{75m}Ge	^{75}Ge
Emission probability	2.0	10.0 / 9.6^a
Peak area	2.8 - 5.4	0.8 - 3.3
Detector efficiency	1.8	1.5 - 1.8
Correction for decay during activation/waiting/measurement		
due to beam-shutter	1.5 - 2.3	< 0.1
due to half-life time	0.5 - 1.1	< 0.1
Target inhomogeneity	2	2
γ-ray attenuation	≤ 0.2	≤ 0.1
Neutron self shielding	< 0.1	< 0.1
Number of ^{74}Ge nuclei	0.2	0.2
Monitored neutron flux (gold ref.)	2.7	2.3 - 2.7^b

^{a} line dependent

^{b} detector dependent

probabilities. The error for the capture cross section to the isomeric state on the other hand is reduced by this work significantly from 10 % [57] to below 5 %.

Altough no Monte-Carlo simulations were run to determine the production rate of ^{75}Ge it can be estimated on basis of the ^{76}Ge(n,γ) cross section $(6 + 137 = 143\,\text{mb}$, sect. 1.3). With the total cross section for ^{74}Ge(n,γ) $(\sigma^t = 497\,\text{mb})$ and an abundance ratio of 87.1:12.7 about 0.5 nuclei/(kg y) are produced in the crystals.

Table 3.11: Results obtained in this work for the thermal cross sections of ^{74}Ge(n,γ)^{75m}Ge and ^{74}Ge(n,γ)^{75}Ge compared with previous publications.

Cross section [mb]			Year	Reference
^{75m}Ge	^{75}Ge			
	Total	Direct		
	380 ± 76		1947	[52]
	600 ± 60		1952	[51]
40 ± 8		180 ± 40	1957	[15]
	550 ± 55		1960	[36]
200 ± 20			1962	[57]
143 ± 16			1968	[40]
	400 ± 200		1987	[32]
130.5 ± 5.6	497 ± 52	365 ± 51	2010	this work

Chapter 4

γ-ray intensities in the ^{77}Ge decay

In chapter 3 the cross section measurement of the ^{76}Ge(n,γ)-reaction is presented. The results show, that there is a severe discrepancy between the emission probabilities given in Nuclear Data Sheets 81 (NDS81) [19] that are based on the PhD thesis of Lent [34] and the experimental results in this work. The same inconsistency was found by two groups in Karlsruhe [38] and Geel, Belgium [56].

The relative intensities have been remeasured at the PGAA instrument of the research reactor FRM II in Garching. The goal of this measurement was to determine the emission probabilities. No efforts were made to find new lines or to check the decay scheme proposed by Lent.

4.1 Available data

The emission probabilities mostly used are the ones given in the NDS81 [19]. These values are inconsistent with other data such as measured by Ng [46] using NaI detectors. The intensities from both references are compared in table 4.1 to the values suggested by the cross section measurements done by the Karlsruhe group and this work. The intensities of the 367 keV and 558 keV peak resulting from our measurement are normalized to the previously determined (sect. 3.3.2) intensities of 211 keV and 215 keV line (second column), the Karlsruhe group used additionally the 264 keV transition for normalization.

4.2 Experiment

The decay spectrum of ^{77}Ge was measured following the measurement of the prompt radiation in the enriched target (chapter 6). The sample ($m = 580.1$ mg) was irradiated for ~15 hours. After a waiting period of more than 20 min (suppression of short lived isotopes like: ^{20}F, ^{28}Al, ^{75m}Ge, ^{77m}Ge) the decay spectrum of ^{77}Ge, *i.e.* the γ-lines in ^{77}As

Table 4.1: Emission probabilities per 100 neutron captures in the ^{77}Ge decay. The intensities obtained in chapter 3 are normalized in column "old normalization" to the intensities of of the 211 keV and 215 keV by NDS81 (30.8 % and 28.6 %), in column "new normalization" to those of the remeasurement (29.6 % and 27.7 %) presented in this chapter.

E_γ	I_γ [%]					
[keV]	NDS81 [19]	Ng [46]	Karlsruhe [38]	chapter 3		remeasur.
				old norm.	new norm.	
211.0	30.8 ± 1.0	26.9 ± 1.7	-	-	-	29.6 ± 1.1
215.5	28.6 ± 0.9	25.7 ± 1.7	-	-	-	27.7 ± 1.0
367.4	14.0 ± 0.3	16.71 ± 0.17	15.3 ± 0.4	16.4 ± 0.6	15.8 ± 0.6	15.2 ± 0.6
558.0	16.1 ± 0.4	18.3 ± 1.7	18.8 ± 0.5	19.2 ± 0.7	18.5 ± 0.7	18.0 ± 0.7
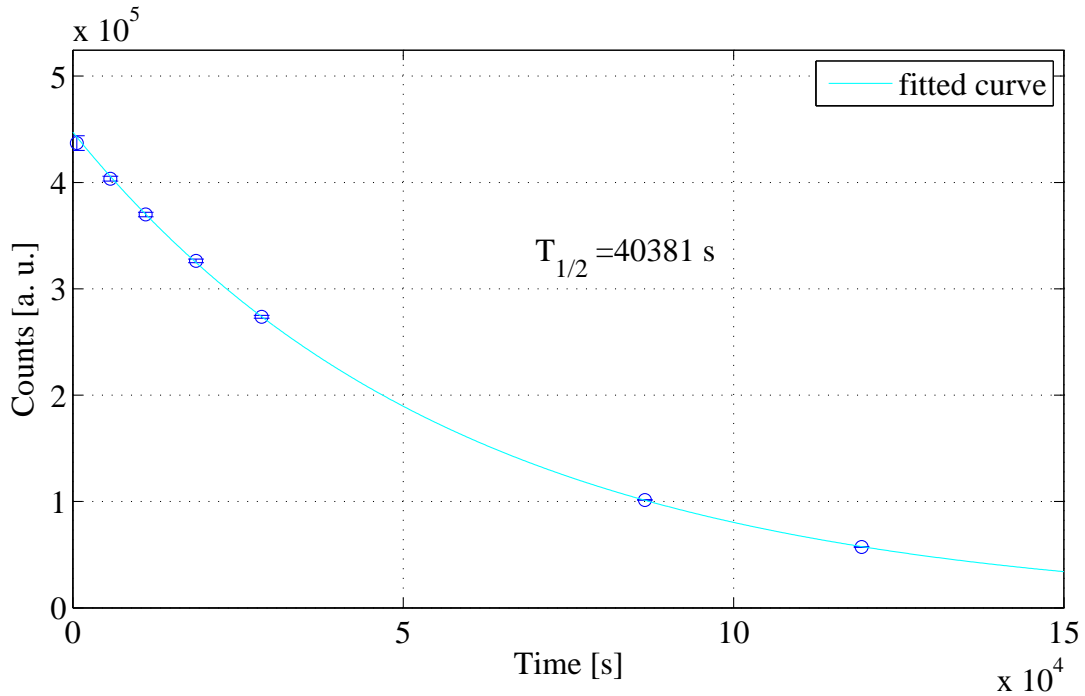
Figure 4.1: Decay curve of the 558 keV peak. The fitted exponential function is consistent with the half-life of ^{77}Ge.
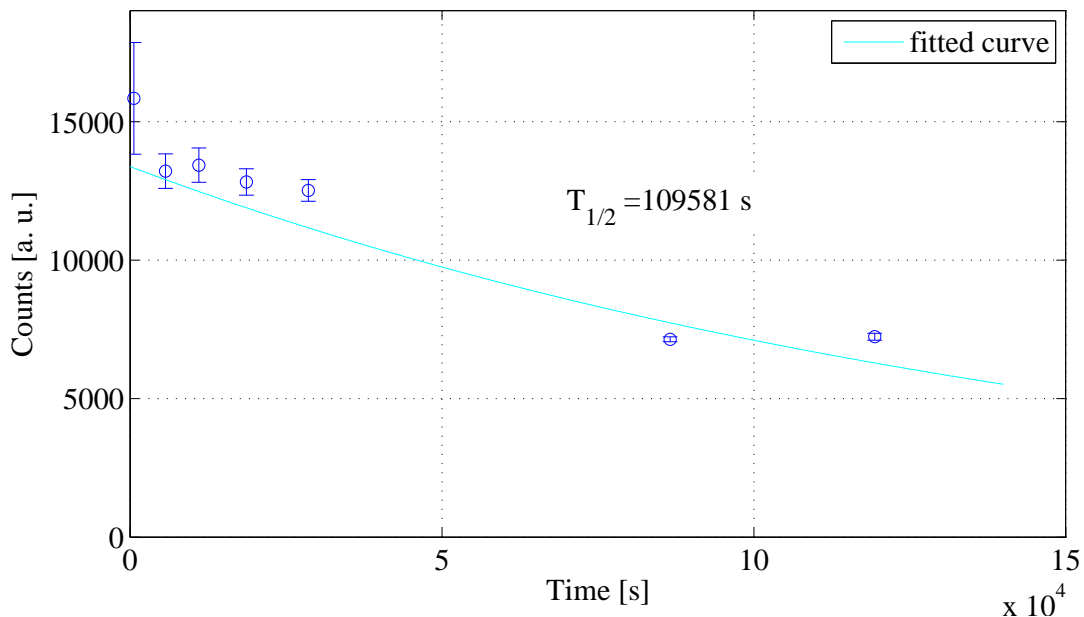
Figure 4.2: Decay curve of the 520 keV peak. The fit is not consistent with the half-life of ^{77}Ge. The peak contains a strong contribution by the longer lived ^{77}As isotope ($T_{1/2} = 38.8$ h).

was recorded for more than 33 h. Dividing this time span into 16 subspectra, the decrease in rate for individual peaks could be measured.

4.3 Results

The γ-spectrum was analyzed using the "Tv"-software [54]. The peaks were fitted applying a gaussian with a left tail. To obtain the intensities the detector efficiency (sect. 2.3.3) and γ-ray attenuation in the sample were considered. In a first step all peak areas were normalized to the strongest line at 264.4 keV. The intensity per 100 neutron captures was determined using the ground state transitions in the decay scheme published by Lent [34]. It was assumed that there is no direct β-decay into the ground state of ^{77}As without emitting γ-rays. The uncertainties of the energy contain a general systematic uncertainty of 0.1 keV added quadratically. The peak areas were corrected for contributions by ^{75}Ge, ^{77}As and ^{24}Na.

The 16 subspectra were used to obtain the half-life time by an exponential fit of individual lines. Comparing this value with the known half-life of ^{77}Ge ($T_{1/2} = 11.3$ h) one has an additional handle to identify the source of the peak. All transitions with intensities

Table 4.2: Decay γ-rays of ^{77}Ge. Only transitions to the ground state (marked with $\star$) or transitions used to derive the cross section of ^{76}Ge(n,γ) in chapter 3 are stated. To obtain the intensity per 100 decays the relative intensity was multiplied by 0.537(14). This factor was determined assuming the sum of the ground state transitions given by Lent to be 100 %. The isotopes in the last column were identified in the spectrum and subtracted from the intensity measured for ^{77}Ge.

E_γ [keV]	Relative intensity	Intensity per 100 decays	Comments
194.72(10)	2.99(8)	1.61(6)	$\star$
211.05(10)	55.1(14)	29.6(11)	
215.51(10)	51.6(13)	27.7(10)	$\star$
264.37(11)	100.0	53.8(14)	$\star$,^{75}Ge
367.33(10)	28.4(7)	15.2(6)	
475.49(10)	2.18(6)	1.17(5)	$\star$
558.03(10)	33.5(8)	18.0(7)	
614.43(10)	1.25(15)	0.57(8)	$\star$
631.87(10)	14.6(4)	7.83(28)	$\star$
634.41(10)	4.18(11)	2.25(8)	$\star$
714.39(10)	14.9(4)	7.99(28)	
784.83(10)	2.73(7)	1.47(6)	$\star$
875.26(10)	1.63(5)	0.87(4)	$\star$
889.38(56)	0.011(7)	0.006(4)	$\star$
1164.79(15)	0.054(6)	0.029(4)	$\star$
1193.33(10)	5.30(13)	2.85(10)	
1201.43(14)	0.134(13)	0.072(7)	$\star$
1280.02(11)	0.366(13)	0.197(9)	$\star$
1319.76(11)	0.548(17)	0.295(12)	$\star$
1399.59(34)	0.012(4)	0.0062(20)	$\star$
1528.46(12)	0.100(7)	0.054(4)	$\star$
1538.90(11)	0.298(11)	0.160(8)	$\star$
1573.80(11)	1.40(4)	0.755(28)	$\star$
2000.27(11)	1.16(4)	0.625(24)	$\star$
2341.84(11)	1.014(29)	0.545(21)	$\star$

$I_\gamma > 1\,\%$ were checked by this method for contributions by other isotopes. An example of a pure ^{77}Ge peak is the 558 keV line (fig. 4.1). On the contrary the fit in fig. 4.2 does not correspond the ^{77}Ge decay. The raise in rate at the end of the measurement is due to ^{77}As, the longer lived daughter nucleus of ^{77}Ge.

The complete set of transitions and their intensities can be found in table C.6 in the appendix. The ground state transitions and the peaks used in the cross section measurement (chapter 3) are summarized in table 4.2.

Chapter 5

Known levels and transitions in ^{77}Ge and ^{75}Ge

From previous measurements of the ^{76}Ge(n,γ) reaction a limited number of 17 prompt transitions after neutron capture on ^{76}Ge are known (table 5.2). Starting from the initial level at $S_n = 6072\,\mathrm{keV}$, six excited states, including the metastable level (159.7 keV) are populated. Some of these transitions are placed into the decay scheme, but except for the direct transition to the metastable level ($E_\gamma = 5912.9\,\mathrm{keV}$ [24]) no complete decay path from the initial level to the ground state was reported.

Other reactions like ^{76}Ge(^{13}C,^{12}C), ^{76}Ge(d,p) or β-decay of ^{77}Ga give information about the level scheme in ^{77}Ge as well [19, 28].

The properties of the ^{74}Ge(n,γ) reaction are better known because of the larger cross section and the higher abundance reached in the enrichment process [20].

In this chapter relevant data for the level schemes of ^{77}Ge and ^{75}Ge are discussed. The rather simplistic tables with transitions in ^{77}Ge are given in this chapter, the more elaborate tables of ^{75}Ge can be found in the appendix (tables A.3 and A.1).

5.1 Data from (n,γ) reactions

5.1.1 Hasselgren

Hasselgren [25] measured the (n,γ)-reaction of even germanium isotopes (for isotopic composition see table 5.1) at the 1 MW water reactor R1 in Stockholm. Targets of about 500 mg were irradiated close to the reactor core with an thermal neutron flux of $3 \times 10^{12}\,\mathrm{n/(cm^2\,s)}$. A Ge(Li) detector ($1.5\,\mathrm{cm^3}$) at a distance of 4.5 m was used to measure the γ-rays. The target chamber was evacuated to reduce background by neutron capture on nitrogen. Above the pair production threshold the Ge(Li) crystal was used together with NaI detectors as a pair spectrometer. For lower energies these NaI crystals were used

Table 5.1: Isotopic composition of the germanium targets used by Groshev et al. and Hasselgren for the ^{74}Ge(n,γ) and ^{76}Ge(n,γ) measurements.

Target	Groshev *et al.* [24]					Hasselgren [25]				
	Content [%]									
	^{70}Ge	^{72}Ge	^{73}Ge	^{74}Ge	^{76}Ge	^{70}Ge	^{72}Ge	^{73}Ge	^{74}Ge	^{76}Ge
^{nat}Ge	20.52	27.43	7.76	36.54	7.76					
^{74}Ge	1.5	2.4	1.8	92.7	1.6	0.69	1.14	1.56	95.8	0.82
^{76}Ge	3.26	4.75	1.49	7.20	83.3	4.4	6.7	3.1	9.8	76.0

for an anti-coincidence Compton suppression system. The detector signal was digitized by a 4096-channel pulse-height analyzer. The intensities were normalized to the primary transitions found in this measurement. The transitions found in ^{77}Ge and ^{75}Ge are listed in table 5.2 and A.3 respectively.

5.1.2 Groshev *et al.*

The measurement by L.V. Groshev *et al.* [24] was carried out in the external thermal neutron beam of the IRT-M reactor at the I.V. Kurchatov Atomic Energy Institute in 1973. Targets of different isotopic compositions (table 5.1) were irradiated in the neutron beam with a flux of $\sim 10^7$ n/(cm^2 s). Ge(Li) crystals with a volume of 5 cm^3 and 0.5 cm^3 were used as detectors. The efficiency calibration was done with standard sources and the prompt chlorine spectra. With this efficiency curve the relative emission probabilities could be obtained. For normalization to absolute intensities a germanium target of natural isotopic abundance was irradiated. Knowing the isotopic composition of the target and the absolute intensity of the 7262.3 keV line in ^{74}Ge ($I_\gamma = 1.49\%$ per neutron capture [39]) the intensities in the other isotopes were determined. Since there were no lines of ^{77}Ge in the spectrum of the natural target, the absolute intensities were extracted from the spectrum of the target enriched in ^{76}Ge using the same transition in ^{74}Ge. In the more recent publication by Islam *et al.* [27] the emission intensity of this line is given as $I_\gamma = (2.5 \pm 0.5)\%$. The obtained transitions and their intensities are listed in table 5.2.

Table 5.2: Known transitions in ^{77}Ge after neutron capture on ^{76}Ge. The intensities given by Hasselgren are normalized to the primary transitions, those by Groshev *et al.* to the 7262 keV line in ^{74}Ge. The relative intensities in the IAEA data base are normalized to the strongest transition with $E_\gamma = 1250.55$ keV.

Hasselgren [25]		Groshev *et al.* [24]		IAEA data base [1]	
E_γ [keV]	I_γ [%]	E_γ [keV]	I_γ [%]	$E_{\gamma,rel}$ [keV]	I_γ [%]
		159.5†	0.32		
		195.6	0.15		
		431.5	0.82		
		808.2	2.25		
		850.8	1.62		
				862,20	10,91
				1250,55	100,00
				1903,80	16,36
3895.2	13.4				
4008.5	9.3			4008,70	46,36
4193.2	30(9)			4193,20	64,45
		4514.3*	0.24		
		4821.8*	0.16	4821,60	2,73
5050.8*	39(2)	5047.4*	2.25	5050,30	36,36
5420.1	9(3)				
5444.7*	3(1)			5443,70	3,64
5912.8*	57(7)	5912.9*	4.65	5912,4	72,73

* Primary transition
$\dagger$ ground state transition

5.1.3 Islam *et al.*

The ^{70,72,73,74}Ge(n,γ)-reaction was measured at the McMaster Nuclear Reactor by Islam *et al.* [27]. The target of natural composition was exposed to a neutron flux of 5×10^{12} n/(cm^2 s) and the emitted γ-rays were detected by a pair-spectrometer (HPGe + NaI). To obtain the absolute intensities the germanium powder was mixed with melamine (C$_3$H$_6$N$_6$). The intensity values were then derived relative to ^{14}N. Because of the pair-spectrometer mode only high energetic γ-rays were measured (above 4707 keV).

5.1.4 Weishaupt and Rabenstein

The prompt γ-rays in ^{71,73,74,75}Ge emitted by a natural germanium sample were measured by Weishaupt and Rabenstein [58] in two different ways. Firstly, a sample was irradiated and the emitted γ-radiation measured by a Ge(Li) detector close by. Secondly, germanium detectors themselves were activated and the radiation deposited in the crystal was detected. In the latter mode very low-energy γ-rays and even conversion electrons can be measured. On the other hand summing of γ-rays affects the peak size, dependent on the volume of the detector. To quantify this effect two detectors of different size were used. To assign the lines to the isotopes a γ-γ-coincidence measurement was carried out. Only energies up to 2014 keV are reported. In this range four transitions in ^{75}Ge were observed (60.5(2) keV, 80.1(1) keV, 139.69(5) keV and 177.3(1) keV).

5.1.5 Discussion of discrepancies of intensities in ^{75}Ge

The absolute values of the intensities collected in table A.3 are of poor agreement while they fit rather well together if they are renormalized. Since the method of normalization used by Hasselgren is not expected to deliver correct absolute values, Groshev *et al.* and Islam use both an adequate procedure. Nevertheless their values differ by a factor of ≈ 2. As discussed by Islam *et al.* this may result from the intensity of the 7262 keV line, used by Groshev. It was calculated by Magruder relative to carbon, having its strongest transition at 4945.3 keV. But there is a strong transition in ^{74}Ge only 6 keV higher in energy that possibly not has been resolved from the carbon line. This would have lead to a lower intensity of the 7262 keV line and subsequently to lower intensities of transitions derived by Groshev *et al.*. The intensity given by Islam *et al.* for $E_\gamma = 7260$ keV is $I_\gamma = (2.54 \pm 0.11)\,\%$, excluding an error of 14 % for the cross section of ^{73}Ge(n,γ).

5.1.6 ^{13}C(n,γ)^{12}C reaction

In a recent measurement by Kay *et al.* [28] excited states in ^{77}Ge were measured with the ^{76}Ge(^{13}C,^{12}C)^{77}Ge reaction. A thin isotopically enriched ^{76}Ge target was irradiated by a ^{13}C beam provided by the Argonne Tandem Linear Accelerator System (ATLAS). The γ-rays were detected by the detector array Gammasphere (GS) consisting out of 99 Compton suppressed HPGe detectors. γ-γ coincidences were determined using only the GS data. For coincidences of nuclear recoil and γ-rays a fragment mass analyzer was used, allowing the determination of angular distributions. Kay reported 26 transitions and 10 levels with a maximum energy of 1385 keV.

The ^{76}Ge(^{13}C,^{12}C)^{77}Ge reaction was measured before by A.E. Zobov *et al.* [59] detecting only part of the transitions given by Kay *et al.*. Only one line with $E_\gamma = 1385$ keV connecting the 1385 keV level with the ground state found by Zobov *et al.* is not stated by Kay *et al.*.

Table 5.3: Properties of excited states in ^{77}Ge obtained with the ^{76}Ge(^{13}C,^{12}C)-reaction by Kay *et al.* [28]. The uncertainties in energy are 0.1 keV. Square brackets indicate that the multiplicity was extracted from the level scheme.

E_{level} [keV]	I_i^π	E_γ [keV]	I_γ [%]	γ multipolarity	I_f^π
224.9	$9/2^+$	224.9	$\equiv$100	M1/E2	$7/2^+$
421.4	$(5/2)^+$	421.4	124(3)	(M1/E2)	$7/2^+$
492.0	$5/2^{(-)}$	332.4	1.3(9)	[E])	$1/2^-$
		492.0	23(1)	(E1)	$7/2^+$
504.8	$5/2^+$	83.5	37(2)	[M1/E2]	$(5/2)^+$
		279.9	4.3(9)	[E2]	$9/2^+$
		504.8	96(3)	M1/E2	$7/2^+$
618.9	$3/2^+$	114.0	0.14(3)	[M1/E2]	$5/2^+$
		126.8	0.36(5)	[E1]	$5/2^{(-)}$
		197.5	6.3(7)	[M1/E2]	$(5/2)^+$
		459.2	32(2)	E1	$1/2^-$
		618.9	8(2)	[E2]	$7/2^+$
629.7	$3/2^-$	470.0	61(2)	M1/E2	$1/2^-$
760.6	$7/2^+$	255.7	14(1)	M1/E2	$5/2^+$
		535.6	24(1)	M1/E2	$9/2^+$
		760.6	8.1(10)	M1/E2	$7/2^+$
884.3	$5/2^+$	884.3	33(2)	M1/E2	$7/2^+$
910.6	$(5/2,7/2)^+$	224.9	100		$3/2^+$
		418.5	8.4(8)	[E1]	$5/2^{(-)}$
		685.6	3.8(5)		$9/2^+$
1385.3	$5/2^+$	624.7	39(2)	M1/E2	$7/2^+$
		755.6	30(2)	[E1]	$3/2^-$
		766.5	17(1)	[M1/E2]	$3/2^+$
		880.5	36(2)	M1/E2	$5/2^+$
		893.3	5.2(6)	[E1]	$5/2^-$
		963.9	11(1)	[M1/E2]	$(5/2)^+$

5.2 Further reactions

The levels in ^{77}Ge and ^{75}Ge can also be populated by β-decay of ^{77}Ga and ^{75}Ga respectively. Table 5.4 summarises the evaluated data for ^{77}Ge presented in [19]. The data for ^{75}Ge can be found in tableA.1.

The ^{76}Ge(d,p) reaction was also used to determine the level structure in ^{77}Ge together with the corresponding quantum numbers. But the energy information gained by this method is very inaccurate ($\sim 10\,\text{keV}$). Table A.2 in the appendix shows the results collected in [19].

Table 5.4: States and transitions in ^{77}Ge after β-decay of ^{77}Ga [19]. The uncertainty in E_γ is 1.0 keV for all transitions.

E_{level} [keV]	I_i^π	E_γ [keV]	I_γ [%]
0.0	$7/2^+$		
160.0(10)	$(1/2)^-$	160.0	
581.3(13)	$1/2, 3/2, 5/2^-$	420.9	
619.0(13)	$1/2, 3/2, 5/2^-$	458.6	48
629.4(15)	$3/2^-$	469.4	100
778.3(12)	$1/2, 3/2, 5/2^-$	196.7	
		618.2	
1021.4(12)	$1/2, 3/2, 5/2^-$	242.6	
		401.9	
		861.4	
1047.9(15)	$1/2^-, 3/2^-$	887.9	
1358.9(17)		739.9	
1663.6(13)	$(1/2, 3/2, 5/2)^-$	641.4	
		1504.4	
1823.6(17)	$(1/2)^+$	1242.3	
2816.7(18)		2187.3	

5.3 Discussion

The data provided for the ^{76}Ge(n,γ) reaction were measured in the early 70s using Ge(Li) detectors of very small volumes ($0.5\,\text{cm}^3$ - $5\,\text{cm}^3$) compared to modern HPGe detectors. This results in a worse Compton to peak ratio and very intense single and double escape peaks. The targets used by Hasselgren and Groshev *et al.* are both isotopically enriched

in ^{76}Ge, but all other isotopes have a significant abundance. Since ^{76}Ge has the lowest neutron capture cross section of all germanium isotopes, the spectra contain a large number of peaks from these isotopes. These two facts makes it very difficult to identify transitions in ^{77}Ge. The targets used in the ^{74}Ge(n,γ) measurement had a higher isotopic enrichment and the cross section ratio was more appropriate. Therefore the number of lines and levels is considerable higher.

Using the ^{13}C(n,γ)^{12}C reaction with a 4π detection system a very detailed picture with good statistics was gained by Kay et $al..$ The drawback of this reaction is that the initial state has an excess energy of only 1385 keV, much lower than the 6072 keV binding energy gained by neutron capture. The population of levels differs from the (n,γ) reaction that is of interest in the GERDA experiment as well. The same holds for the β-decay of ^{77}Ga, where levels up to 2816 keV are populated. Some discrepancies to the β-decay data were found by Kay et $al..$

The (d,p) reaction allows to gain valuable spin information for levels, but the achieved energy information is too unprecise to compare with HPGe spectroscopy.

The level scheme and the transitions in ^{75}Ge are known much better. For the ^{74}Ge(n,γ)-reaction most of the lines at the lower and upper end of the energy spectrum have been placed into the decay cascade. This information is supplemented by data from ^{75}Ga decay measurements.

In summary the knowledge of the decay scheme is very poor for ^{77}Ge, while the levels and transitions in ^{75}Ge are rather well known. To satisfy the need of the GERDA experiment (as discussed in chapter 1) a new measurement of the prompt radiation after neutron capture on ^{76}Ge was planned and carried out at the research reactor FRM II as described in the next chapter.

Chapter 6

Prompt γ-rays

The prompt γ-radiation after neutron capture on ^{76}Ge was measured with the same setup as the cross sections and the decay spectrum of ^{77}Ge. In the first section the data taking and analysis of the single spectra will be described, the second section is dedicated to the coincidence measurement. Combining both data the level scheme in ^{77}Ge was reconstructed. In the last part of this chapter the results of the two experiments are discussed. The spectra recorded were also used to determine the transitions and the level scheme in ^{75}Ge. The partial γ-ray production cross section σ_γ defined in chapter 2 are abbreviated in the following with *partial cross section*.

6.1 Data taking of single spectra

6.1.1 Experiment

The single spectra were measured using both HPGe detectors (I: 60 % and II: 36 % relative efficiency). The larger detector covered an energy range up to 8.7 MeV, while the smaller detector was tuned for lower energies (<2600 keV). The energy resolution at 1.3 MeV

Table 6.1: Experimental parameters for the prompt measurements.

Target	Mass [mg]	Detector	Real time [s]	Dead time [%]	Data acquisition
enriched	580.1	I+II	53 666	2.8/2.7	standard
enriched	580.1	I	54 459	5.9	Multiport II
depleted	435.7	I+II	52 770	5.4/6.0	standard
empty	-	I+II	53 667	1.3/1.1	standard
enriched (coinc.)	304.1	I+II	713 790	-	coincidence
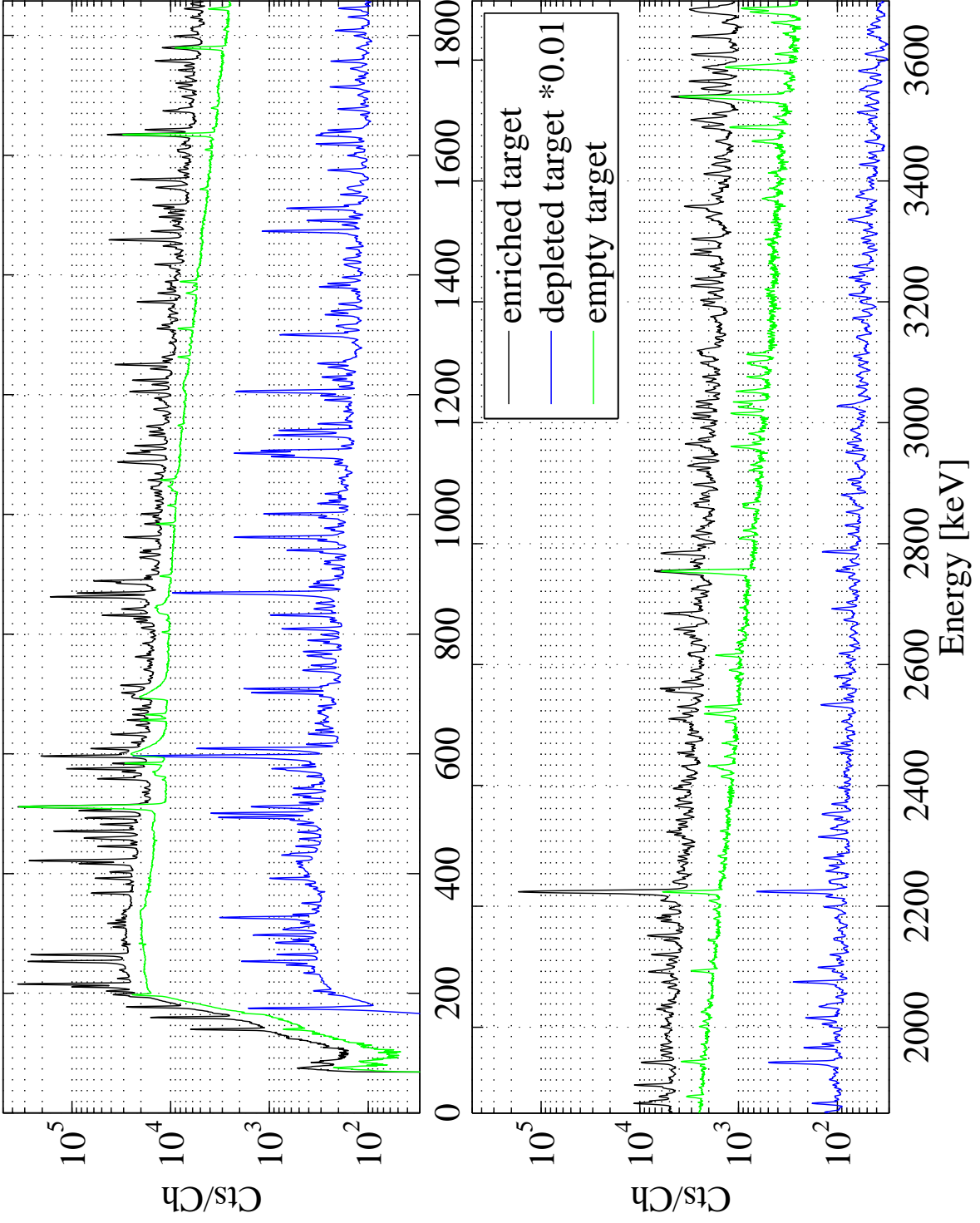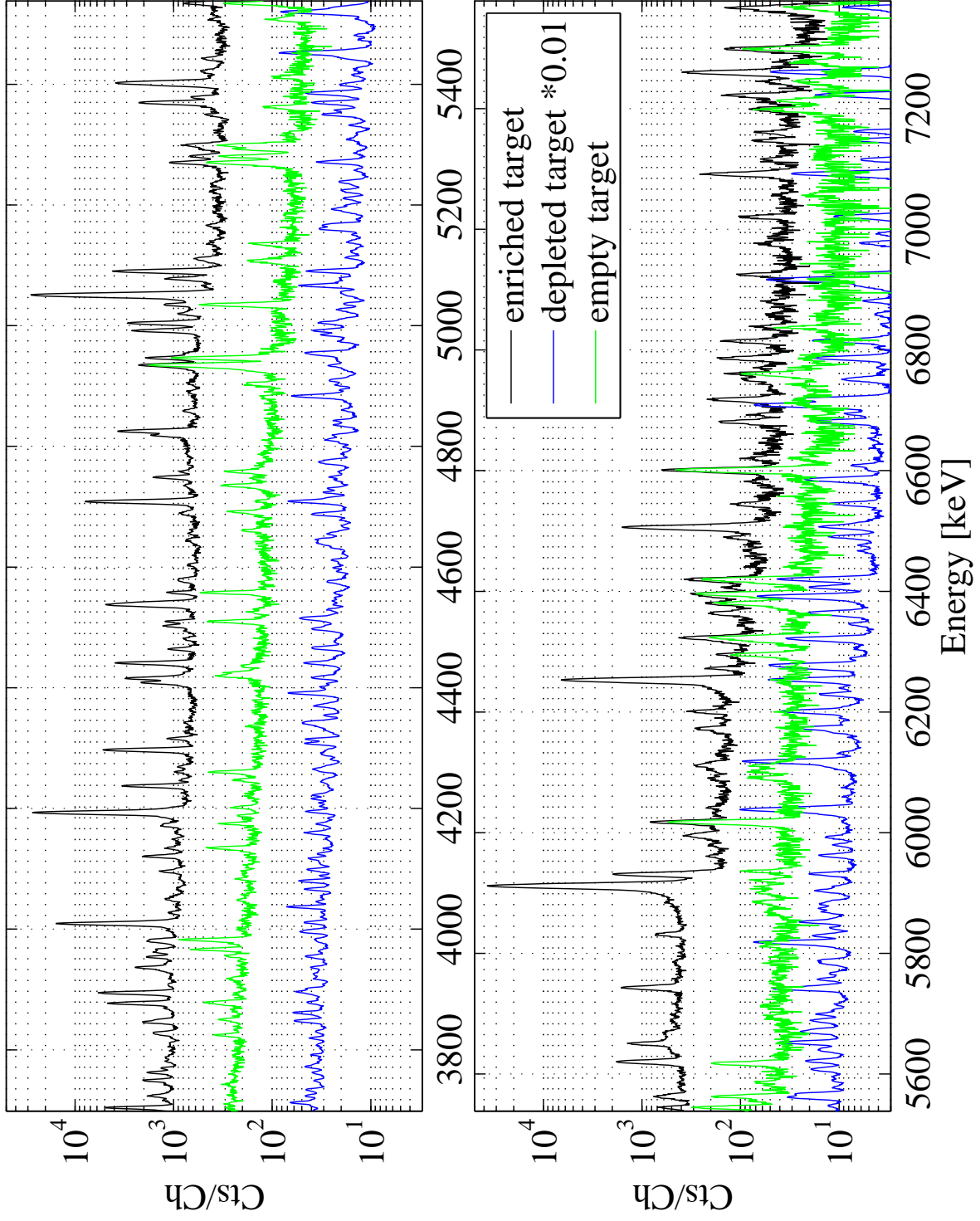
Figure 6.1: Prompt spectra of the enriched, the depleted and the empty target.

was 2.14 keV (FWHM) for detector I and 2.27 keV (FWHM) for detector II. The target chamber was evacuated during irradiation to reduce background by nitrogen in air.

Due to the relatively small cross section of ^{76}Ge an isotopically enriched GeO$_2$ target (^{76}Ge: 87.0 %, ^{74}Ge: 12.7 %, ^{70,72,73}Ge: 0.3 % [56]) with a mass of 580.1 mg was employed in our measurement. Samples of natural composition do not show any peaks of ^{76}Ge. To identify peaks resulting from neutron capture on ^{74}Ge a second sample of GeO$_2$ powder, depleted in ^{76}Ge (^{76}Ge: 0.58 %, ^{74}Ge: 39.02 %, ^{73}Ge: 8.42 %, ^{72}Ge: 29.57 %, ^{70}Ge: 22.03 %) was used. The GeO$_2$ powder was sealed in a FEP (Fluorinated Ethylene-Propylene) bag. An empty target consisting only of the FEP bag was used to determine the background. To obtain good statistics all targets were exposed for about 15 h to the neutron beam. For the depleted target a lower neutron flux than for the others was chosen, taking into account the higher cross section of ^{70}Ge and ^{73}Ge. The spectra of the enriched, the depleted and the empty targets are shown in fig. 6.1, the target properties and the parameters of the measurement are given in table 6.1. All targets are different from those used for the cross section measurements, the decay of ^{77}Ge in contrast was measured with the same enriched sample.

6.1.2   Analysis

Transitions in the different germanium isotopes were identified by comparing the spectra of the enriched, the depleted and the empty targets. For the spectrum analysis the "Tv"-software [54] was used. The peaks were fitted with gaussian distributions, extended by a left tail and an *erf*-step function if needed. To the uncertainty of the measured γ-ray energy E_γ a systematic contribution from energy calibration of 0.10 keV was added quadratically. A detailed description of the energy and efficiency calibration can be found in sect. 2.3.3. In the analysis neutron self-shielding was not considered since it has a very small effect on the relative γ-ray intensities. The γ-ray attenuation in the sample on the other hand was included, it amounts to approximately 5 % for low energies ($E_\gamma \sim 100$ keV) and to 0.5 % at 4 MeV.

The enriched spectrum shows peaks due to ^{76}Ge, ^{74}Ge and ^{73}Ge, while the depleted spectrum contains all germanium isotopes except for ^{76}Ge (fig. 6.1). The ratio between peaks of ^{74}Ge or ^{73}Ge occurring in both spectra is constant. Therefore, if a peak in the depleted spectrum was identified to be due to neutron capture of ^{74}Ge or ^{73}Ge, the corresponding contribution in the enriched spectrum could be subtracted if peaks were overlapping. The ^{70,72,73}Ge(n,γ peaks were identified using the "database of prompt gamma rays from slow neutron capture for elemental analysis" published by the IAEA [1]. Figure 6.2 shows the case where a peak remains unidentified. In the upper plot the depleted spectrum is shown with an unidentified peak at 1904 keV. If the peak is due to ^{74}Ge(n,γ) a peak, represented by the pink gaussian, in the lower plot has to be subtracted from the peak area of ^{76}Ge(n,γ). The contribution if the unidentified peak is due to ^{73}Ge(n,γ) is
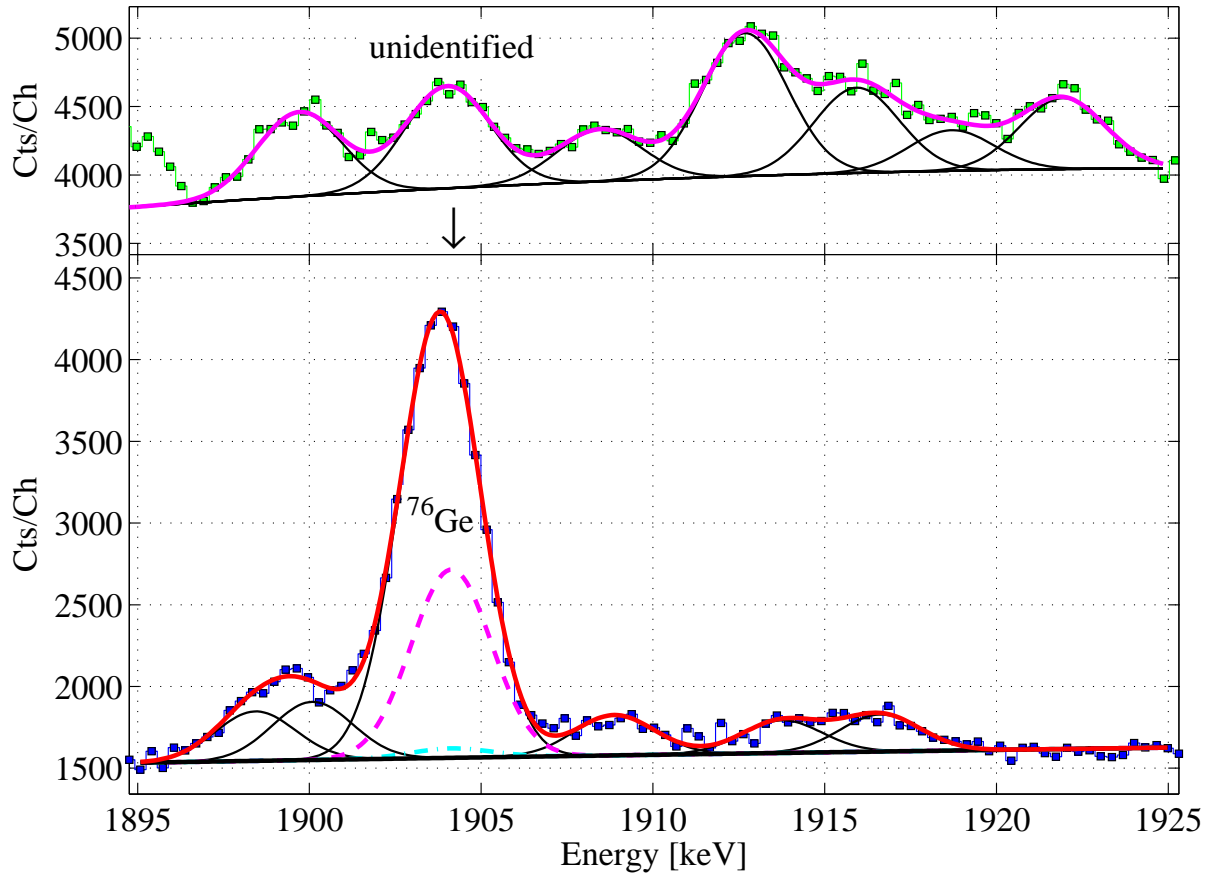
Figure 6.2: Subtraction of an unidentified peak. If the peak in the depleted (upper) spectrum is due to ^{74}Ge(n,γ) the contribution in the enriched (lower) spectrum is shown by the pink, for ^{73}Ge(n,γ) by the turquoise gaussian.

shown in turquoise. If ^{70}Ge or ^{72}Ge is the source of the line, no events are expected in the enriched spectrum. To cover all possible options, half of the potential ^{74}Ge contribution is subtracted from the ^{76}Ge(n,γ) peak. At the same time the uncertainty is increased by the same amount.

After correction for the detector efficiency the intensities were normalized to the strongest transition with $E_\gamma = 5911 \, \text{keV}$ (=100 %). The partial cross sections σ_γ were obtained relative to the partial cross section of the prompt line in gold at 247 keV. In principle a pill of GeO$_2$ should have been irradiated together with a piece of gold. Knowing their thickness and masses the intensities of the prompt γ-rays in the germanium isotopes could be related to the reference transition in gold. Due to the very different cross sections of ^{76}Ge and gold (0.0688 b : 98.65 b) the prompt spectrum would be dominated by gold only if both targets were irradiated together. Therefore the activation

was done separately. After irradiation, for each target the decay spectrum was measured. The connection between the spectra was established by the 211 keV and 367 keV line of the decay of ^{77}Ge and the 411 keV line emitted by the decay of ^{198}Au that was measured simultaneously in the cross section measurement (chapter 3). The cross sections for three lines in ^{77}Ge (159 keV, 504 keV and 862 keV) were determined relative to the 247 keV transition in gold with $\sigma_\gamma = 5.56(8)$ b [1]. The evaluation was elaborated using both detectors and the two targets employed in the previous cross section measurement (chapter 3). The results are presented in table 6.2 (top).

$$
\boxed{
\begin{array}{c|c|c}
\begin{array}{lr} ^{76}\text{Ge} & \Longleftrightarrow & ^{77}\text{Ge} \\ \text{Prompt} & & \text{Decay} \end{array}
& \Longleftrightarrow \ \begin{array}{c} ^{77}\text{Ge}/^{198}\text{Au} \\ \text{Decay/Decay} \end{array} \ \Longleftrightarrow
& \begin{array}{lr} ^{198}\text{Au} & \Longleftrightarrow & ^{197}\text{Au} \\ \text{Decay} & & \text{Prompt} \end{array}
\end{array}
}
$$

Activation	Cross section	Activation
GeO$_2$	measurement	Au
	(chapter 3)	
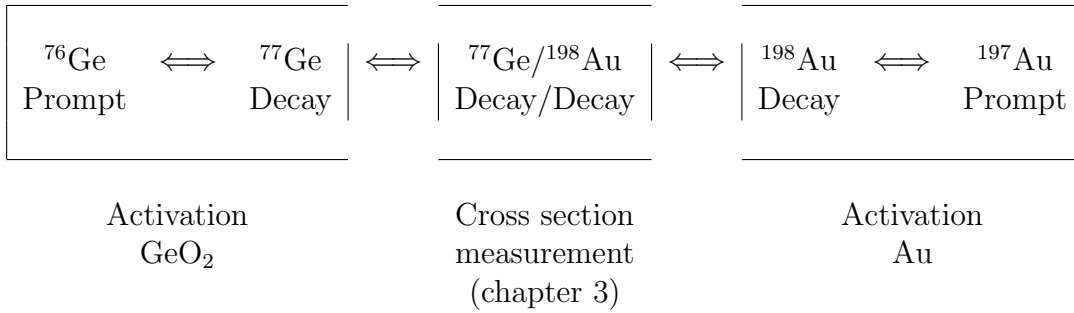
Alternatively, the partial cross sections were derived from the decay peaks of ^{77}Ge observed in the prompt spectrum. The known partial cross sections of the decay γ-rays with 211 keV and 367 keV were used to derive those of the prompt 159 keV, 504 keV and 862 keV transitions. Both detectors were used for the energies above 220 keV, for lower energies the evaluation was based only on detector II. Although transitions of the ^{77}Ge decay were used, the problem of the discrepancy in the emission probabilities discussed in chapter 3 does not play a role. With the relation $\sigma_\gamma = I_\gamma \times \sigma^t$ and eqs. 3.1 and 3.5 it can be shown that the intensity I_γ cancels out and the prompt partial cross sections are directly connected to the 411 keV reference line in gold. The results of both approaches are in good agreement and can be found in table 6.2.

Applying the renormalization factor of 0.395(15) from table 6.2 to the relative intensities in table 6.6 the partial cross sections can be calculated. Example for the 862 keV line: $\sigma_\gamma = I_\gamma \times \text{factor} = 51.4 \times 0.395 = 20.3$; $\Delta \sigma_\gamma = \sqrt{(1.8/51.4)^2 + (0.015/0.395)^2} \times 20.3 = 1.1$. To obtain the absolute intensity per 100 neutron captures the partial cross sections have to be divided by the total cross section. The cross sections were determined in [41] to be $\sigma_{tot} = (46.9 + 115) \, \text{mb} = 161.9 \, \text{mb}$. As discussed in the same paper, discrepancies in the intensities given in the literature were observed. With new emission probabilities (table 3.7) the total cross section was recalculated to be (154.9 ± 16.8) mb. The multiplication factor derived with the new value that has to be applied to the relative intensities is 0.255(30).

In similar manner the prompt approach was also used to calculate the partial cross sections of the 253 keV and 574 keV transition occurring in the ^{74}Ge(n,γ) reaction. The normalization factor to obtain the partial cross sections was determined in table 6.3 with 1.57(10). The corresponding factor for the intensity per 100 neutron captures is 0.32(4).

Table 6.2: Partial cross sections for several prompt transitions in ^{77}Ge. The upper part shows the values obtained from decay peaks observed in the prompt spectrum. The partial cross sections in the lower part were derived from a prompt spectrum of ^{76}Ge(n,γ) relative to the prompt 247 keV transition in gold. The normalization factor (ratio of the weighted mean of the partial cross sections and the relative intensities given in table 6.6) is 0.395(15). "A" and "B" denote the target used (chapter 3).

Detector	Ref. [keV]	159 [keV]	504 [keV]	862 [keV]
II	211	11.46 ± 0.78	6.75 ± 0.46	21.78 ± 1.48
	367	10.84 ± 0.62	6.38 ± 0.37	20.60 ± 1.19
I	367	-	6.53 ± 0.37	19.81 ± 1.11
Mean (decay)		$\mathbf{11.15 \pm 0.70}$	$\mathbf{6.55 \pm 0.40}$	$\mathbf{20.73 \pm 1.26}$
II A	211	11.11 ± 0.48	6.41 ± 0.27	20.73 ± 0.87
	367	11.12 ± 0.51	6.42 ± 0.29	20.75 ± 0.92
II B	211	11.51 ± 0.49	6.63 ± 0.28	21.41 ± 0.89
	367	11.65 ± 0.51	6.71 ± 0.29	21.67 ± 0.92
I A	367	-	6.59 ± 0.28	19.46 ± 0.86
I B	367	-	6.61 ± 0.28	20.00 ± 0.85
Mean (prompt)		$\mathbf{11.35 \pm 0.50}$	$\mathbf{6.56 \pm 0.29}$	$\mathbf{20.67 \pm 0.89}$
Mean (total)		$\mathbf{11.3 \pm 0.6}$	$\mathbf{6.6 \pm 0.4}$	$\mathbf{20.7 \pm 1.1}$
Rel. Int. (table 6.6)		$\mathbf{28.9 \pm 1.1}$	$\mathbf{16.7 \pm 0.6}$	$\mathbf{51.4 \pm 1.8}$
Norm. factor (ratio)		$\mathbf{0.389 \pm 0.025}$	$\mathbf{0.394 \pm 0.025}$	$\mathbf{0.403 \pm 0.025}$

Table 6.3: Partial cross sections σ_γ^p for the 253 keV and 574 keV transition in ^{76}Ge derived by the prompt approach. To obtain σ_γ^p multiply the relative intensities in table C.4 by 1.57(10). "A" and "B" denote the target used (chapter 3).

Detector	Ref. [keV]	253 [keV]	574 [keV]
II B	211	158.1 ± 8.2	79.8 ± 4.2
B	367	160.0 ± 8.3	80.8 ± 4.2
II A	211	156.0 ± 8.1	78.1 ± 4.1
A	367	152.2 ± 8.2	76.3 ± 4.2
I B	367	153.0 ± 8.2	74.3 ± 3.9
I A	367	156.6 ± 8.3	77.3 ± 4.2
Mean (prompt)		**156 ± 9**	**78 ± 5**
Rel. Int. (table 6.8)		**100**	**49.5 ± 1.7**
Norm. factor (ratio)		**1.56 ± 0.09**	**1.58 ± 0.10**

6.2 Data taking of coincidence spectra

6.2.1 Setup

For the coincidence measurement the standard PGAA setup with two HPGe detectors was used. The neutron flux at the target position was $1.48 \times 10^9 \, \mathrm{n}_{th}/(\mathrm{cm}^2 \, \mathrm{s})$ and again the target chamber was evacuated to avoid background by neutron reactions in air. GeO$_2$ powder was used as a target, which is isotopically enriched in ^{76}Ge with a mass of $m = 304.1 \, \mathrm{mg}$.

In the following paragraphs the data acquisition, the applied cuts and the analysis of the coincidence spectra are discussed in detail. To continue with the results of the prompt measurements please go to sect. 6.3 "Results".

6.2.2 Data acquisition

For the data acquisition (DAQ) a combination of NIM and VME modules was utilized. For the trigger logic and the signal amplification the NIM standard was used, while the analog to digital conversion and the communication with the PC was realized with VME modules. A schematic view of the circuit and the module types used can be found in fig. 6.3.

Both detector preamplifiers provide two identical signal outputs. One of them was used for the trigger logic. After amplification and shaping by a fast filter amplifier (FFA) the timing information of the event was obtained by a constant fraction discriminator (CF). The logic signal was delayed and adapted in width using discriminators. The delay was adjusted in the way that the logic pulses from detector I arrived later at the coincidence
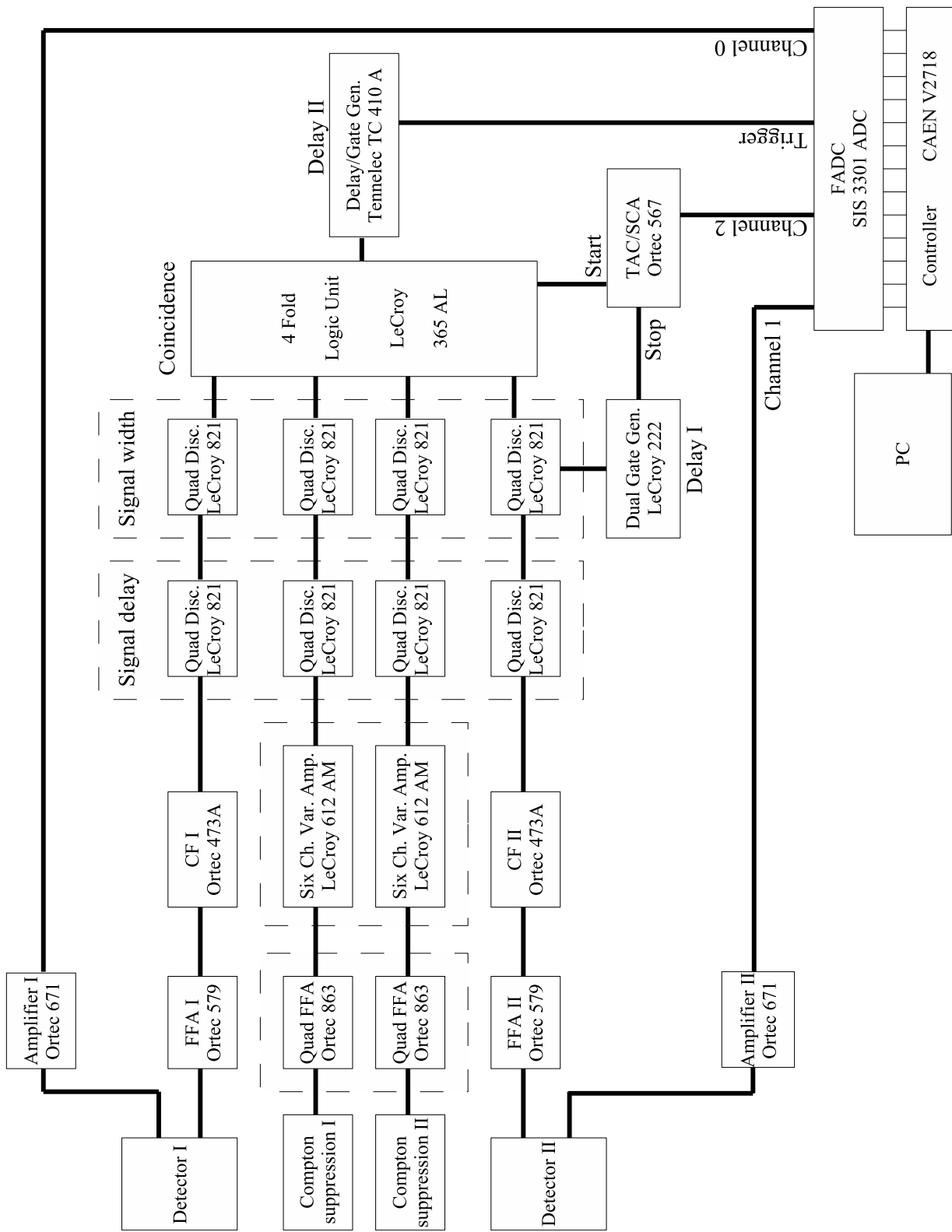
Figure 6.3: Scheme of the electronic circuit used for the coincidence measurement. Dashed rectangles indicate modules used for more than one channel.
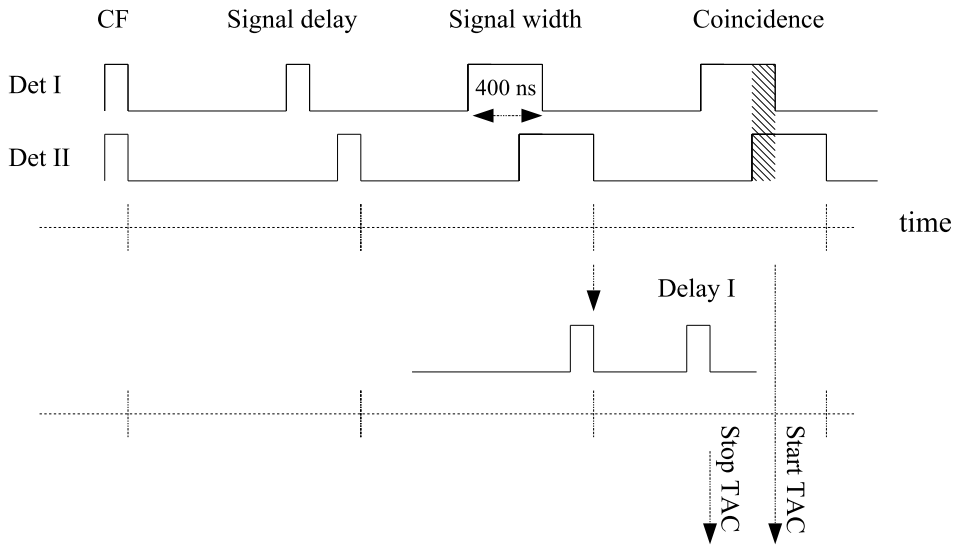
Figure 6.4: Logic pulses for the coincidence trigger and TAC start/stop.

unit (4-fold) than those from detector II if the events were in true coincidence (fig. 6.4). The coincidence window was set to a width of 400 ns. If the coincidence condition was met, a start signal was sent to the time to analog converter (TAC). Delaying the pulse of detector I, the time of the start signal corresponds always to the time of this pulse. The stop signal for the TAC was created by the second discriminator used to adjust the width of the signal from detector II. To prevent the stop signal reaching the TAC earlier than the start signal, it was delayed by a gate generator. The TAC created an analog pulse, whose height was proportional to the time difference between events in the two detectors.

The signals of the Compton suppression system were implemented at the 4 fold logic unit in the anti-coincidence mode.

The pulse used as start signal for the TAC was sent also to a delay/gate generator to trigger the FADC. The controller used to run the FADC was connected to a PC by an optical link.

The maximum length of the traces that can be recorded by the 14-bit FADC (Struck SIS 3301) is 1311 μs. To reduce traffic between the FADC and the PC the trace was divided into 32 sections (41 μs), each containing one coincident event. As soon as the memory was full the data were transferred to the PC, meanwhile a second memory in the FADC of the same capacity was available.

Three of the eight channels of the FADC were used. Channel 0 and Channel 1 were fed by spectroscopy amplifiers of detector I and detector II, respectively. Channel 2 recorded the output of the TAC.

The DAQ software[1] determined the pulse heights by subtracting the baseline from the maximum of the trace. The values for the pulse heights and baselines of the three channels were written to file together with the corresponding time stamp.

Since the highest relevant energy in the spectra is 6505 keV (S_n of ^{74}Ge(n,γ)) the gain of the amplifiers was adjusted to cover this range.

6.2.3 Measurement

The pulse rate of a single detector was in the order of ~ 4000 counts per second without Compton suppression. Assuming that each photon has exactly one other photon in coincidence and the detector efficiency is about $\epsilon \sim 10^{-4}$ (sect. 2.3.3), a rough estimation of the resulting count rate for true coincident events in the second detector gives about 0.4 Hz (compare to table 6.5). Higher rates could have been accomplished using a larger target mass or a higher neutron flux. Both options imply a higher signal rate in the detectors, increasing the number of overlapping signals and decreasing the energy resolution because of incomplete baseline restoration. An enhanced detector efficiency realized by a larger diameter of the collimators was tested but the gain in statistics was compensated by the additional background.

The target was irradiated for 8.26 days ($\hat{=}$ 713 790 s), interrupted only by short beam shut downs to refill the dewars of the detectors with liquid nitrogen. Because of varying electronic noise the threshold of the CF discriminators was increased on the fifth day of measurement. A small decrease in the count rate due to the change of the threshold can be seen in fig. 6.5. This threshold limits the spectra to energies above 100 keV.

The two energy spectra and the spectrum of time differences using all recorded data are shown in fig. 6.6. The time resolution achieved in this measurement was about 20 ns (FWHM). The probability for pile up peaks in the spectra is negligible because of the very low detector efficiency. Due to the small rate and the two memories of the FADC the dead time is assumed to be zero, except for the periods with increased rate because of electronic noise.

6.2.4 Selection of data

Checking the two energy spectra during the experiment no eye-catching artifacts were observed, while the time spectrum showed a clear artifact at maximum time differences and a bump on the right side of the coincidence peak (around channel 5000). Since the electronic noise was not constant for the whole time of measurement the rate of recorded data is time dependent. In fig. 6.5 the rate of events is shown with a binning of 1800 s. The black line represents the complete set of taken data. In several periods the rate increased massively. The majority of these peaks vanish if proper cuts in the energy and

---

[1] The software for the DAQ was based on a program written by F. Ritter.
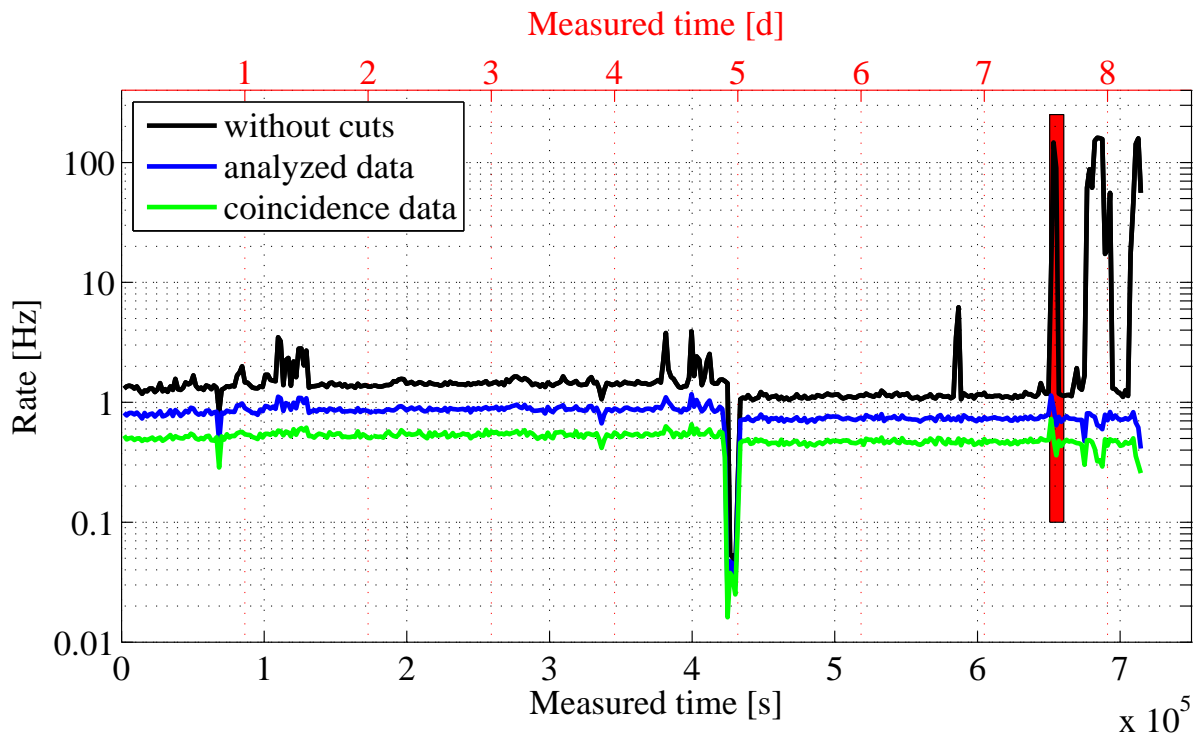
Figure 6.5: Rate of coincident events during the measurement. The raw data (black) show peaks caused by electronic noise that can be suppressed applying different cuts (blue, green). The corresponding cuts can be found in table 6.5. The remaining dips are due to neutron beam shut downs for testing and refilling of nitrogen in the dewars. For analysis only data left from the red bar ($t = 650\,986\,\mathrm{s}$) were taken into account. The bin width is $1800\,\mathrm{s}$.
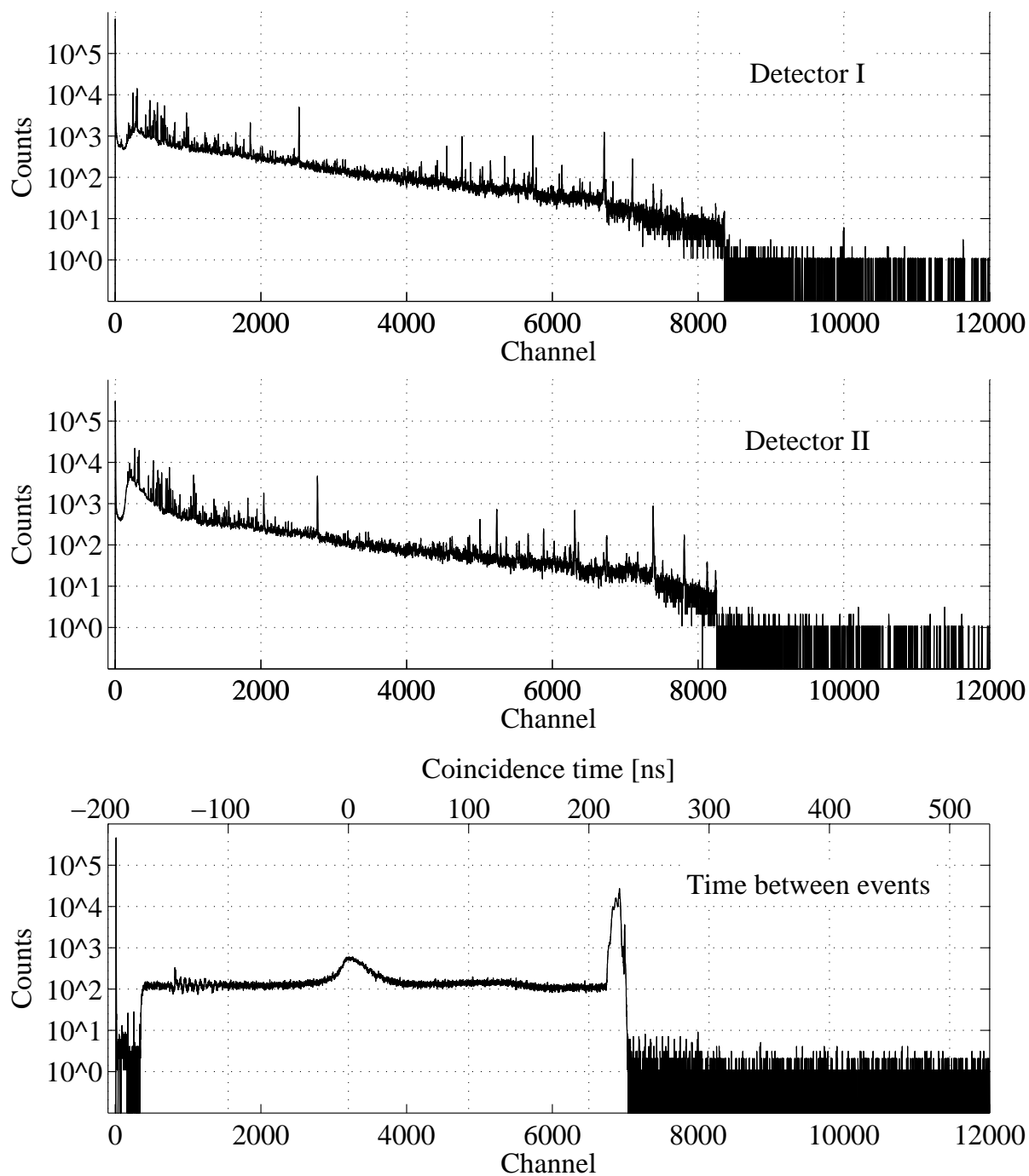
Figure 6.6: The upper two plots show the spectra recorded with detector I and II. The lower spectrum shows the time differences between events in the two detectors. The peak at "coincidence time" $= 0$ ns is due to real coincidences, the flat component arises from random coincidences.

65

the timing spectra were set. For low energies (below channel 100) a cut is applied to suppress electronic noise. Energies higher than channel 8000 are treated as out of range and cut away as well. In the timing spectrum only events between channel 1500 and 5500 were used for the analysis (blue line). Almost no peaks in the rate can be seen any more when the range is reduced to channel 2400 - 4200 (green line). Small dips occur due to beam shut downs to refill the dewars. The lower count rate in these dips has no effect on the energy spectrum, therefore these periodes were used as well.

At the end of the measurement the raw data show temporary increases of more than a factor 100. At the same time periods the count rate suffers a decrease if the cuts are applied. It seems that the maximum traffic of the optical link to the FADC was reached and real events were missed because of dead time due to data transfer. To avoid any influence of these massive rate changes only data to the left of the red bar ($t = 650\,986\,\mathrm{s}$, fig. 6.5) are considered for the analysis.

In the following the restriction in the energy spectra to channels 100 - 8000 is called cut "A". Six different cuts in the time spectrum ("B1 - 6") were tested for good statistics and low background due to random coincidences (table 6.4). The number and rate of true and random coincidences resulting from these cuts can be found in the appendix (B.1). The amount of random coincidences below the peak of true coincidences was determined evaluating the flat regions beside the peak (channels 1500 - 2400 and 4200 - 5500) named "R" (fig. 6.7). After normalization to the width of the cuts this value was subtracted from the measured events in the peak area resulting in the number of true coincidences. The

Table 6.4: Cuts used for the analysis. If the complete time range was used the data are marked with "c".

Cut	data	Range [channel]	Comments
A	energy spectra	100 - 8 000	
B1	timing spectrum	1 500 - 5 500	
B2	timing spectrum	2 400 - 4 200	true coincidences
B3	timing spectrum	3 043 - 3 560	
B4	timing spectrum	3 107 - 3 446	
B5	timing spectrum	3 144 - 3 351	
B6	timing spectrum	3 196 - 3 248	
c	measured time	0 - 713 790 s	total period
		0 - 650 986 s	analyzed period
R	timing spectrum	1 500 - 2 400	random coincidences
		4 200 - 5 500	random coincidences
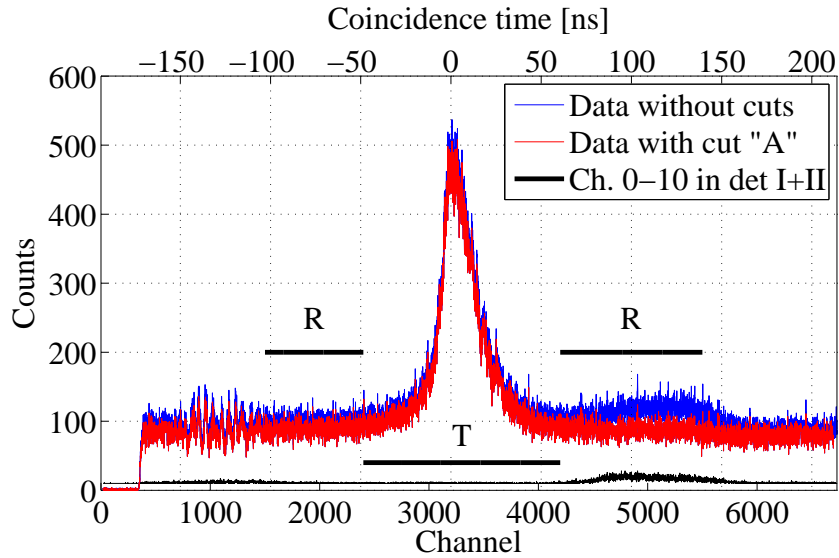
Figure 6.7: Time spectrum with cut "A" and without cuts on the energy spectra. The bump right of the coincidence peak disappears setting cut "A". If only channels 0 - 10 are selected in detector I+II the bump is reproduced (plotted with offset of 10 counts/ch.). Hence it corresponds to events with no signal in both detectors.

ratio between true and random coincidences becomes better for the narrow regions while the statistics become worse. Cut "AB2" was found to be a good compromise between the need for a sufficient amount of events in the peaks and low background due to random coincidences. Region "AB2" together with "R" is consistent with "AB1", called "analyzed region" (table 6.5).

A closer look at the energy spectra show, that the peaks in detector II have a rather bad energy resolution at high energies, while low energies are not strongly affected. It was found that the resolution was declined by drifting as shown in fig. 6.8. The bad energy resolution at high energies is no serious problem, because of the small peak density in this region. Detector I did not drift significantly (fig. 6.9).

The bump in the time spectrum described earlier disappears as soon as cut "A" was applied to the energy spectra (fig. 6.7) Furthermore it can be shown that the artefact at maximum time differences in fig. 6.6 arises during the last two days. Obviously this artifact corresponds to the increase of the rate seen in fig. 6.5. These data were excluded by reducing the time range.
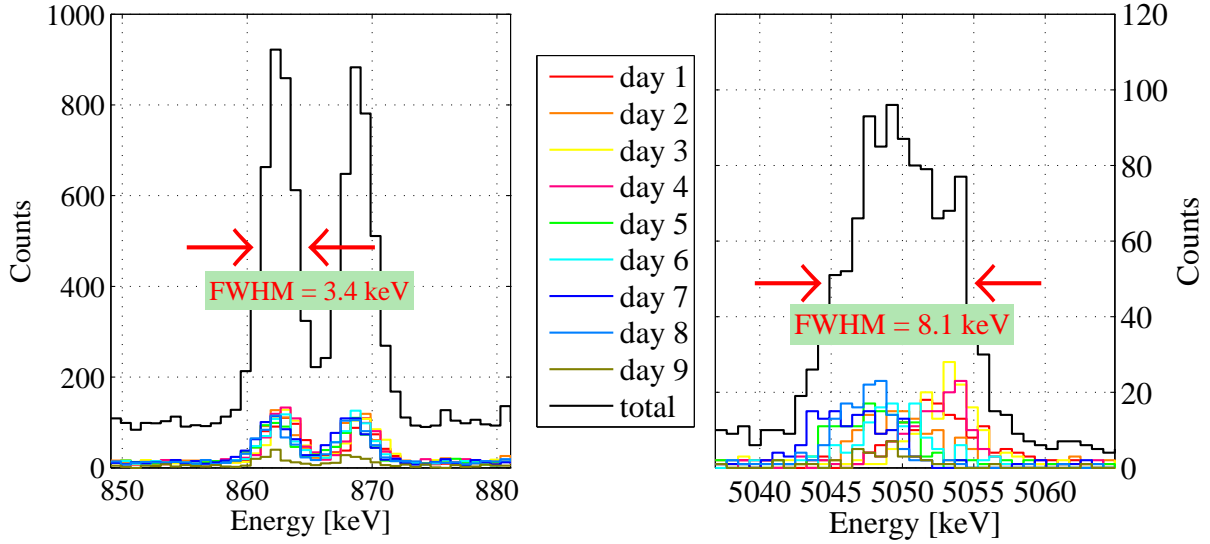
Figure 6.8: Energy drift of detector II for the peaks at 861 keV and 5049 keV. Each spectrum represents a time interval of 86 400 s. Cuts: "AB1c".
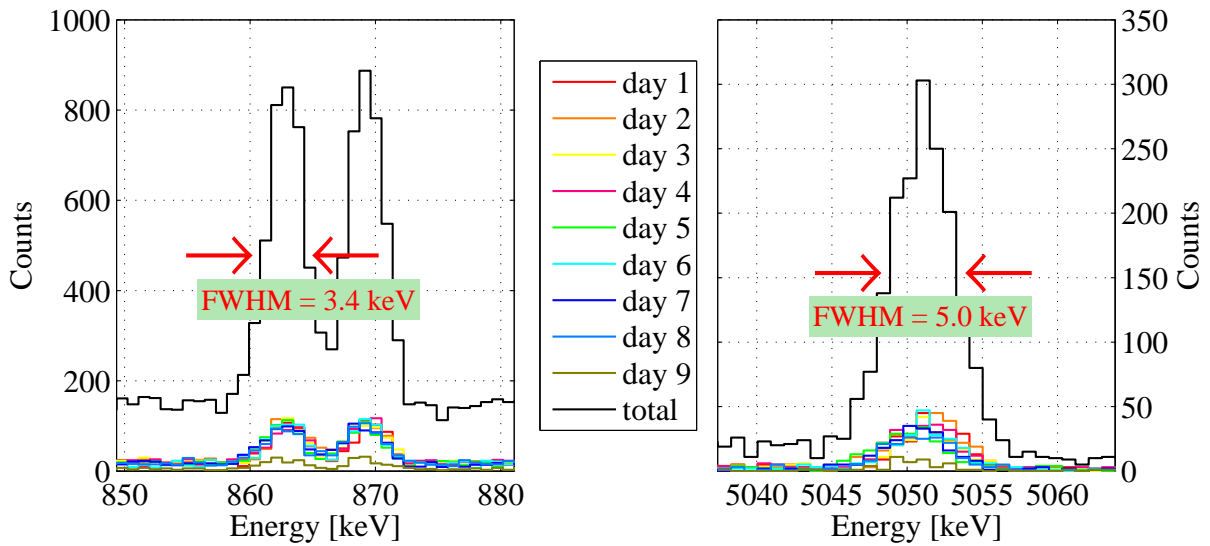
Figure 6.9: Energy drift of detector I for the peaks at 861 keV and 5049 keV. Each spectrum represents a time interval of 86 400 s. Cuts: "AB1c".

Table 6.5: Number of events after applying different cuts. The rate in the first raw contains also triggers on electronic noise and should not be used to obtain the coincident signal rate.

Data	time [s]	Number of events	Rate [Hz]
All data "c"	713 790	3 807 275	5.3339
Only time cut	650 986	875 963	1.3456
Analyzed region "AB1"	650 986	509 918	0.7833
Coincidence region "AB2"	650 986	316 223	0.4857

6.2.5 Analysis

Picking one peak in the energy spectrum of *e.g.* detector I the corresponding coincidence spectrum in detector II was generated applying cut "AB2". This spectrum was then searched for significant peaks. An example of a coincidence spectrum for the 392 keV line is shown in fig. 6.10. This particular spectrum shows a peak at 5050 keV and some more at energies of few hundred keV. To determine which of these peaks has a significant coincidence with the 392 keV line the background has to be calculated quantitatively. The peak in the spectrum of detector I sits usually on a flat Compton plateau (fig. 6.11). The Compton plateau can be divided into two layers. One part of it results from true coincidences that deposit energy by Compton scattering (green), the other part arises from Compton scattering in a random coincidence (red area). The peak in detector I contains besides true coincidences also background produced by random coincidences (indicated by the red Gaussian). So, only the counts between the blue curve and the red line (hatched area) are due to coincident photo absorptions.

From the data themselves it is impossible to identify whether an event corresponds to the peak area or the background below the peak. That means, that the spectra of detector II are "contaminated" by background. One has to account for this statistically. Figure 6.12 gives an example how the background was subtracted from the events measured. In the true coincidence spectrum (blue, cut "AB2") the channels representing the peak (colored bars) were summed up. The same was done for the spectrum created from random coincidences (red) using cut "R". The rectangular red area represents the "random Compton" and the red peak the "random peak" events. The number of "coincident Compton" events (green) was determined by the difference of the area below the plateau (blue) and the red rectangle from randoms.

When the three types of background contributions in detector I were determined quantitatively their influence on the spectrum in detector II was calculated. The background of "random" origin (Compton and peak) was obtained by normalizing the spectrum of ran-
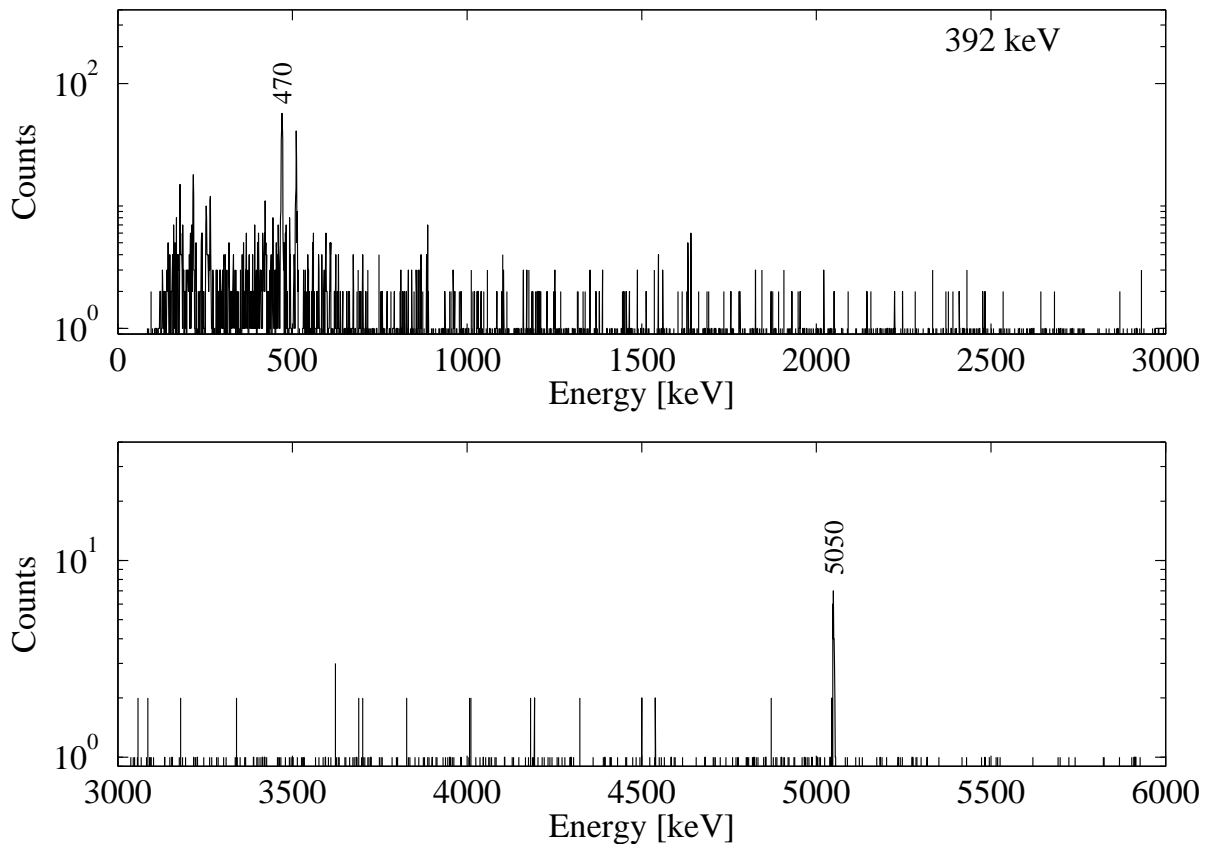
Figure 6.10: Spectrum of events coincident with the 392 keV line.

dom background (cut "R") for detector II to the corresponding number of random events. The "coincidence Compton" events are assumed to produce a spectrum like the spectrum obtained for true coincidences in the second detector. This approximation works well for peaks with low energies in detector I but not very accurately for higher energies. At low energies all peaks contribute to the background by Compton scattering, while at high energies only few peaks above the treated peak contribute. But, since the background at high energies is very low, this approximation was used over the whole energy range.

The spectrum obtained for detector II suffers of Compton background as well. True coincident events in detector I may have a partner in detector II that is Compton scattered, *i.e.* produces a flat distribution. To estimate this part quantitatively the "coincidence Compton" contribution of detector II (analog to the green area in detector I) was determined. Normalizing the spectrum in detector I to this value the number of counts in the true coincidence peak give the background by Compton scattering. This correction has to be calculated for each peak in detector II separately.
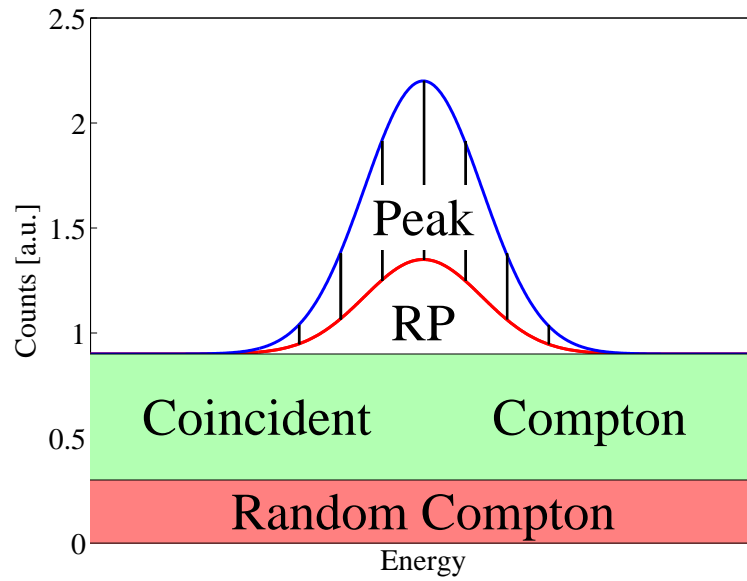
Figure 6.11: Schematic view of the background composition, RP denotes "random peak".
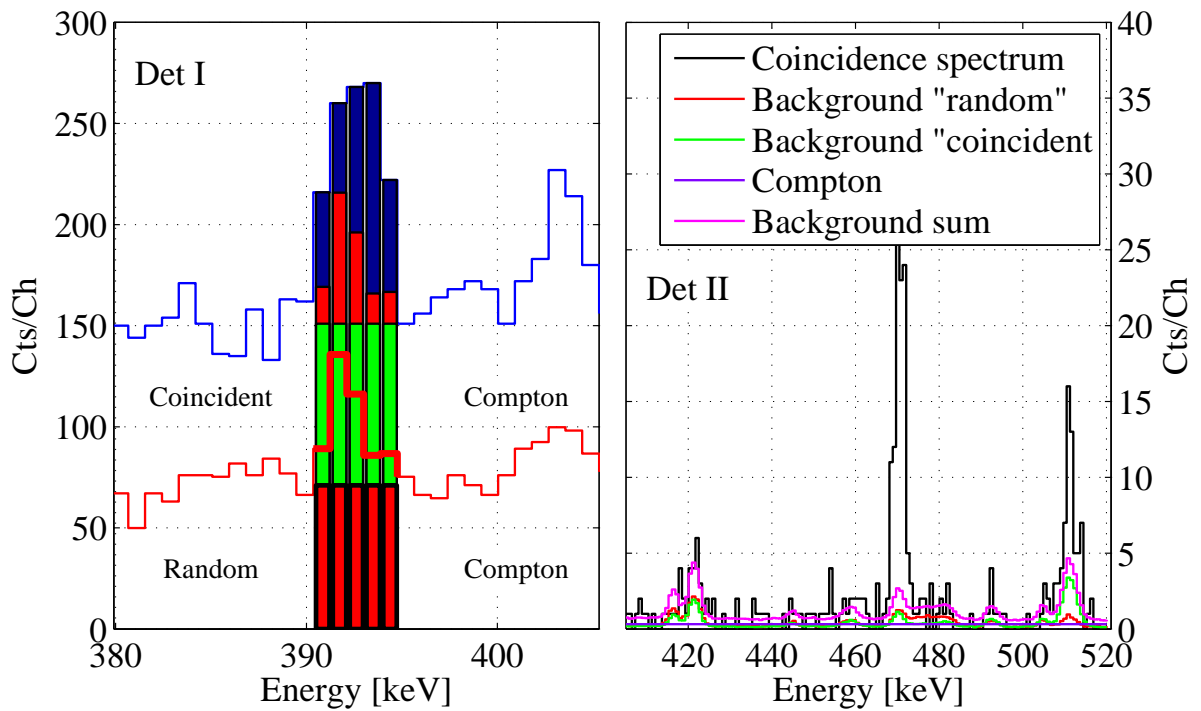
Figure 6.12: Quantitative determination of the background in coincidence spectra. The left side presents the region selected for analysis in detector I with the different background contributions. The right side shows the corresponding background in detector II.
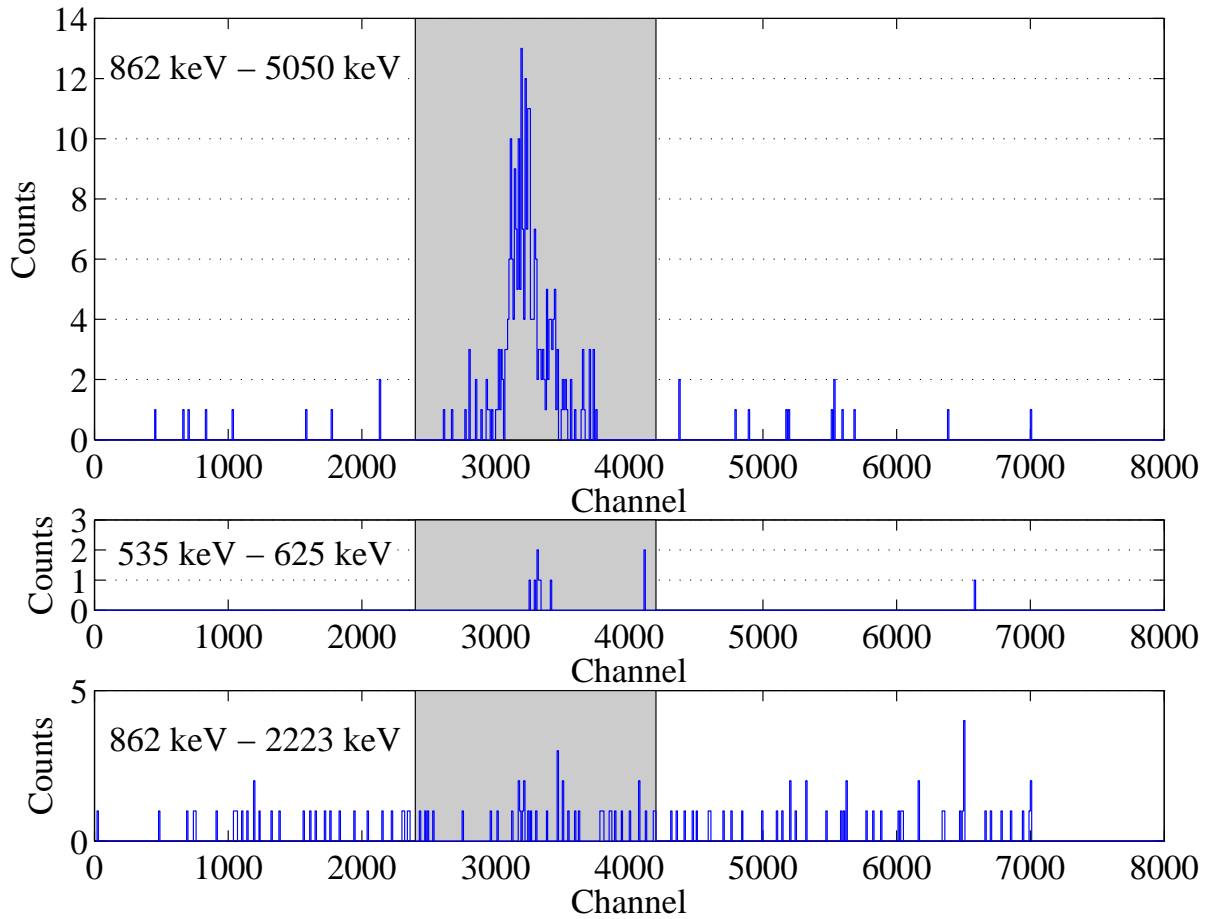
Figure 6.13: Time spectrum for three coincidence pairs. The transitions in the upper two plots are in coincidence, almost all events are within the window for true coincidences. In the lower plot the events are more equally distributed, hence it is dominated by random coincidences.

The background that has to be subtracted is very low. A good illustration is given in fig. 6.13 showing the timing spectrum if two peaks are checked for coincidence. In both energy spectra a peak was selected and the corresponding time spectrum plotted. For strong coincidences (top: 862 keV - 5050 keV) almost all events ($> 90\%$) are in the region "B2", even though it covers only about 26% of the channels (0 - 7000). The same was obtained for the 535 keV - 625 keV pair, only one random event was found, all other counts are in the coincidence window. In contrary the independent 862 keV and 2223 keV (H(n,γ)D) peaks have a rather equal distribution over the whole range in the time spectrum. The small enhancement in region "B2" can be explained by coincident Compton events in the flat background below the peaks.

Because of the small count rate most of the peaks in the second detector contain a relatively small number of events (fig. 6.14). Zooming into the spectrum one can see that the background is very low as well (fig. 6.15) and the significance of these peaks is good enough for an unambiguous identification of coincidence. For the spectra created with cut "AB2" a confidence level of $2\,\sigma$ was required to verify their simultaneous occurrence.

In most decays more than two transitions take part to emit the excess energy of 6072 keV. To establish a decay chain all partners were needed to be in coincidence with each other with a C.L. of $2\,\sigma$. To be defined as a branch of an existing decay chain a connection with at least one peak of this chain was required. Since the angular correlation might suppress some coincidences, some transitions could only related to an already established decay path. An example is given in fig. 6.16. The coincidence between 4008 - 1558 - 505 and 1558 - 279 - 224 transitions was well established with the required significance. But there is no significant connection between 4008 and 279 - 224. In this case the 1558 transition, coincident with both was used as link and 279 - 224 could be included in the decay scheme.

An additional check provides the analysis of the ratio between the numbers of true and random coincidences for different cuts. An example is given in fig. 6.17. Selecting the 5050 keV peak in one detector the counts obtained for the six cuts ("AB1 - 6") for the 862 keV peak in the other detector (blue line) are compared with the expected background events (black line). The red curve represents the true coincidences, *i.e.* the black curve subtracted from the blue one. The X-axis is normalized to the peak area in the time spectrum (table B.1). Therefore, coincident peaks should result in a straight line (blue curve) as it can be seen for 862 keV. If a tested peak is not of the same cascade and contains only random coincidences the blue curve show a significantly different behavior. The red curve is then compatible with zero.
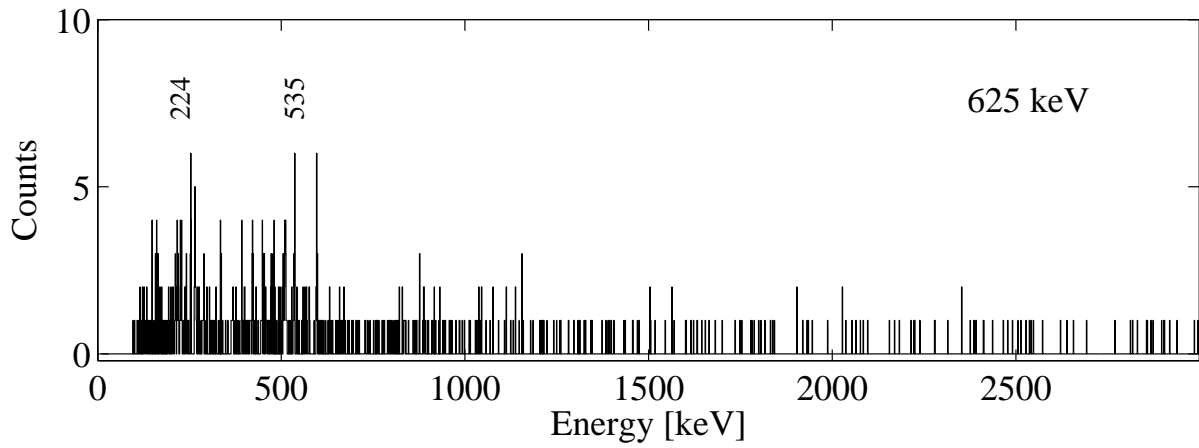
Figure 6.14: Example for coincidence spectra of low intensity.
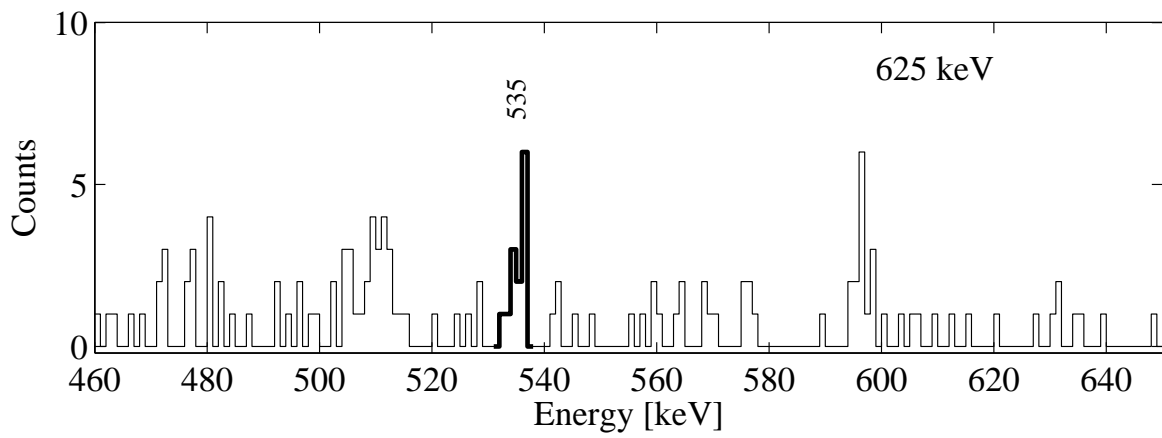
Figure 6.15: Zoom into the spectrum in coincidence with the 625 keV peak. The peak at 535 keV is in true coincidence, the other the lines (511 keV and 595 keV) fit in the estimated background.

6071

4008

2063

1904
1642
1571

1558

505

505

279

224

^{77}Ge
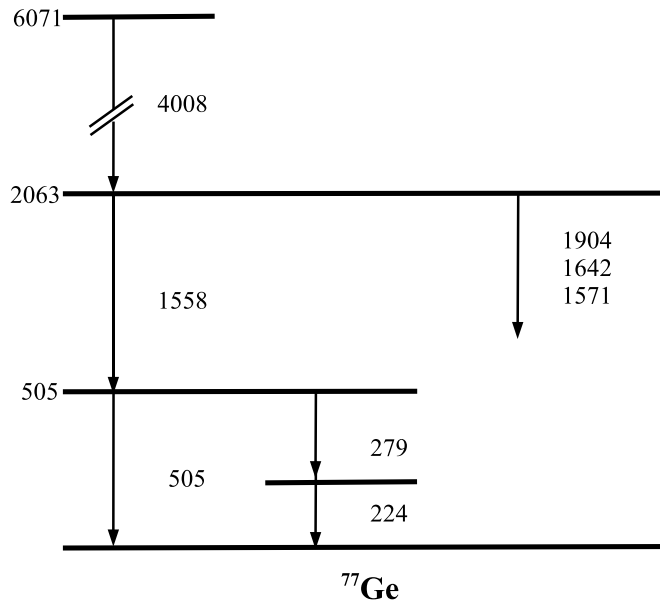
Figure 6.16: Decay branches following the 4008 keV transition.
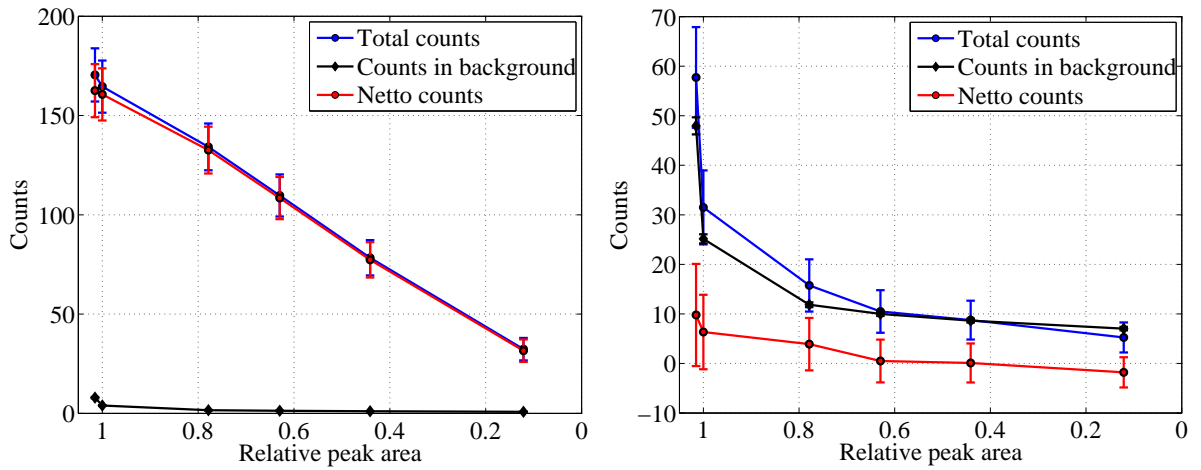
Figure 6.17: Determination of coincidences by count ratios. The number of counts plotted agains the relative peak area (defined as ratio of true coincidences with cut "ABx"/"AB2", table B.1) gives a straight line if two peaks are in coincidence. Left: Peak at 862 keV in detector II coincident with peak at 5050 keV in detector I. Right: Hydrogen peak at 2223 keV in detector II coincident with peak at 862 keV in detector I. Since this transition has no coincidences at all, the shape of the blue curve is typical for events of pure random coincidence.

6.3 Results

In this section an overview of the results of the prompt γ-ray measurements including the transition energies and intensities is given. The energies and intensities were determined from the single spectra, while the level information was derived from the coincidence data. A collection of γ-rays of special interest are discussed in more detail. In the last subsection the consequences of these results on the GERDA experiment are studied.

6.3.1 ^{76}Ge(n,γ)

119 of the γ-ray lines found could be assigned to the ^{76}Ge(n,γ) reaction, 84 of them were placed into the level scheme, including 21 placements done according to other experiments (^{76}Ge(^{13}C,^{12}C)^{77}Ge [28] or β-decay of ^{77}Ga [19]). All peaks with a relative intensity above 10 % and those discussed in this section are presented in table 6.6; the complete list of transitions is given in the appendix (table C.2). The level scheme was reconstructed using the information from the coincidence measurement. Unless otherwise noted in these tables, a transition was placed in the level scheme only if the complete path from the capture state to the ground state or the isomeric state could be reconstructed with 2 σ C.L.. If a coincidence with a transition that is not part of an established decay path was observed, the energy of this coincident line is shown in the third column. Some transitions only could be placed into the decay scheme using information from other reactions. For transitions marked with "a" or "b" the reference was used only for the placement into the level scheme, while in cases "c" and "d" the transition was identified unambiguously as ^{76}Ge(n,γ) with the help of the reference. Lines marked with "e" were placed tentatively by energy. The sequence of the 2783 keV and 2785 keV lines could not be clarified ("f").

Table C.3 shows the level energies and the corresponding transitions depopulating the state. The level energies were calculated by weighted means with γ-ray energies corrected for recoil. Transitions whose placement in the scheme was suggested by energy ("e") were not used for this purpose. Since the 1901 keV and 2119 keV levels are depopulated only by the tentatively placed 1697 keV and 1741 keV transitions, these energies had to be used to derive the level energies. The depopulating intensities I_{dep} are compared with the populating ones I_{pop}, giving a hint for missing intensity. The neutron binding energy was determined to be 6071.29(5) keV, about 1 keV less than the values found in previous measurements (table 6.7).

Because of the lack of a good energy calibration below 100 keV the energy for the 83.5 keV line was adopted from Kay *et al.* [28]. As expected, no direct transition from the capture state ($S_n = 6071$ keV) with a spin configuration of $J^\pi = +1/2$ to the ground state with a spin of $J^\pi = +7/2$ was observed.

Similar to ref. [28], we also could not observe the 581 keV level given in [19]. The 420.9 keV transition claimed to deexcite this level to the isomeric state is identical to

Table 6.6: Selection of the most important prompt γ-rays after neutron capture on ^{76}Ge. The uncertainty of the measured γ-ray energy E_γ contains a systematic contribution of 0.10 keV added quadratically. The relative intensity was normalized to the strongest transition at 5911 keV (100%). To obtain the partial cross section in mbarn multiply the relative intensity by 0.395(15), for the absolute intensity by 0.255(30).

E_γ [keV]	Relative intensity	Coincident transitions [keV]	E_i [keV]	E_f [keV]	Comments
83.5	6.12(23)		505	421	a,b, energy by [28]
159.62(10)	28.9(11)		160	0	$t_{1/2} = 52.9\,$s
197.17(33)	1.25(7)	421	619	421	a
421.34(10)	60.9(21)		421	0	
459.15(10)	13.2(6)		619	160	
469.99(10)	34.3(12)	755, 2684	630	160	
504.79(10)	16.7(6)		505	0	
618.86(24)	1.64(15)		619	0	
831.22(10)	11.1(5)	445	1879	1048	
861.82(15)	51.4(18)		1021	160	
888.34(15)	15.1(6)	1147	1048	160	
893.15(11)	1.21(5)	492	1385	492	a
1242.24(18)	2.4(4)		1664	421	
1249.43(18)	10.7(5)		1879	630	
1457.84(10)	17.3(7)		1879	421	
1697.40(12)	1.08(6)	421	2119	421	e
1741.35(11)	1.52(7)		1901	160	e
2026.37(14)	0.55(4)				
2029.60(11)	1.44(8)				
2035.48(13)	1.07(10)		2195	160	
2782.91(11)	3.00(12)		3287	504	f
2785.11(15)	1.30(14)		6071	3287	f
4007.96(10)	21.0(15)		6071	2063	
4192.00(20)	38.5(12)		6071	1879	
5049.69(10)	56.0(23)		6071	1021	
5911.33(10)	100.0		6071	160	

a) Placement in level scheme according to [28]
b) Placement in level scheme according to [19]
c) Identification based on [28]
d) Identification based on [19]
e) Placement in level scheme suggested by energy
f) Sequence of transitions unclear

Table 6.7: Binding energy of the neutron in ^{77}Ge and ^{75}Ge. The result of this work is compared to values from other measurements.

| | Binding energy [keV] | | | |
	Q-value calculator [4]	Groshev *et al.* [24]	Islam *et al.* [27]	This work
^{77}Ge	6072.3 ± 2.37	6072.7 ± 1.3	-	6071.29 ± 0.05
^{75}Ge	6505.31 ± 2.31	6505.9 ± 1.1	6505.26 ± 0.08	6505.84 ± 0.05

the 421.3 keV line to the ground state in our work. The transitions assumed to populate the 581 keV level (196.7 keV, 1242.3 keV) are shifted downwards in our level scheme by 159.7 keV. Accordingly, no levels at 778 keV (shifted to 618 keV) and 1823.3 keV (1663 kev) exist. No evidence for the third transition supposed to feed the 581 keV level (242.6 keV) was found.

In ref. [24] prompt peaks at 808.2 and 850.8 keV were reported. Our analysis assigns the lower line to a transition in ^{74}Ge while at 850 keV no significant peak could be observed. No evidence was found for the 4514.3 keV peak stated in the same work.

The 831 keV line shows coincidences with the 445 keV peak, assigned to ^{74}Ge(n,γ). Whether this is a hint for a contribution of ^{74}Ge(n,γ) in 831 keV or of ^{76}Ge(n,γ) in 445 keV is not clear.

The origin of the peak at 5420.1 keV reported by [25] could not be clarified. The peak is a multiplet of at least two peaks. One of them has its origin in the single escape peak of 5930 keV (^{74}Ge(n,γ)). The other one could not be assigned unambiguously to ^{76}Ge.

Comparing the results of Kay *et al.* (table 5.3) with those from this work a very good agreement in the measured transition energies was found. The branching of the γ-rays depopulating the different levels match within the errorbars except the 197 keV, 618 keV and 893 keV line. While for the first two the difference amounts a factor of two, the latter is one order of magnitude higher in our measurement. One possible explanation could be that the 893 keV consists of two different transitions, one of them does not occur after the ^{76}Ge(^{13}C,^{12}C) reaction.

To estimate how much of the emitted energy was detected, the energy weighted intensities have to be summed up and normalized to the total expected emissions with

$$v = \frac{\sum E_i \sigma_i}{S_n \sigma_{tot}} = \frac{\sum E_i I_i}{S_n}. \tag{6.1}$$

Taking into account all transitions presented in table C.2, a fraction of $v = 65.5\,\%$ was detected, a value much higher than the old one (10.6 %, sect. 1.3.2). But this improvement is mostly due to the new intensities derived in this work. If the old lines (only those that were confirmed by our measurement) are weighted with the new intensities a v of

49.7 % is calculated, 43.6 % of this value are contributed by the strongest three lines. This illustrates that the effort needed to push v to even higher values will increase drastically.

6.3.2 ^{74}Ge(n,γ)

Different from ^{76}Ge, ^{74}Ge is present in the isotopic composition of both targets. The peaks due to ^{74}Ge(n,γ) have a constant ratio in the two spectra, but it can be shifted by overlying peaks from ^{70,72,73}Ge in the depleted spectrum and from ^{73,76}Ge in the enriched one. Therefore the identification of new ^{74}Ge(n,γ) peaks was based only on the coincidence measurement because it refers new lines to well established ones, although this strong requirement limited the discovery potential of new lines. Additionally, transitions given in [20] were confirmed if besides the correct peak position the population of the initial level was shown by the coincidence measurement. Following these rules 68 peaks were assigned to the prompt radiation in ^{75}Ge (tables 6.8 and C.4), 32 of them were not observed before in the neutron capture reaction (compare to table A.3). Most of these transitions were observed in other reactions like ^{75}Ga decay (table A.1) or (d,pγ) on ^{74}Ge before. Six peaks are reported for the first time (648 keV, 1496 keV, 1607 keV, 1873 keV, 2091 keV and 2119 keV).

The coincidence data show, that three of these transitions (1496 keV, 1873 keV and 2119 keV) populate the 192 keV level. The sum of all intensities populating this state exceeds the depopulation strength by more than a factor of 3 (table C.5). No hint for the missing intensity was found. In ref. [20] a line with an energy of 2089.7 keV is reported (table A.3), still, the placement in the level scheme is different to the 2091.2 keV line measured here.

From literature three transitions around 444 keV are known [20], but in the measured spectra only two lines were resolved with energies of 443.5 keV ($I_{rel} = 1.22(9)$) and 444.9 keV ($I_{rel} = 16.0(6)$). The observed coincidences (177 keV, 204 keV and 1285 keV) are in agreement with the literature, but the correct distribution of the intensities and the exact energies of the three peaks remain unclear.

The transitions at 4415 keV and 4440 keV differ almost by 4 keV from the position given in [20] (4410.6 keV and 4436.4 keV respectively), but since their intensity ratio and their distance are in good agreement to each other they are believed to be the same two lines.

The 5420 keV line that was assignedd by Hasselgren [25] to ^{76}Ge(n,γ) and ^{74}Ge(n,γ) could not be confirmed. The intensity of the peak at this position is compatible with the expected single escape (SE) contribution from the 5931 keV transition. Also the weak 4012 keV line that is overlapped by the very strong 4008 keV peak could not be verified. All other lines above 4 MeV reported in ref. [20] were observed in this work as well.

The intensities derived are in good agreement with the values of Islam *et al.* [27] for most of the transitions. Only the 4817 keV peak differs significantly. Our value is

Table 6.8: Selection of the most important prompt γ-rays after neutron capture on ^{74}Ge. The uncertainty of the measured γ-ray energy E_γ contains a systematic contribution of 0.10 keV added quadratically. The relative intensity was normalized to the strongest transition at 253 keV (100 %). To obtain the partial cross section in mbarn multiply the relative intensity by 1.57(10), for the absolute intensity by 0.32(4).

E_γ [keV]	Relative intensity	Coincident transitions [keV]	E_i [keV]	E_f [keV]	Comments
52.5	10.8(6)		192	140	h, energy by [20]
124.75(11)	2.12(10)		316	192	h
			886	762	h
139.81(10)	35.8(10)		140	0	
177.29(11)	20.2(7)		317	140	
253.01(10)	100.		253	0	
443.48(11)	1.22(9)	1285	583	140	g,i
444.95(10)	16.0(6)	177	762	317	g,i
		204	901	457	g,i
457.24(10)	12.0(4)	1045	457	0	g
481.71(10)	15.0(4)		674	192	
574.98(10)	49.5(17)		575	0	
647.67(11)	3.14(13)	25			
1223.33(10)	11.5(4)		1798	575	
1495.98(11)	4.63(19)		1688	192	
1606.82(40)	0.96(17)		2066	457	
1873.27(15)	6.6(7)		2066	192	
2091.21(15)	4.6(9)		2091	0	
2119.42(16)	5.4(10)		2312	192	f
4414.54(11)	7.70(28)	253	6506	2091	
4439.95(11)	10.3(4)		6506	2066	
4817.46(14)	3.25(30)		6506	1688	
5089.21(11)	14.5(6)		6506	1415	
5743.20(41)	3.4(6)		6506	762	e, overlap with 6252(SE)
5930.68(11)	8.6(4)		6506	575	
6252.24(11)	36.4(13)		6506	253	
6505.40(11)	9.5(4)		6506	0	

e) Placement in level scheme suggested by energy
f) Sequence of transitions unclear
g) Placement in level scheme according to [20]
h) Placement and identification based on [20]
i) Correct intensity, energy and placement unclear
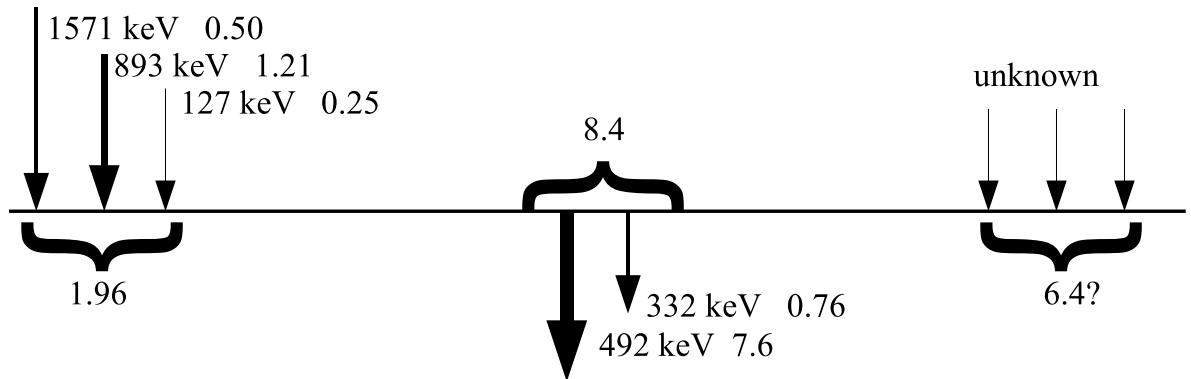
Figure 6.18: Origin of the difference between measured and simulated intensities. The numbers represent the relative intensities.

supported by Groshev *et al.* [24] if the correction factor of 2 is applied to their intensity as discussed in sect. 5.1.5.

Using the recoil corrected γ-ray energies the level scheme was reconstructed. Two new levels were found at 2091 keV and 2311 keV. The 2066 keV level corresponds to the 2069 keV reported by Groshev *et al.* [24]. The shift is caused by the lower energy given for the populating 4436 keV transition (see above). The capture state and accordingly the neutron binding has an energy of $S_n = 6505.84(5)$ keV (table C.5).

The fraction of emitted energy found in our measurement reaches $v = (53 \pm 4)\,\%$, slightly less than calculated from the data reported by Groshev *et al.* ($v \sim 60\,\%$ with correction factor of 2). Because of the conservative requirements for acception some transitions at mid energies were not recognized as ^{75}Ge.

6.3.3 Consequences for the GERDA experiment

The Monte-Carlo simulation of the detection efficiency presented in chapter 1 was repeated with the actual decay scheme and emission probabilities obtained in the present work [49]. All levels in table C.3 that are populated were used; the 911 keV, 1385 keV and 2814 keV levels were ignored since no populating transitions from the capture state were found. The IT with an energy of 160 keV was not included in the simulation because of the delayed decay with a half-life of 52.9 s. Since the decay scheme is not completely known, the simulated emission probabilities differ from the ones measured. While the high energetic primary γ-rays are exactly reproduced, the low energetic transitions at the end of the cascade deviate by a factor of up to 2, in one case (level 492 keV) even about 10. This is a result of the typical PGAA spectra, where the identification probability is best for the lower and upper end of the spectrum. For example the 492 keV level is depopulated
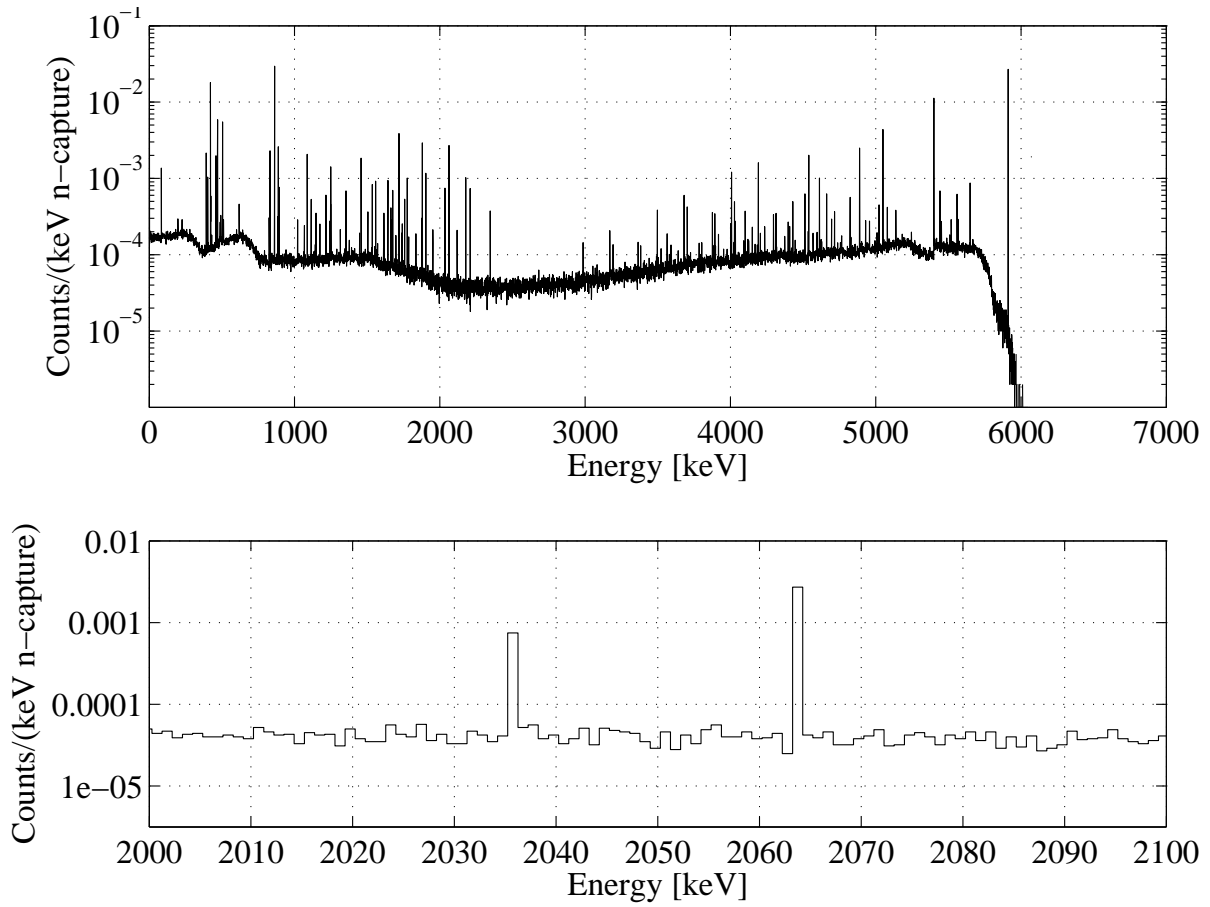
Figure 6.19: Simulated prompt spectrum in ^{77}Ge for a single phase I detector. The counts in bin 2063 represent the sum peak corresponding to the 2063.2 keV level.

by two low-energetic transitions with a total intensity of 8.4 %. But only an intensity of 1.96 % was found to populate this state (fig. 6.18), the rest of the incoming intensity is likely to be from the mid-energy range that is hard to analyze. Since these transitions are missing in the simulation, the probability of this level to occur is lower than in the measurement. Taking into account the same effect in preceding steps the factor of 10 can easily be explained. The 2035 keV transition in the region of interest is not affected by this problem, hence the populating and depopulating intensities of the 2195 keV level are identical (table C.3).

1 000 000 nuclei with an excitation energy of 6071 keV were simulated in a single 2.8 kg phase I detector (fig. 6.19). Counting all energy depositions above 20 keV, a detection efficiency of 68.2 % was found compared to 37.7 %, assuming a single photon emission with $E_\gamma = 6$ MeV (table 1.1). Still, this value is a rough estimation since the fraction

of emitted energy v used in the simulation is only $60.7\,\%$[2]. Of the remaining $39.3\,\%$ no significant contribution is expected to exceed an energy of $4\,\mathrm{MeV}$ because in this range the spectrum is well understood. So, the most conservative case is the emission of two $3\,\mathrm{MeV}$ γ-rays with a detection efficiency of $64.7\,\%$ (table 1.1). Weighting the two efficiencies with their probability they add up to $\epsilon_{Ge} = 66.8\,\%$.

The GERDA phase I array of 8 enriched and 6 natural germanium detectors has an simulated detection efficiency of $74.7\,\%$. The increase in efficiency is rather small due to the limited number of diodes deployed. Taking again into account the $39.3\,\%$ of intensity not used in the simulation with a detection efficiency of $84.8\,\%$ (table 1.1, $2\,\gamma$s $2\,\mathrm{MeV}$ $+4\,\mathrm{MeV}$) a weighted value of $\epsilon_{Ge} = 78.7\,\%$ is obtained. The total rejection efficiency (eq. 1.3) of the delayed decay of ^{77m}Ge in phase I will be $\epsilon = 75\,\%$[3] for the conservative approach. For the simulations the ^{77}Ge nuclei were placed only in the enriched crystals as the production probability depends more on the enrichment than on mass.

For the alternative trigger condition with a minimum energy deposition of $4\,\mathrm{MeV}$ (sect. 1.3.1) an efficiency of $26.1\,\%$ for the single detector and $27.8\,\%$ for the detector array was obtained. Obviously this method is less capable to start the dead time for the veto of the ^{77m}Ge decay.

Another background arises from Compton scattering of high-energetic γ-rays. In the region of interest a Compton plateau of $b_C = 0.43 \times 10^{-4}$ counts/(keV n-capture) was result of simulations for the single detector setup. One can assume that the level and shape of the plateau is not changed significantly by the transitions not included in the simulations.

In the region of interest for $0\nu\beta\beta$-decay around $2039\,\mathrm{keV}$ five peaks were observed (fig. 6.20, table 6.9). Those at $2026\,\mathrm{keV}$ ($I_\gamma = 0.55$) and $2030\,\mathrm{keV}$ ($I_\gamma = 1.44$) appear only in the enriched spectrum, hence they are due to ^{76}Ge. At $2035\,\mathrm{keV}$ ($I_\gamma = 1.07$) the peak could not be assigned to ^{76}Ge(n,γ) using only the single spectra. But, because of the coincidence found with the $3876\,\mathrm{keV}$ transition this line could be placed into the level scheme. The peak nearby is a combination of ^{19}F (empty-spectrum), ^{73}Ge (depleted-spectrum) and the $2038\,\mathrm{keV}$ decay line from ^{77}Ge (decay-spectrum). The peak with an energy of $2043.7\,\mathrm{keV}$ consists of a superposition of prompt emissions in ^{74}Ge, ^{20}F and the single escape peak of the $2555\,\mathrm{keV}$ transition in ^{77}Ge. A contribution from ^{76}Ge(n,γ) could not be excluded (relative intensity $< 0.28\,\%$). The simulation shows a peak at $2063\,\mathrm{keV}$ as well that is due to the summing of transitions depopulating the corresponding level. This line did not show up in the experimental data taken in this work because the prompt decay happend outside the detectors resulting in a negligible efficiency for sum peaks.

Multiplying the relative intensity of the $2035\,\mathrm{keV}$ line (table 6.9) with the normalization factor 0.255 (sect. 6.1.2) this transition has a probability of 27×10^{-4} events/n-capture (table 6.10). The corresponding simulated efficiency for the single detector is

---

[2] v for the transitions used in the simulations

[3] The muon veto efficiency was here assumed to be $\epsilon_{mv} = 0.995$ [31]
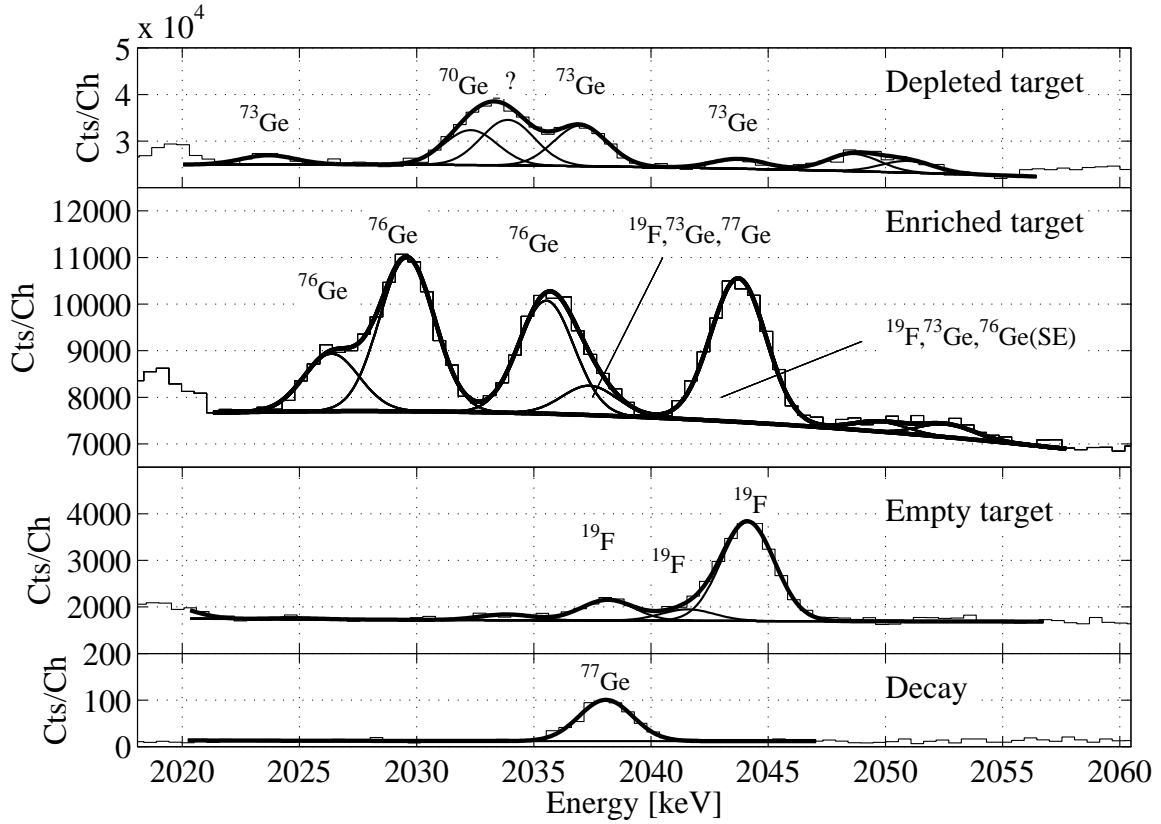
Figure 6.20: Spectra of the depleted, enriched (prompt and decay) and empty target in the region of interest around 2039 keV. The spectra were normalized for comparison in the way that the most important isotope occurs with the same intensity as in the enriched spectrum (depleted: ^{74}Ge(n,γ), empty: ^{19}F(n,γ), decay: ^{77}Ge decay.

$\epsilon(2035) = 6.3\%$, *i.e.* 1.7×10^{-4} counts/n-capture are expected close to $Q_{\beta\beta}$. The efficiency for photoabsorption in the detector array is only 5.6%, resulting in 1.5×10^{-4} counts/n-capture. This astonishing decrease in efficiency if more than one crystal is used can be explained by the high mass of 2.8 kg of the single detector, whereas the average crystal used in GERDA weights only 2.2 kg (17.66 kg/8 crystals). In the case of the single detector simulation all created photons profit from the higher efficiency of the large volume, while in the array most of the ^{77}Ge nuclei are produced in crystals with lower mass. Observing the same effect for the most important sum peaks at 5911 keV and 6071 keV one can exclude an explanation where events are stolen from individual peaks and added into the sum peak. Still, the probability for Compton scattering is higher for the array, resulting in a Compton level of $b_C = 0.55 \times 10^{-4}$ counts/(keV n-capture).

Adding up the flat contributions due to neutron capture on ^{76}Ge in table 6.10, a continuous background of approximately 3.8×10^{-4} counts/(keV n-capture) is expected. The effect of the 2035 keV peak in counts per keV depends strongly on the energy resolution of the detectors.

Running the simulation for the phase I array with the data determined for the prompt transitions in ^{75}Ge a background level from Compton scattering in the region of interest of $b_C = 0.5 \times 10^{-4}$ counts/(keV n-capture) was obtained. Since the abundance of ^{74}Ge is much lower than of ^{76}Ge (12.7 %/87.1 %), at the same time the cross section is higher (497 mb/154.9 mb), only 0.5 nuclei/(kg y) are produced, *i.e.* to obtain the absolute value of b_C the result in table 6.10 has to be divided by 2.

The ^{77}Ge decay line at $E_\gamma = 2038$ keV has a probability 7×10^{-4} counts/n-capture (table C.6). Accounting for the efficiencies discussed above for the prompt 2035 keV peak a background contribution of 0.39×10^{-4} counts/n-capture is expected almost directly at $Q_{\beta\beta} = 2039$ keV.

Table 6.9: Peaks in the region of interest for $0\nu\beta\beta$ around 2039 keV. The intensity is given relative to the strongest line of ^{76}Ge(n,γ). For peaks with an uncertain ^{76}Ge contribution the maximal possible intensity is given.

Energy (keV)	Relative I_γ (%)	Isotope
2026.4	0.55(4)	^{76}Ge
2029.6	1.44(8)	^{76}Ge
2035.5	1.07(10)	^{76}Ge
2037.4	-	^{19}F & ^{73}Ge & ^{77}Ge
2043.7	< 0.28	^{73}Ge & ^{19}F & SE ^{76}Ge(2555) & ^{76}Ge

The γ-radiation can be effectively suppressed by PSA, while at least 75 % of the background by β-particles can be eliminated applying the rejection strategy for the ^{77m}Ge decay discussed in chapter 1. Hence a background index due to neutron capture and its subsequent radiative emissions of $\sim 10^{-4}$ counts/(keV n-capture) should be achievable.

Table 6.10: Background in the region of interest (2032 keV - 2046 keV) without suppression by PSA. While the value in the first row is derived directly from the measured intensity, the simulated ones account for the detector efficiency as well. In case of the 2035 keV and 2038 keV peaks the number of counts per keV depends on the energy resolution. The contributions by ^{77,77m}Ge decay are adopted from ref. [50] and corrected for the new cross sections (chapter 3). These values were derived from a simulation for an array of 21 18-fold segmented detectors.

Source	Radiation	Background [10^{-4}counts/(keV n-capture)]		
		Measurement	Simulation	
			Single detector	Phase I array
Prompt ^{76}Ge(n,γ)				
Peak (2035 keV)	γ	27/resolution	1.7/resolution	1.5/resolution
Compton scattering	γ		0.43	0.55
Prompt ^{74}Ge(n,γ)				
Compton scattering	γ			0.5
Decay				
^{77}Ge	β, γ			1.1
^{77m}Ge	$\beta, (\gamma)$			2.1
^{77}Ge peak (2038 keV)	γ	7.0/resolution	0.44/resolution	0.39/resolution

Chapter 7

Conclusions

This PhD thesis was performed in the framework of the GERDA experiment searching for neutrinoless double beta ($0\nu\beta\beta$)-decay in ^{76}Ge. Due to the long half-life of $0\nu\beta\beta$ decay, background has to be reduced to a very low level. The goal of GERDA is a background rate of 10^{-3} counts/(keV kg y) in the region of interest around 2039 keV for phase II. One contribution with 2.1×10^{-4} counts/(keV n-capture)[1] is given by the β-decay of ^{77m}Ge produced by neutron capture on ^{76}Ge. If the instant of the neutron capture is known, this background can be rejected by introducing a dead time of several half lives ($T_{1/2} = 52.9$ s). Goal of this PhD thesis was to establish the prompt γ-cascade in ^{77}Ge that reveals the moment of neutron capture.

For quantitative estimations of the background the knowledge of the neutron capture cross section is crucial. The values given in literature have a broad spread, therefore new measurements were performed at the PGAA facility of the research reactor FRM II in Garching applying the activation method. By irradiation of GeO$_2$, isotopically enriched in ^{76}Ge together with a gold foil the capture cross sections were determined relative to the gold standard. The analysis showed that the emission probabilities for the ^{77}Ge decay in the literature do not match with our experimental results. Remeasuring the intensities of the γ-rays in the ^{77}Ge decay consistent values for the cross section to the ground state could be obtained. While the rate for the ^{77m}Ge production in GERDA was not changed significantly applying the new cross sections, the rate for ^{77}Ge (g.s.) was increased. The background by the latter decay amounts therefore to 1.1×10^{-4} counts/(keV n-capture).

GeO$_2$ samples of different isotopic composition were irradiated with neutrons to measure the prompt γ-radiation. The spectra of the prompt ($t_m \sim 15$ h) and the decay ($t_m \sim 33$ h) radiation were recorded and by comparison the peaks were assigned to the different isotopes. To gain information about the level scheme in ^{77}Ge a longterm mea-

---

[1] Note the different units: counts/(keV kg y) vs. counts/(keV n-capture). Simulations predict ~ 1 n-capture/(kg y), therefore the values are approximately the same for both units.)

surement ($t_m \sim 8\,\mathrm{d}$) searching for coincidences was carried out.

In this work 119 prompt transitions in ^{77}Ge were found, 84 of them could be placed into a level scheme. Beforehand only 14 lines were known with doubtful position in the decay scheme. The total intensity, weighted by the energy of the photon, was increased from about 10 % to 65 %. Implementing the transitions placed into the level scheme in a Monte-Carlo simulation the expected prompt spectra for a single germanium detector and the whole phase I array were calculated. With the detection probability of the prompt cascade of $\epsilon_{Ge} = 78.7\,\%$ (phase I array), the muon veto efficiency of $\epsilon_{mv} = 99.5\,\%$ and the fraction of ^{77m}Ge nuclei decayed within the dead time of $\epsilon_{dec} = 96\,\%$ follows a total suppression capability of $\epsilon = 75\,\%$. Applying the rejection by dead time the ^{77m}Ge decay adds only 0.5×10^{-4} counts/(keV n-capture) to the background.

Besides for the triggering of the veto the prompt radiation has to be known because it contributes directly to the background. Three new prompt γ-ray peaks at 2026 keV, 2030 keV and 2035 keV were found in the region of interest around 2039 keV. The background expected from the 2035 keV transition in phase I is 1.5×10^{-4} counts/n-capture, the 2038 keV peak from ^{77}Ge (g.s.) decay adds another 0.39×10^{-4} counts/n-capture around $Q_{\beta\beta}$. Additionally high-energetic γ-rays may deposit energy close to $Q_{\beta\beta}$ by Compton scattering. The contribution by Compton scattering was obtained from the simulated spectra and is with 0.55×10^{-4} counts/(keV n-capture) similar to the one from the ^{77m}Ge decay.

The isotope ^{74}Ge has an abundance of about 12.7 % in the GERDA diodes, therefore similar measurements like for ^{76}Ge were carried out. 68 prompt transitions in ^{75}Ge were found, none of them in the region of interest. Since the Q-value in the β-decay of ^{75}Ge and ^{75m}Ge is smaller than $Q_{\beta\beta}$ the only background contribution around 2039 keV comes from Compton scattering of the prompt γ-rays with energies up to 6506 keV. Simulations give a value of 0.5×10^{-4} counts/(keV n-capture) for the phase I detector array.

From the experimental point of view the number of identified peaks could be increased if a target with higher isotopic enrichment of ^{76}Ge would be used. At the same time the abundance of the light germanium isotopes, especially ^{73}Ge should not exceed the value of the target used in this work. If the depleted target would be replaced by one isotopically enriched in ^{74}Ge the discrimination of transitions in ^{77}Ge and ^{75}Ge could be improved.

Using an array of HPGe detectors would not help to obtain more information from single spectra because statistics is not an issue. But, for the coincidence mode an increase of coincidence count rate would be an important improvement. Also spins of levels could be determined from the angular distribution of the coincident γ-rays. The PGAA facility offers only limited space for additional detectors because good shielding has to be provided for each detector due to the easily scattered neutrons. Shielding can be reduced if other reactions like (^{13}C,^{12}C) with more focused beams are used to add a neutron to the nucleus, but the levels populated are different from those in the (n,γ)-reaction occurring in GERDA.

Effort should be made to solve the unsatisfying situation of the branching in the

^{77m}Ge decay. Due to this uncertainty the cross section to the isomeric state of ^{77}Ge can not be calculated precisely. To measure the branching one has to detect the γ- and β-radiation in coincidence and in single mode. If all β-transitions into exited states and the ground level of ^{77}As are found, the branching can be determined in comparison with IT to the ground state of ^{77}Ge (γ, internal conversion). The main challenge is to extract the energies from the continuous spectrum of the β-particles. Such a measurement could be carried out at the PGAA facility using additional detectors for β-particle detection (Si-stack). In principle, also other instruments like mass spectrometers can be used to separate radioactive ^{77m}Ge nuclei and to observe their decay. Still, the challenge of β-particle detection stays the same.

From theory the direct transition from the ground state of ^{77}Ge ($J^\pi = 7/2+$) to the ground state of ^{77}As ($J^\pi = 3/2-$) is forbidden, but the experimental limit is rather high ($I_\beta < 10\,\%$ [19]). It is important to explore this decay as well more in-depth to know how much non-coincident background by β-particles has to be expected in GERDA.

The simulations using the decay scheme of ^{77}Ge obtained in this work should be repeated with an array of BEGe detectors used in phase II to explore the rejection strength of pulse shape analysis for the energies in the prompt cascade.

Appendix

A Known levels and transitions in ^{77}Ge and ^{75}Ge

Table A.1: States and transitions in ^{75}Ge after β-decay of ^{75}Ga [12]. The uncertainty in E_γ is 0.2 keV.

E_{level} [keV]	E_γ [keV]	I_γ [%]	E_{level} [keV]	E_γ [keV]	I_γ [%]
139.3	139.3		1240.3	783.2	2.1(2)
252.8	252.8	100		987.5	1.4(2)
316.8	177.0	13.5(10)		1239.5	0.3(1)
	316.8	3.3(7)	1427.0	1174.6	1.5(2)
457.1	203.9	5.3(8)		1427.0	0.9(2)
	457.1	4.5(4)	1501.1	927.2	6.6(5)
574.7	321.6	2.0(4)		1043.3	2.6(2)
	574.7	31.6(20)		1248.5	5.5(3)
584.1	444.8	1.6(2)		1501.1	4.5(5)
	584.1	1.5(1)	1796.4	1222.5	1.3(2)
761.3	761.3	1.2(3)		1543.0	1.1(2)
	442.8	0.9(1) tentatively		1796.4	0.6(1)
placed, poor energy fit (evalutors [20])			2103.7	2103.7	0.20(5)
885.4	124.3	0.8(3)	2664.4	2089.7	0.20(5)
	310.4	6.6(10)			
	428.3	1.1(3)	not placed in decay scheme		
	568.5	2.4(4)			
	632.2	5.5(3)		279.3	2.9(6)
	885.4	11.1(7)		1182.3	1.4(2)
1222. 5?	1222.5 ? double placed			1358.8	0.4(1)
	1.8(2)	11.1(7)		1745.6	< 0.1

Table A.2: Levels in ^{77}Ge from ^{77}Ga β-decay, ^{77}Ge IT decay, ^{76}Ge(n,γ), ^{76}pol d,p),(d,p) and ^{76}Ge(^{13}C,12Cγ) [19].

E_{level} [keV]	J^π	E_{level} [keV]	J^π
0.0	7/2+	1954(10)	(3/2+,5/2+)
159.70(10)	1/2-	2060(10)	
224.9(7)	9/2+	2088(10)	(7/2+,9/2+)
421.0(7)	3/2+,5/2+	2120(10)	(3/2+,5/2+)
491.9(10)		2260(10)	
504.8(6)	5/2+	2305(10)	(3/2+,5/2+)
581.0(8)	1/2,3/2,5/2-	2442(10)	(3/2+,5/2+)
618.8(7)	1/2,3/2,5/2-	2479(10)	(1/2+)
629.4(8)	3/2-	2515(10)	
760.5(6)	5/2+,7/2,9/2+	2556(10)	
778.0(7)	1/2,3/2,5/2-	2783(10)	
884.3(10)	5/2+	2816.7(13)	
1021.1(7)	1/2,3/2,5/2-	2873(10)	(1/2+)
1047.6(10)	1/2-,3/2-	2929(10)	
1109?(10)		2960(10)	(1/2+)
1189?(10)	(7/2+,9/2+)	2998(10)	
1250.4(10)	1/2+	3090(15)	
1358.7(12)		3135(10)	
1385.0(6)	5/2+	3147(10)	
1536(10)	1/2+	3242(10)	(3/2+,5/2+)
1610(10)		3257(10)	(1/2+)
1663.3(8)	(1/2,3/2,5/2-)	3364(15)	(3/2+,5/2+)
1777(10)	1/2+	3388(15)	
1804(10)	3/2+	3443(15)	
1823.3(13)	(1/2+)	3496(15)	
1883(10)		3547(15)	

Table A.3: Known transitions and their absolute intensities in ^{75}Ge after neutron capture on ^{74}Ge ([24, 25, 27]). The intensities for the high energy region ($E_\gamma > 928.1$ keV) given by [25] are normalized to 100% for the primary transitions. In the low-energy region the values are normalized to 11.2 for the 265 keV line. The intensities in [24] are obtained relative to the 7262 keV line in ^{74}Ge. [27] normalized the intensities relative to ^{14}N. An additional error of 16% has to be added to corresponding uncertainties given in the table due to the uncertainty of the cross section of ^{74}Ge.

Hasselgren [25]		Groshev et al. [24]		Islam et al. [27]		Weishaupt [58]		IAEA [1]	
E_γ[keV]	I_γ[%]	E_γ[keV]	I_γ[%]	E_γ[keV]	I_γ[%]	E_γ[keV]	I_γ[%]	E_γ[keV]	I_γ[%]
								52.31(5)	0.0103(6)
						60.5(2)			
						80.1(1)			
112.7(15)	9.5	111.8	0.40						
		121.1	0.43					124.76(9)	0.0016(3)
139.6(15)	7.0	139.2	7.09			139.69(5)	6.53(60)		
		177.3	2.18			177.3(1)	1.83(50)	177.49(4)	0.0118(5)
		204.0	0.95					201.82(25)	0.0022(5)
223.7(15)	2.3								
253.3(15)	64.3	253.7	9.30					253.21(5)	0.0609(16)
264.5(15)	11.2					264.6(2)			
299.7(15)	2.6							300.2(6)	0.00106(25)
								317.07(8)	0.0045(5)
444.6(15)	2.9	445.2	2.34					445.4(6)	0.0054(13)
		455.8	1.59					455.02(24)	0.0031(7)
								569.76(11)	0.0052(8)

Continued on next page

93

Hasselgren [25]		Groshev et al. [24]		Islam et al. [27]		Weishaupt [58]		IAEA [1]	
E_γ[keV]	I_γ[%]	E_γ[keV]	I_γ[%]	E_γ[keV]	I_γ[%]	E_γ[keV]	I_γ[%]	E_γ[keV]	I_γ[%]
575.2(10)	12.8	574.7	13.30					574.91(3)	0.0306(12)
								673.78(12)	0.0040(6)
		737.1	1.31						
		762.4	1.34					762.08(14)	0.0030(7)
841.4(10)	13.2	841.6	1.56					841.9(5)	0.0036(9)
884.5(10)	8.1							885.10(7)	0.0033(8)
928.1(10)	10.2							927.13(7)	0.0035(10)
		932.7	0.93						
		1222.0	4.35						
		1248.8	3.20						
								1426.3(3)	0.0025(7)
		1545.0	3.17					1545.09(23)	0.007(3)
								2069.4(5)	0.0024(8)
3278.5(20)	2.7		0.24						
3303.2(20)	2.6	3302.9	0.43						
3337.9(20)	2.1	3337.7	0.53						
		3348.3	0.36						
3501.1(20)	4.5	3502.2	0.40						
3538.7(20)	2.2								
3551.6(20)	3.3	3553.3	0.58						
3607.8(20)	5.8	3607.5	0.44						
		3635.5	0.29						
3748.1(20)	4.8	3745.3	0.31						
3761.3(20)	3.2								
		3826.1	0.28						
3844.6(20)	5.1	3846.8	0.51						

Table A.3 – continued from previous page

Hasselgren [25]		Groshev et al. [24]		Islam et al. [27]		Weishaupt [58]		IAEA [1]	
E_γ[keV]	I_γ[%]	E_γ[keV]	I_γ[%]	E_γ[keV]	I_γ[%]	E_γ[keV]	I_γ[%]	E_γ[keV]	I_γ[%]
3934.1(20)	3.4	3934.9	0.46						
		3979.5	0.20						
4012.1(20)	2.9								
4194.4(20)	3.1								
4414.7(20)	22.7	4410.6	1.01					4410.6(8)	0.0023(6)
4439.6(20)	28.5	4436.4	1.51					4435.9(5)	0.0035(8)
4500.9(20)	2.2							4500.7(9)	0.00090(22)
4707.4(20)	28.5	4706.0	3.50	4707(1)	7.14(32)			4706.98(23)	0.0151(13)
4748.2(20)	3.5	4746.1	0.40	4747.63(8)	0.78(12)			4747.67(5)	0.00092(22)
4816.9(20)	4.6	4815.0	0.59	4816.86(11)	3.06(85)			4816.91(7)	0.0014(3)
4990.8(20)	8.6	4988.5	1.13	4990(2)	1.97(23)			4989.5(4)	0.0062(14)
5002.5(20)*	11.3	5000.3	1.30	5003.22(6)	2.27(12)			5003.23(6)	0.0033(8)
5077.9(20)	2.6	5075.9	0.54					5079.0(3)	0.0012(3)
5088.9(20)*	14.7	5088.0	2.06	5088(1)	4.35(19)			5088.4(5)	0.0047(11)
5368.7(20)*	9.1	5368.6	1.26	5368(2)	2.45(14)			5367.9(3)	0.0091(19)
5420.7(20)	2.6								
5620.4(20)*	8.3	5621.1	0.84					5620.12(6)	0.0041(15)
5744.0(20)*	1.7			5745(2)	0.61(8)			5743.14(15)	0.00069(17)
5831.4(20)*	3.0			5620.09(8)	2.35(11)			5831.42(13)	0.0012(3)
5930.6(20)*	11.6	5930.9	1.38	5930.34(5)	2.91(13)			5930.29(4)	0.0033(8)
6252.4(20)*	33.1	6252.1	6.13	6252.16(4)	11.75(51)			6251.97(6)	0.0188(18)
6505.6(20)*	8.9	6505.6	1.56	6505.09(6)	2.83(15)			6505.15(4)	0.0070(10)

B Coincidences

Table B.1: Number of events after applying cuts "AB1-6". The stated rate is valid for the true coincidences.

Data	Recorded events	Random coincidences	True coincidences	Rate (true) [Hz]
Region B1	509 918	348 166 ± 1825	161 752 ± 1825	0.2485 ± 0.0028
Region B2	316 223	156 894 ± 687	159 329 ± 687	0.2448 ± 0.0011
Region B3	169 188	45 125 ± 187	124 063 ± 187	0.1906 ± 0.0003
Region B4	129 980	29 622 ± 123	100 358 ± 123	0.1542 ± 0.0002
Region B5	88 424	18 124 ± 75	70 300 ± 75	0.1080 ± 0.0001
Region B6	23 939	4 619 ± 19	19 320 ± 19	0.0297 ± 0.0001
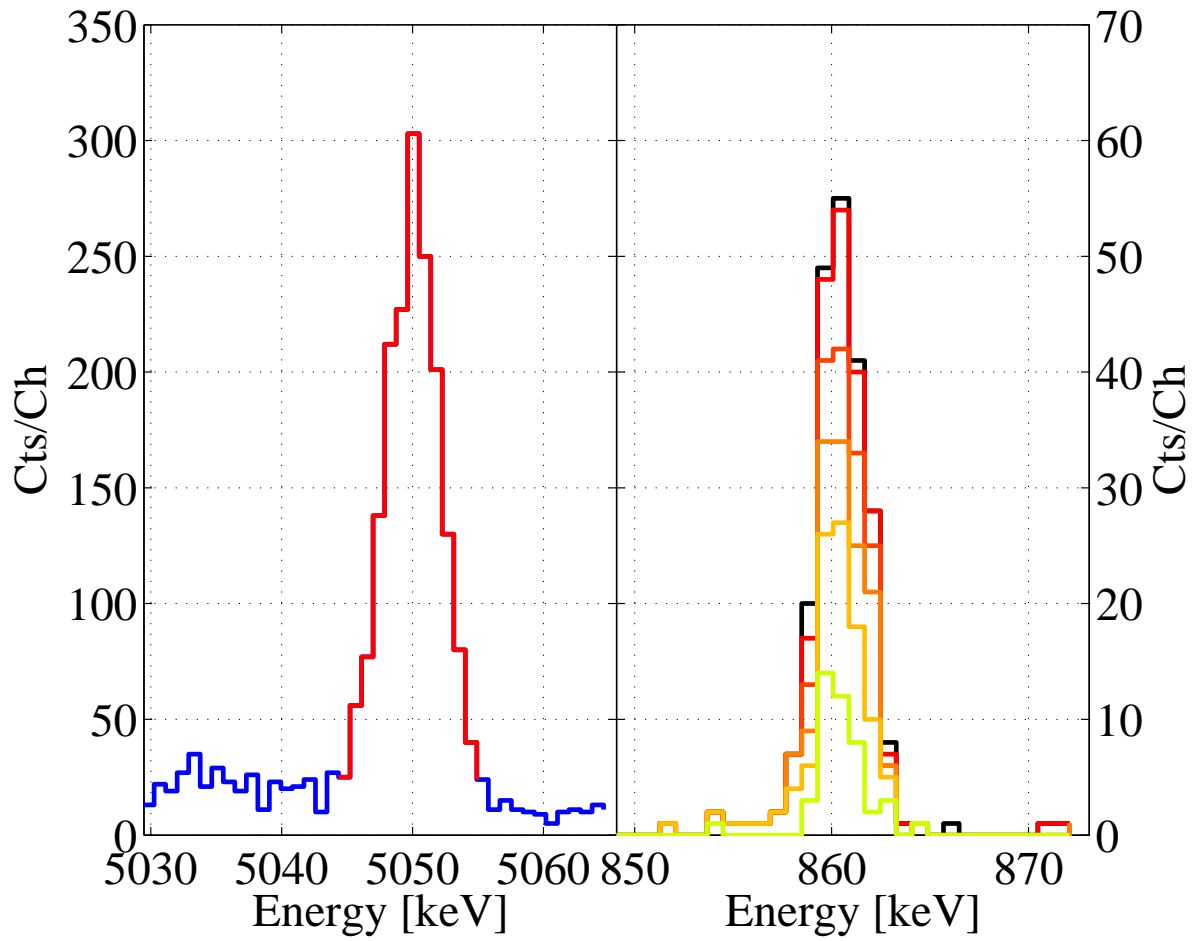
Figure B.1: Coincidence of the 5050 keV peak with the 862 keV line. The red marked area in the left spectrum (detector I) shows the channels used to plot the coincident events in detector II. The six different colors correspond to the range "AB1-6" given in table 6.4.

C Results

Table C.2: Prompt γ-rays after neutron capture on ^{76}Ge. The uncertainty of the measured γ-ray energy E_γ contains a systematic contribution of 0.10 keV. The relative intensity was normalized to the strongest transition at 5911 keV (100 %). To obtain the partial cross section in mbarn multiply the relative intensity by 0.395(15), for the absolute intensity per 100 neutron captures by 0.255(30).

E_γ [keV]	Relative intensity	Coincident transitions [keV]	E_i [keV]	E_f [keV]	References/ comments
83.5	6.12(23)		505	421	a,b, energy by [28]
126.85(13)	0.25(12)		619	492	a
159.62(10)	28.9(11)		160	0	$t_{1/2} = 52.9\,\text{s}$
197.17(33)	1.25(7)	421	619	421	a
224.88(10)	1.94(9)		225	0	
255.78(42)	0.36(10)		760	505	a,b,c,d
279.74(11)	0.82(10)		505	225	
291.80(16)	0.19(9)		911	619	a
332.32(11)	0.76(13)		492	160	a
392.04(10)	7.79(29)		1021	630	
402.59(10)	4.05(15)		1021	619	
418.61(26)	0.84(8)		911	492	a,c
421.34(10)	60.9(21)		421	0	
423.00(11)	2.8(4)	470,1316	1053	630	b
429.10(14)	0.65(4)	831, 4192	1048	619	e
449.72(11)	1.09(5)				
459.15(10)	13.2(6)		619	160	
469.99(10)	34.3(12)	755, 2684	630	160	
487.24(11)	0.43(20)		1535	1048	
491.98(24)	7.6(19)		492	0	
504.79(10)	16.7(6)		505	0	
535.48(11)	0.85(5)	225,625	760	225	a,b
600.33(11)	1.00(5)				
618.86(24)	1.64(15)		619	0	
624.73(18)	0.37(20)	225,535	1385	760	a,b
642.19(12)	0.40(19)	862	1664	1021	b

Continued on next page

Table C.2 – continued from previous page

E_γ [keV]	Relative intensity	Coincident transitions [keV]	E_i [keV]	E_f [keV]	References/ comments
740.46(11)	1.44(7)	459	1359	619	b
755.17(26)	0.72(22)	470	1385	630	a,b
760.22(30)	0.40(25)		760	0	a,b
766.64(23)	0.37(7)		1385	619	a,b
794.44(21)	0.28(4)				
825.55(10)	2.99(12)	421	1247	421	e
831.22(10)	11.1(5)	445	1879	1048	
861.82(15)	51.4(18)		1021	160	
880.37(17)	0.69(10)		1385	505	a,b
884.09(15)	5.0(6)	1068	884	0	a,b
888.34(15)	15.1(6)	1147	1048	160	
893.15(11)	1.21(5)	492	1385	492	a
897.00(22)	0.99(11)				
935.80(10)	2.69(11)				
963.88(17)	0.24(12)		1385	421	a,b,c,d
1042.09(12)	1.26(9)				
1067.66(11)	1.02(5)		1952	884	e
1087.31(10)	8.55(30)		1247	160	
1113.84(18)	4.0(12)		1535	421	
1142.45(11)	0.98(4)		2195	1053	
1145.53(18)	1.70(10)		1775	630	
1146.95(18)	1.40(12)		2195	1048	
1173.68(12)	1.11(7)		2195	1021	
1216.06(12)	2.07(9)	459	1835	619	e
1242.24(18)	2.4(4)		1664	421	
1249.43(18)	10.7(5)		1879	630	
1315.59(11)	1.60(7)		2368	1053	
1342.90(12)	0.69(11)				
1353.94(10)	6.06(22)		1775	421	
1375.47(11)	1.43(20)				
1446.87(16)	1.05(13)		1952	505	e
1448.14(13)	1.15(13)				
1457.84(10)	17.3(7)		1879	421	
1504.05(12)	0.90(6)		1664	160	b
1558.48(10)	9.2(4)		2063	505	
1571.09(15)	0.50(4)		2063	492	

Table C.2 – continued from previous page

E_γ [keV]	Relative intensity	Coincident transitions [keV]	E_i [keV]	E_f [keV]	References/ comments
1608.73(27)	0.60(9)				
1641.85(23)	5.78(21)		2063	421	
1673.22(15)	3.2(5)		2178	505	
1697.40(12)	1.08(6)	421	2119	421	e
1719.58(32)	1.1(6)				
1741.35(11)	1.52(7)		1901	160	e
1756.86(42)	4.0(11)		2178	421	
1877.02(11)	1.80(7)	470	2507	630	e
1903.55(18)	3.2(11)		2063	160	
1953.52(15)	0.84(11)				
1961.71(15)	0.80(25)				
2026.37(14)	0.55(4)				
2029.60(11)	1.44(8)				
2035.48(13)	1.07(10)		2195	160	
2102.59(15)	0.68(7)				
2150.67(11)	3.21(20)				
2184.60(11)	1.38(7)	470	2814	630	b
2208.76(23)	1.23(30)		2368	160	
2301.94(12)	0.55(22)				
2321.63(65)	1.6(4)				
2377.28(40)	0.91(17)				
2399.16(35)	0.88(25)				
2407.27(32)	0.65(24)				
2509.51(23)	1.7(4)				
2555.18(11)	2.7(7)				
2559.48(15)	3.10(13)				
2683.76(15)	3.1(4)	470			
2782.91(11)	3.00(12)		3287	504	f
2785.11(15)	1.30(14)		6071	3287	f
2806.05(42)	0.34(9)				
2921.14(28)	0.74(63)				
2941.21(27)	1.15(25)				
3252.7(10)	0.39(11)				
3285.11(11)	1.58(30)				
3357.17(11)	2.57(25)				
3410.85(13)	1.28(20)				

Continued on next page

Table C.2 – continued from previous page

E_γ [keV]	Relative intensity	Coincident transitions [keV]	E_i [keV]	E_f [keV]	References/ comments
3564.44(11)	2.62(10)	470	6071	2506	e
3638.68(42)	2.1(10)				
3689.09(35)	0.52(7)				
3702.92(15)	4.4(11)		6071	2368	
3875.97(15)	4.72(22)		6071	2195	
3893.12(15)	6.78(29)		6071	2178	
3952.53(11)	1.25(7)	421	6071	2119	e
4007.96(10)	21.0(15)		6071	2063	
4119.53(24)	1.90(9)		6071	1952	e
4170.19(34)	0.54(10)		6071	1901	e
4192.00(20)	38.5(12)		6071	1879	
4236.33(11)	4.14(21)	458	6071	1835	e
4295.92(11)	7.0(10)		6071	1775	
4407.53(11)	2.45(21)		6071	1664	
4535.81(18)	3.9(9)		6071	1535	
4824.31(11)	5.56(27)		6071	1247	
5018.75(16)	0.53(4)	470	6071	1053	e
5049.69(10)	56.0(23)		6071	1021	
5442.06(18)	0.30(7)		6071	630	e
5649.71(11)	1.94(9)		6071	421	
5911.33(10)	100.0		6071	160	

a) Placement in level scheme according to [28]

b) Placement in level scheme according to [19]

c) Identification based on [28]

d) Identification based on [19]

e) Placement in level scheme suggested by energy

f) Sequence of transitions unclear

Table C.3: Levels E_i in ^{77}Ge determined by weighted means. The γ-transitions were corrected for recoil. All transitions marked with "e" in table 6.6 were not used to calculate the level energies. The relative intensities of transitions known to depopulate a level I_{dep} and their sum are given. For comparison the known transitions populating a certain level I_{pop} are stated as well. The population intensity of the 159 keV level (232.3(27) was multiplied by a factor of 0.103(11) ref. [19] accounting for the second decay channel to ^{77}As via β-decay.

E_i [keV]	E_γ [keV]	E_f [keV]	I_{dep} [%]	I_{pop} [%]
159.62(10)	159.6	0	28.9(11)	
			28.9	23.9(26)
224.88(10)	224.9	0	1.94(9)	
			1.94(9)	1.67(12)
421.34(10)	421.3	0	60.9(21)	
			60.9(21)	53.2(19)
491.99(24)	492.0	0	7.6(19)	
	332.3	159.6	0.76(13)	
			8.4(20)	1.96(14)
504.74(9)	504.8	0	16.7(6)	
	279.7	224.9	0.82(10)	
	83.5	421.3	6.12(23)	
			23.6(7)	14.5(7)
618.80(11)	618.9	0	1.64(15)	
	459.1	159.6	13.2(6)	
	197.2	421.3	1.25(7)	
	126.8	492.0	0.25(12)	
			16.3(7)	8.58(21)
629.62(15)	470.0	159.6	34.3(12)	
			34.3(12)	27.2(8)

Continued on next page

Table C.3 – continued from previous page

E_i [keV]	E_γ [keV]	E_f [keV]	I_{dep} [%]	I_{pop} [%]
760.35(13)	760.2	0	0.40(25)	
	535.5	224.9	0.85(5)	
	255.8	504.7	0.36(10)	
			1.61(28)	0.37(20)
884.10(16)	884.1	0	5.0(6)	
			5.0(6)	1.02(5)
910.60(16)	418.6	159.6	0.84(8)	
	291.8	618.8	0.19(9)	
			1.03(13)	
1021.49(10)	861.8	159.6	51.4(18)	
	402.6	618.8	4.05(15)	
	392.0	629.6	7.79(29)	
			63.2(19)	57.5(24)
1047.96(18)	888.3	159.6	15.1(6)	
	429.1	618.8	0.65(4)	
			15.7(6)	12.9(6)
1052.62(18)	423.0	629.6	2.8(4)	
			2.8(4)	3.11(11)
1246.91(10)	1087.3	159.6	8.55(30)	
	825.6	421.3	2.99(12)	
			11.5(4)	5.56(27)
1359.27(16)	740.5	618.8	1.44(7)	
			1.44(7)	
1385.12(10)	963.9	421.3	0.24(12)	
	893.2	492.0	1.21(5)	
	880.4	504.7	0.69(10)	
	766.6	618.8	0.37(7)	
	755.2	629.6	0.72(22)	
	624.7	760.4	0.37(20)	

Continued on next page

Table C.3 – continued from previous page

E_i [keV]	E_γ [keV]	E_f [keV]	I_{dep} [%]	I_{pop} [%]
			3.60(35)	
1535.19(21)	1113.8	421.3	4.0(12)	
	487.2	1048.0	0.43(20)	
			4.4(13)	3.9(9)
1663.67(10)	1504.1	159.6	0.90(6)	
	1242.3	421.3	2.4(4)	
	642.2	1021.5	0.40(19)	
			3.7(5)	2.45(21)
1775.25(12)	1354.0	421.3	6.06(22)	
	1145.5	629.6	1.70(10)	
			7.76(25)	7.0(10)
1834.87(16)	1216.1	618.8	2.07(9)	
			2.07(9)	4.14(21)
1879.17(10)	1719.6	159.6	1.1(6)	
	1457.9	421.3	17.3(7)	
	1249.4	629.6	10.7(5)	
	831.2	1048.0	11.1(5)	
			40.2(12)	38.5(12)
1900.99(15)	1741.4	159.6	1.52(7)	
			1.52(7)	0.54(10)
1951.70(14)	1446.9	504.7	1.05(13)	
	1067.7	884.1	1.02(5)	
			2.07(14)	1.90(10)
2063.21(9)	1903.6	159.6	3.2(11)	
	1641.9	421.3	5.78(21)	
	1571.1	492.0	0.50(4)	
	1558.5	504.7	9.2(4)	
			18.7(12)	21.0(15)

Table C.3 – continued from previous page

E_i [keV]	E_γ [keV]	E_f [keV]	I_{dep} [%]	I_{pop} [%]
2118.76(15)	1697.4	421.3	1.08(6)	
			1.08(6)	1.25(7)
2178.01(15)	1756.9	421.3	4.0(11)	
	1673.2	504.7	3.2(5)	
			7.2(13)	6.78(29)
2195.12(9)	2035.5	159.6	1.07(10)	
	1173.5	1021.5	1.11(7)	
	1147.0	1048.0	1.40(12)	
	1142.5	1052.6	0.98(4)	
			4.56(19)	4.72(22)
2368.33(13)	2208.8	159.6	1.23(30)	
	1315.6	1052.6	1.60(7)	
			2.8(4)	4.4(11)
2506.67(18)	1877.0	629.6	1.80(7)	
			1.80(7)	2.62(10)
2814.26(31)	2184.6	629.6	1.38(7)	
			1.38(7)	
6071.29(5)	5911.6	159.6	100.0	
	5649.9	421.3	1.94(9)	
	5442.3	629.6	0.30(7)	
	5049.9	1021.5	56.0(23)	
	5018.9	1052.6	0.53(4)	
	4824.5	1246.9	5.56(27)	
	4536.0	1535.2	3.9(9)	
	4407.7	1663.7	2.45(21)	
	4296.1	1775.3	7.0(10)	
	4236.5	1834.9	4.14(21)	
	4192.1	1879.2	38.5(12)	
	4170.3	1901.0	0.54(10)	
	4119.7	1951.7	1.90(9)	
	4008.1	2063.2	21.0(15)	

Table C.3 – continued from previous page

E_i [keV]	E_γ [keV]	E_f [keV]	I_{dep} [%]	I_{pop} [%]
	3952.6	2118.8	1.25(7)	
	3893.2	2178.0	6.78(29)	
	3876.1	2195.1	4.72(22)	
	3703.0	2368.3	4.4(11)	
	3564.5	2506.7	2.62(10)	
			264.(4)	

Table C.4: Prompt γ-rays after neutron capture on ^{74}Ge. The uncertainty of the measured γ-ray energy E_γ contains a systematic contribution of $0.10\,\text{keV}$. The relative intensity was normalized to the strongest transition at $253\,\text{keV}$ $(100\,\%)$. To obtain the partial cross section in mbarn multiply the relative intensity by $1.57(10)$, for the absolute intensity per 100 neutro captures by $0.32(4)$.

E_γ [keV]	relative intensity	Coincident transitions [keV]	E_i [keV]	E_f [keV]	Comments References
52.5	10.8(6)		192	140	h, energy by [20]
124.75(11)	2.12(10)		317	192	h
			886	762	h
139.81(10)	35.8(10)		140	0	
177.29(11)	20.2(7)		317	140	
204.09(10)	9.5(4)		457	253	
236.25(11)	0.98(6)		1137	901	h
253.01(10)	100.		253	0	
310.89(10)	4.02(18)	574	886	575	g
317.14(10)	6.14(25)	568	317	0	g
321.89(21)	3.4(5)		575	253	
443.48(11)	1.22(9)	1285	584	140	g,i
444.95(10)	16.0(6)	177	762	317	g,i
			901	457	g,i
457.24(10)	12.0(4)	1045	457	0	g
481.71(10)	15.0(4)		674	192	
562.28(13)	1.35(12)	574	1137	575	g
568.89(23)	1.01(20)	317	886	317	g
570.02(20)	4.1(8)		762	192	h
574.98(10)	49.5(17)		575	0	
632.40(29)	5.7(21)	253	886	253	g
647.67(11)	3.14(13)	25			
673.96(15)	4.41(30)		674	0	h
679.89(12)	2.10(13)	204	1137	457	g
762.51(22)	3.6(4)		762	0	h
783.58(23)	1.5(4)	204	1241	457	g
820.13(10)	5.08(18)		1137	317	h
840.69(52)	1.36(15)	481	1515	674	g
841.44(42)	5.8(24)		1416	575	

Table C.4 – continued from previous page

E_γ [keV]	relative intensity	Coincident transitions	E_i [keV]	E_f [keV]	Comments References
885.83(11)	7.85(27)		886	0	
927.39(11)	5.00(24)		1502	575	
987.80(14)	0.99(9)		1241	253	h
1045.30(31)	2.1(7)	204,457	1502	457	g
1137.15(11)	4.08(30)		1137	0	h
1175.54(11)	3.27(24)		1429	253	
1223.33(10)	11.5(4)		1798	575	
1249(1)	3.2(14)	253	1502	253	g
1285.29(16)	1.18(14)	443	1869	584	g
1416.45(11)	5.97(21)		1416	0	
1428.67(12)	1.07(6)		1429	0	a
1495.98(11)	4.63(19)		1688	192	
1502.34(11)	2.37(13)		1502	0	h
1514.85(11)	7.63(29)		1515	0	
1545.06(11)	6.79(24)		1798	253	
1606.82(40)	0.96(17)		2066	457	
1798.30(11)	4.48(16)		1798	0	
1873.27(15)	6.6(7)		2066	192	
2091.21(15)	4.6(9)		2091	0	
2119.42(16)	5.4(10)		2312	192	
4193.90(52)	4.1(18)		6506	2312	
4414.54(11)	7.70(28)	253	6506	2091	
4439.95(11)	10.3(4)		6506	2065	
4501.58(12)	2.37(11)		6506	2003	h
4707.51(10)	25.8(10)		6506	1798	
4747.80(11)	3.63(15)				h
4817.46(14)	3.25(30)		6506	1688	
4990.92(11)	7.94(30)		6506	1515	
5003.38(11)	9.4(4)		6506	1502	
5077.00(11)	3.09(15)		6506	1429	
5089.21(11)	14.5(6)		6506	1416	
5368.38(16)	7.8(11)		6506	1137	
5619.97(31)	6.2(6)		6506	886	
5743.20(41)	3.4(6)		6506	762	h
5831.58(32)	1.73(11)		6506	674	
5930.68(11)	8.6(4)		6505	575	

Continued on next page

Table C.4 – continued from previous page

E_γ [keV]	relative intensity	Coincident transitions	E_i [keV]	E_f [keV]	Comments References
6252.24(11)	36.4(13)		6506	253	
6505.40(11)	9.5(4)		6506	0	

g) Placement in level scheme according to [20]

h) Placement and identification based on [20]

i) Correct intensity, energy and placement unclear

Table C.5: Levels E_i in ^{75}Ge determined by weighted means. The γ-transitions were corrected for recoil. The relative intensities of transitions known to depopulate a level I_{dep} and their sum are given. For comparison the known transitions populating a certain level I_{pop} are stated as well.

E_i [keV]	E_γ [keV]	E_f [keV]	I_{dep} [%]	I_{pop} [%]
139.81(10)	139.8	0	35.8(10)	
			35.8(10)	31.0(10))
192.31(15)	52.5	139.8	10.8(6)	
			10.8(6)	35.7(16)
253.01(10)	253.0	0	100.0	
			100.0	69.3(30)
317.13(9)	317.1	0	6.14(25)	
	177.3	139.8	20.2(7)	
			26.3(8)	5.08(18)
457.19(9)	457.2	0	12.0(4)	
	204.1	253.0	9.5(4)	
			21.5(6)	3.6(9)
574.95(9)	575.0	0	49.5(17)	
	321.9	253.0	3.4(5)	
			52.9(20)	34.9(25)
584	444	139.8		
				1.18(14)
674.07(10)	674.0	0	4.41(30)	
	481.7	192.3	15.0(4)	
			19.4(6)	3.09(19)
762.43(11)	762.5	0	3.6(4)	
	570.0	192.3	4.1(8)	
	444	317.1		

Table C.5 – continued from previous page

E$_i$ [keV]	E$_\gamma$ [keV]	E$_f$ [keV]	I$_{dep}$ [%]	I$_{pop}$ [%]
			7.7(9)	3.4((6)
885.88(8)	885.8	0	7.85(27)	
	632.4	253.0	5.7(21)	
	310.9	575.0	4.02(18)	
			17.6(22)	6.2(6)
901	444	457.2		
				0.98(6)
1137.17(8)	1137.2	0	4.08(30)	
	820.1	317.1	5.08(18)	
	236.2	901	0.98(6)	
			10.1(4)	7.8(11)
1240.81(15)	987.8	253.0	0.99(9)	
	783.6	457.2	1.5(4)	
			2.6(5)	
1416.47(11)	1416.5	0	5.97(21)	
	841.4	575.0	5.8(24)	
			11.8(4)	14.5(6)
1428.68(10)	1428.7	0	1.07(6)	
	1175.6	253.0	3.27(24)	
			4.34(25)	3.09(15)
1502.37(13)	1249	253.0	3.2(14)	
	1045.3	457.2	2.1(7)	
	927.4	575.0	5.00(24)	
			10.3(16)	9.4(4)
1514.86(11)	1514.9	0	7.63(29)	
	840.7	674.0	1.36(15)	
			9.0(4)	7.94(30)
1688.31(18)	1496.0	192.3	4.63(19)	

Continued on next page

Table C.5 – continued from previous page

E_i [keV]	E_γ [keV]	E_f [keV]	I_{dep} [%]	I_{pop} [%]
			4.63(19)	3.25(30)
1798.26(8)	1798.3	0	4.48(16)	
	1545.1	253.0	6.79(24)	
	1223.3	575.0	11.5(4)	
			22.8(5)	25.8(10)
1869	1285.3	584	1.18(14)	
			1.18(14)	
2065.61(11)	1873.3	192.3	6.6(7)	
			6.6(7)	10.3(4)
2091.24(11)	2091.2	0	4.6(9)	
			4.6(9)	7.70(28)
2311.76(22)	2119.5	192.3	5.4(10)	
			5.4(10)	4.1(18)
6505.84(5)	6505.7	0	9.5(4)	
	6252.6	253.0	36.4(13)	
	5930.9	575.0	8.6(4)	
	5831.8	674.0	1.73(11)	
	5743.4	762.4	3.4(6)	
	5620.2	885.9	6.2(6)	
	5368.6	1137.2	7.8(11)	
	5089.4	1416.5	14.5(6)	
	5077.2	1428.7	3.09(15)	
	5003.6	1502.4	9.4(4)	
	4991.1	1514.9	7.94(30)	
	4817.6	1688.3	3.25(30)	
	4707.7	1798.3	25.8(10)	
	4440.1	2065.6	10.3(4)	
	4414.7	2091.2	7.70(28)	
	4194.0	2311.8	4.1(18)	
			159.7(31)	

Table C.6: γ-rays in ^{77}As after the decay of ^{77}Ge. To obtain the intensity per 100 decays the relative intensity was multiplyed by 0.5376(134). This factor was determined assuming the sum of the ground state transitions given by Lent to be 100 %. The transitions used are marked with $\star$.

E_γ [keV]	Relative intensity	Intensity per 100 decays	References comments
150.46(15)	0.078(16)	0.042(9)	
156.33(11)	1.11(4)	0.0.598(23)	
159.40(35)	0.077(30)	0.041(16)	
177.27(13)	0.152(17)	0.082(9)	
194.72(10)	2.99(8)	1.61(6)	$\star$
208.68(11)	2.37(7)	1.27(5)	
211.05(10)	55.1(14)	29.6(11)	
215.51(10)	51.6(13)	27.7(10)	$\star$
254.57(11)	0.345(16)	0.185(10)	
264.37(11)	100.0	53.8(14)	$\star$,^{75}Ge
313.5(10)	0.042(10)	0.023(6)	
325.5(10)	0.044(11)	0.024(6)	
337.42(15)	0.36(5)	0.192(27)	
338.54(12)	1.45(12)	0.78(7)	^{75}Ge
339.60(40)	0.13(10)	0.07(6)	
350(1)			
367.33(10)	28.4(7)	15.2(6)	
398.93(11)	0.215(16)	0.115(9)	
416.29(10)	44.5(11)	23.9(9)	
419.71(11)	2.29(8)	1.23(5)	^{75}Ge
439.49(11)	0.404(16)	0.217(10)	^{77}As
444.76(18)	0.044(8)	0.023(5)	
461.37(10)	2.63(7)	1.41(5)	
471(1)	0.043(20)	0.023(11)	
475.49(10)	2.18(6)	1.17(5)	$\star$
504.10(12)	0.119(9)	0.063(6)	
520.61(99)	0.49(26)	0.26(14)	^{77}As
531.20(14)	0.076(11)	0.041(6)	
535.00(15)	0.059(10)	0.032(6)	
558.03(10)	33.5(8)	18.0(7)	

Continued on next page

Table C.6 – continued from previous page

E_γ [keV]	Relative intensity	Intensity per 100 decays	References comments
569.55(11)	0.423(18)	0.227(11)	
582.58(10)	1.57(5)	0.84(4)	
610.80(14)	0.142(11)	0.076(6)	
614.43(10)	1.24(4)	0.666(25)	⋆, a
614	1.05(15)	0.57(8)	⋆, b
614	0.185(26)	0.099(14)	b
624.73(11)	0.374(13)	0.201(9)	
631.87(10)	14.6(4)	7.83(28)	⋆
634.41(10)	4.18(11)	2.25(8)	⋆
639.27(15)	0.053(8)	0.029(4)	
655.12(22)	0.029(8)	0.016(4)	
659.92(15)	0.058(9)	0.031(5)	
665.56(42)	0.014(7)	0.008(4)	
673.14(10)	1.45(4)	0.779(29)	a
680.44(14)	0.077(8)	0.041(5)	
685.24(11)	0.181(10)	0.097(6)	a
698.60(11)	0.445(17)	0.239(11)	
705.26(11)	0.206(10)	0.111(6)	
712.33(11)	1.70(5)	0.91(4)	
714.39(10)	14.9(4)	7.99(28)	
730.65(18)	0.041(6)	0.022(4)	
743.61(11)	0.385(14)	0.207(9)	
745.80(10)	2.06(6)	1.11(4)	
749.92(10)	1.87(5)	1.00(4)	
766.79(10)	1.64(5)	0.88(4)	
775.93(19)	0.033(7)	0.018(4)	
781.31(10)	2.13(6)	1.15(4)	
784.83(10)	2.73(7)	1.47(6)	⋆
789.00(11)	0.198(10)	0.107(6)	
794.42(11)	0.617(18)	0.332(13)	
798.84(12)	0.111(8)	0.060(5)	
803.00(13)	0.079(8)	0.043(4)	
810.40(10)	4.73(12)	2.54(9)	
813.44(11)	0.277(11)	0.149(7)	
823.37(10)	1.26(4)	0.678(25)	
825.80(12)	0.120(8)	0.065(5)	

Continued on next page

114

Table C.6 – continued from previous page

E_γ [keV]	Relative intensity	Intensity per 100 decays	References comments
843.26(11)	0.425(15)	0.229(10)	
858(1)			
875.26(10)	1.63(5)	0.87(4)	⋆
884.07(23)	0.030(7)	0.016(4)	
889.38(56)	0.011(7)	0.006(4)	⋆
896.56(11)	0.245(10)	0.132(7)	
900.51(13)	0.175(14)	0.094(8)	
907.03(10)	1.97(5)	1.06(4)	
913.90(11)	0.774(22)	0.416(16)	
920.98(13)	0.163(12)	0.088(7)	
923.13(11)	1.49(4)	0.803(30)	
925.51(11)	1.69(5)	0.91(4)	a
928.92(10)	2.16(6)	1.16(5)	
939.42(11)	0.608(20)	0.327(14)	
945.57(18)	0.081(14)	0.043(8)	
959.27(11)	0.162(10)	0.087(6)	
966.74(22)	0.062(13)	0.034(7)	
970.34(19)	0.049(8)	0.027(4)	
985.79(11)	0.238(19)	0.128(11)	
996.56(11)	0.215(11)	0.115(7)	
1007.45(25)	0.026(6)	0.014(3)	
1021.89(26)	0.024(6)	0.013(3)	
1052.58(13)	0.085(8)	0.046(5)	
1055.75(35)	0.020(7)	0.011(4)	
1061.85(12)	0.326(20)	0.175(12)	
1080.86(11)	0.546(19)	0.294(13)	
1085.27(10)	12.7(4)	6.80(24)	
1104.28(13)	0.081(7)	0.043(4)	
1114.90(11)	0.224(10)	0.120(6)	
1125.05(11)	0.256(11)	0.137(7)	
1130.11(35)	0.017(6)	0.009(4)	
1134.74(14)	0.070(7)	0.038(4)	
1151.96(11)	0.392(14)	0.211(9)	
1155.66(26)	0.025(6)	0.013(4)	
1164.79(15)	0.054(6)	0.029(4)	⋆
1186.53(13)	0.092(7)	0.049(4)	

Continued on next page

Table C.6 – continued from previous page

E_γ [keV]	Relative intensity	Intensity per 100 decays	References comments
1193.33(10)	5.30(13)	2.85(10)	
1201.43(14)	0.134(13)	0.072(7)	⋆
1215.45(11)	0.269(11)	0.144(7)	
1234.64(15)	0.053(6)	0.028(4)	
1242.27(11)	0.840(24)	0.452(17)	
1263.95(10)	1.79(5)	0.96(4)	
1280.02(11)	0.366(13)	0.197(9)	⋆
1295.51(11)	0.339(15)	0.182(9)	a
1309.37(11)	1.023(28)	0.550(21)	
1312.88(11)	0.732(21)	0.393(15)	
1319.76(11)	0.548(17)	0.295(12)	⋆
1323.17(23)	0.033(5)	0.0176(27)	
1326.08(13)	0.090(7)	0.49(4)	
1339.37(11)	0.154(8)	0.083(5)	
1354.26(17)	0.043(6)	0.0230(29)	
1358.08(20)	0.032(5)	0.0171(28)	
1368.45(10)	5.79(15)	3.11(11)	^{24}Na
1385.83(23)	0.022(4)	0.0118(22)	
1399.59(34)	0.012(4)	0.0062(20)	⋆
1411.21(32)	0.013(4)	0.0069(20)	
1452.74(11)	0.251(11)	0.135(7)	
1455.09(20)	0.066(7)	0.035(4)	
1465.07(16)	0.133(18)	0.072(10)	a
1476.60(11)	0.501(17)	0.270(12)	
1479.07(11)	0.453(16)	0.244(11)	a
1495.68(11)	1.046(29)	0.562(21)	
1528.46(12)	0.100(7)	0.054(4)	⋆
1538.90(11)	0.298(11)	0.160(8)	⋆
1557.03(22)	0.024(4)	0.0128(22)	
1569.34(12)	0.105(7)	0.057(4)	
1573.80(11)	1.40(4)	0.755(28)	⋆
1624.56(30)	0.031(6)	0.0166(30)	
1639.66(33)	0.015(4)	0.0080(19)	
1643.50(31)	0.016(4)	0.0086(19)	
1709.90(11)	0.653(19)	0.351(14)	
1719.78(11)	0.802(24)	0.431(17)	

Continued on next page

Table C.6 – continued from previous page

E_γ [keV]	Relative intensity	Intensity per 100 decays	References comments
1722.40(14)	0.125(10)	0.067(6)	
1727.30(11)	0.298(11)	0.160(7)	
1735.94(14)	0.057(5)	0.0305(25)	
1759.69(40)	0.028(14)	0.015(8)	
1792.53(24)	0.0276(8)	0.015(5)	
1810.38(14)	0.073(5)	0.0393(29)	
1828.40(54)	0.010(4)	0.0055(19)	
1831.71(33)	0.018(4)	0.0099(20)	
1846.59(11)	0.349(12)	0.187(8)	
1878.91(18)	0.082(7)	0.044(4)	
1881.66(24)	0.036(6)	0.0196(28)	
1911.95(14)	0.052(5)	0.0278(24)	
1929.44(14)	0.050(5)	0.0269(24)	
1949.11(22)	0.020(3)	0.0109(17)	
2000.27(11)	1.16(4)	0.625(24)	⋆
2037.97(12)	0.130(7)	0.070(4)	
2077.39(11)	0.493(16)	0.265(11)	
2089.84(11)	0.548(17)	0.295(12)	
2126.32(11)	0.408(14)	0.219(9)	
2249.03(15)	0.0277(29)	0.0149(16)	
2279.92(30)	0.0087(18)	0.0047(10)	
2328.38(15)	0.035(4)	0.0189(18)	
2341.84(11)	1.014(29)	0.545(21)	⋆

a) Two transitions not resolved [19]
b) intensities divided as given in [19]

List of Figures

120

List of Tables

Bibliography

[1] Database of prompt gamma rays from slow neutron capture for elemental analysis. Vienna: International Atomic Energy Agency, world wide web: http://www-nds.iaea.org/pgaa/ (2006).

[2] Forschungs-Neutronenquelle Heinz Maier-Leibnitz (FRM II), world wide web: http://www.frm2.tum.de/.

[3] Korea Atomic Energy Research Institute, world wide web: http://atom.kaeri.re.kr/ton/.

[4] Q-value calculator, world wide web: http://www.nndc.bnl.gov/qcalc/; based on Audi et al., Nuclear Physics A 729:337-676 (2003) .

[5] C. E. Aalseth et al. IGEX ^{76}Ge neutrinoless double-beta decay experiment: Prospects for next generation experiments. *Phys. Rev. D*, 65:092007, 2002.

[6] G. Altarelli and K. Winter. *Neutrino Mass*. Springer-Verlag, 2003.

[7] F.T. Avignone, S.R. Elliott, and J. Engel. Double beta decay, Majorana neutrinos, and neutrino mass. *Rev. Mod. Phys.*, 80:481–516, 2008.

[8] K.H. Beckurts and K. Wirtz. *Neutron Physics*. Springer-Verlag, 1964.

[9] D. Budjas. *Germanium detector studies in the framework of the GERDA experiment*. PhD thesis, University of Heidelberg, 2009.

[10] L. Canella. priv. comm., 2009 and 2010.

[11] L. Canella, P. Kudejova, R. Schulze, A. Trler, and J. Jolie. Characterisation and optimisation of the new Prompt Gamma-ray Activation Analysis (PGAA) facility at FRM II. *submitted to Nucl. Instrum. Meth. A*, 2010.

[12] M.C. Chacko, L. Dorikens-Vanpraet, and M. Dorikens. The Decay of ^{75}Ga to Levels in ^{75}Ge. *Z. Physik*, 267:359 – 365, 1974.

[13] Z. Chunmei. *Nuclear Data Sheets*, 95:259–347, 2003.

[14] GERDA collaboration. The germanium detector array for the search of neutrinoless double beta decays of ^{76}Ge at Gran Sasso. *http://www.mpi-hd.mpg.de/gerda*, 2004.

[15] E. der Mateosian and M. Goldhaber. Thermal-Neutron Activation Cross Sections of Ge and the Isomeric Ratio Rule. *Phys. Rev.*, 108:766–768, 1957.

[16] C. Dörr and H.V. Klapdor-Kleingrothaus. New Monte-Carlo simulation of the HEIDELBERG-MOSCOW double beta decay experiment. *Nucl. Instrum. Meth. A*, 513:596 – 621, 2003.

[17] G. Douysset et al. Determination of the ^{76}Ge Double Beta Decay Q Value. *Phys. Rev. Lett.*, 86:4259–4262, 2001.

[18] K. Nakamura et al. (Particle Data Group). *JPG*, 37:075021, 2010.

[19] A. R. Farhan and B. Singh. *Nuclear Data Sheets*, 81:417–578, 1997.

[20] A. R. Farhan and B. Singh. *Nuclear Data Sheets*, 86:785–954, 1999.

[21] R.F. Fleming. Neutron self-shielding factors for simple geometrics. *Int. J. Appl. Rad. Isot.*, 33:1263–1268, 1982.

[22] J. Wolf for the KATRIN collaboration. The KATRIN Neutrino Mass Experiment. *arXiv:0810.3281*, 2008.

[23] P. Grabmayr et al. Procurement and analysis of depleted GeO_2 (batch-II) and reduction at PPM. Technical Report GSTR-09-003, University of Tübingen, 2009.

[24] L.V. Groshev, L.I. Govor, and A.M. Demidov. Deexitation of even-odd germanium nuclei after thermal-neutron capture.

[25] A. Hasselgren. Deuteron stripping and thermal neutron capture γ-reactions on the ^{72,74,76}Ge isotopes. *Nucl. Phys.*, A198:353–379, 1972.

[26] J.H. Hubbell and S.M. Seltzer. X-Ray Mass Attenuation Coefficients. *NIST Gaithersburg*, http://physics.nist.gov/PhysRefData/XrayMassCoef/.

[27] M.A. Islam, T.J. Kennett, and W.V. Prestwich. Radiative strength functions of germanium from thermal neutron capture. *Phys. Rev. C*, 43:1086 – 1098, 1991.

[28] B.P. Kay et al. Properties of excited states in ^{77}Ge. *Phys. Rev. C*, 80:017301, 2009.

[29] H.V. Klapdor-Kleingrothaus et al. Latest results from the HEIDELBERG-MOSCOW double beta decay experiment. *Eur. Phys. J. A*, 12:147–154, 2001.

[30] H.V. Klapdor-Kleingrothaus, I.V. Krivosheina, A. Dietz, and O. Chkvorets. Search for neutrinoless double beta decay with enriched ^{76}Ge in Gran Sasso 1990-2003. *Phys. Lett. B*, 586:198–212, 2004.

[31] M. Knapp. *Design, Simulation und Aufbau des GERDA-Myonvetos.* PhD thesis, University of Tübingen, 2009.

[32] L. Koester, K. Knopf, and W. Waschkowski. Neutron interactions with germanium isotopes and amorphous and crystalline GeO$_2$. *Z. Physik A*, 327:129–136, 1987.

[33] P. Kudejova et al. The new PGAA and PGAI facility at the research reactor FRM II in Garching near Munich. *JRNC*, 278:691–695, 2008.

[34] E.M. Lent. *Gamma-Gamma Directional Correlation Studies on ^{77}Ge Decay.* PhD thesis, University of California Davis, 1974.

[35] M.A. Lone, D.C. Santry, and W.M. Inglis. MeV neutron production from thermal neutron capture in Li and B compounds. *Nucl. Instrum. Meth.*, 174:521–529, 1980.

[36] W.S. Lyon. *Nuclear Sci. and Eng.*, 8:378, 1960.

[37] W.S. Lyon and J.S. Eldridge. Radioactive Ge^{77} and Ge^{77m}. *Phys. Rev.*, 107:1056–1057, 1957.

[38] J. Magarniec et al. Neutron capture cross sections of ^{74}Ge, ^{76}Ge, and ^{75}As at 25 keV. *Phys. Rev. C*, 79:065802, 2009.

[39] A.P. Magruder and R.K. Smither. Ge^{73}(n,γ)Ge^{74} Gamma-Ray Spectrum and Energy Levels of Ge^{74}. *Phys. Rev.*, 183:927–944, 1969.

[40] W. Mannhart and H. Vonach. Isomere Wirkungsquerschnittsverhältnisse beim thermischen Neutroneneinfang im Bereich der $2\,p_{1/2}$ und $1\,g_{9/2}$ Schalenmodellzustände. *Z. Physik*, 210:13–31, 1968.

[41] G. Meierhofer et al. Thermal neutron capture cross sections of ^{76}Ge. *Eur. Phys. J A*, 40:61–64, 2009.

[42] G. Meierhofer et al. Thermal neutron capture cross sections of ^{74}Ge. *Phys. Rev. C*, 81:027603, 2010.

[43] P.J. Mohr and B.N. Taylor. The 2006 CODATA Internationally recommended values of the Fundamental Physics Constants. *NIST Gaithersburg*, http://physics.nist.gov/Constants/.

[44] S.F. Mughabghab. *Atlas of Neutron Resonances.* Elsevier, 5 edition, 2006.

[45] S.F. Mughabghab, M. Divadeenam, and N.E. Holden. *Neutron Cross Sections*, volume 1. Academic, New York, 1981.

[46] A. Ng et al. Gamma Rays from the Decay of ^{75}Ge and ^{77}Ge. *Phys. Rev.*, 176:1329–1338, 1968.

[47] E.W. Otten and C. Weinheimer. Neutrino mass limit from tritium β decay. *Rep. Prog. Phys.*, 71:086201, 2008.

[48] L. Pandola. Study of the muon-induced background in the GERDA backup design with stainless-steel cryostat. Technical Report GSTR-06-013, Laboratori Nazionali del Gran Sasso, Italy, 2006.

[49] L. Pandola. priv. comm., 2010.

[50] L. Pandola and C. Tomei. Study of the ^{77m}Ge decay rejection by delayed coincidence. Technical Report GSTR-06-012, Laboratori Nazionali del Gran Sasso, Italy, 2006.

[51] H. Pomerance. Thermal Neutron Capture Cross Sections. *Phys. Rev.*, 88:412, 1952.

[52] L. Seren, H.N. Friedlander, and S.H. Turkel. Thermal Neutron Activation Cross Sections. *Phys. Rev.*, 72:888, 1947.

[53] A. Smolnikov and P. Grabmayr. Conversion of experimental half-life to effective electron neutrino mass in $0\nu\beta\beta$ decay. *Phys. Rev. C*, 81:028502, 2010.

[54] J. Theuerkauf et al. *Program TV*, Institute for Nuclear Physics Cologne, Germany.

[55] S.A. Thomas, F.B. Abdalla, and O. Lahav. Upper Bound of 0.28 eV on Neutrino Masses from the Largest Photometric Redshift Survey. *Phys. Rev. Lett.*, 105:031301, 2010.

[56] P. Vermaercke, L. Verheyen M. Hult, and F. Farina Arboccò. Measurement of the isotopic composition of germanium by k_0-INAA and INAA. *Nuclear Instruments and Methods in Physics Research Section A*, 622:433–437, 2010.

[57] H. Weigmann. Messungen der K-Konversionskoeffizienten und der Aktivierungsquerschnitte der isomeren Atomkerne Se^{77m}, Se^{79m}, Ge^{75m} and Ge^{77m}. *Z. Physik*, 167:549, 1962.

[58] R. Weishaupt and D. Rabenstein. Beiträge zu den Niveauschemata der Ge-Isotope ^{71}Ge,^{73}Ge,^{74}Ge und ^{75}Ge aus der Untersuchung von (n,γ)-Reaktionen in natürlichem Germanium. *Z. Physik*, 251:105 – 134, 1972.

[59] A.E. Zobov et al. Program and thesis. In *Proc. 41st Ann. Conf. Nucl. Spectrosc. Struct. At. Nuclei*, page 54. Minsk, 1991.

List of Publications

With peer review

1. *GERDA - a new neutrinoless double beta experiment using ^{76}Ge,*
   G. Meierhofer for the GERDA collaboration, J. Phys.: Conf. Ser. INPC2010
   (accepted).

2. *The calibration system of the GERDA muon veto Cherenkov detector,*
   F. Ritter, B. Lubsandorzhiev, K. Freund. P. Grabmayr, J. Jochum, M. Knapp,
   G. Meierhofer, and B. Shaibonov, Nucl. Instr. and Meth. A **617** 420-421 (2009).

3. *Thermal neutron capture cross section of ^{74}Ge,*
   G. Meierhofer, P. Grabmayr, J. Jochum, P. Kudejova, L. Canella, and J. Jolie,
   Phys. Rev. C **81**, 027603 (2010).

4. *The GERDA muon veto Cherenkov detector,*
   M. Knapp, P. Grabmayr, J. Jochum, B. Lubsandorziev, G. Meierhofer, F. Ritter, and
   B. Shaibonov, Nucl. Instr. and Meth. A **610** 280-282 (2009).

5. *Fast scintillation light from CaMoO4 crystals,*
   A.V. Veresnikova, B.K. Lubsandorziev, I.R. Barabanov, P. Grabmayr, D. Greiner.
   J. Jochum, M. Knapp, C. Oßwald, R.V. Poleshuk, F. Ritter, B.A.M. Shaibonov,
   Y.E.Vzatchin, and G. Meierhofer, Nucl. Instr. and Meth. A **603** 529 - 531 (2009).

6. *Thermal neutron capture cross-section of ^{76}Ge,*
   G. Meierhofer, P. Kudejova, L. Canella, P. Grabmayr, J. Jochum, and J. Jolie,
   Eur. Phys. J A **40**, 61-64 (2009).

7. *The new PGAA and PGAI facility at the research reactor FRM II in Garching
   near Munich,*
   P. Kudejova, G. Meierhofer, K. Zeitelhack, J. Jolie, R. Schulze, A. Türler, and
   T. Materna, JRNC **278**, 691-695 (2008).

Without peer review

1. *Neutron capture cross sections of ^{74}Ge and ^{76}Ge,*
   G. Meierhofer, P. Grabmayr, J. Jochum, P. Kudejova, L. Canella, and J. Jolie,
   Annual Report 2009, Forschungs-Neutronenquelle Heinz Maier-Leibnitz (FRM II).

2. *Neutron Activation of ^{74}Ge and ^{76}Ge,*
   G. Meierhofer, L. Canella, P. Grabmayr, J. Jochum, J. Jolie, P. Kudejova,
   EPJ Web of Conferences **2**, 05002 (2010).

3. *Prompt Gamma Rays in ^{77}Ge after Neutron Capture on ^{76}Ge,*
   G. Meierhofer, L. Canella, P. Grabmayr, J. Jochum, J. Jolie, P. Kudejova, and
   Nigel Warr, Capture Gamma Ray Spectroscopy and Related Topics:
   13th International Symposium, edited by A. Blazhev, J. Jolie, N. Warr, and
   A. Zilges (AIP, New York, (2009), p. 559;.

128

Acknowledgements

This work would not have been possible without the support and help of many people. I would like to thank ...

... first of all Prof. Peter Grabmayr for the interesting research project and his advise. He supported me in all aspects of the development of this thesis and offered me many oppertunities to broaden my knowledge.

... Prof. Josef Jochum for letting me join his working group and profit from his experience.

... my colleagues in the GERDA group in Tübingen Kai Freund, Markus Knapp and Florian Ritter for their help and the fruitful discussions.

... Petra Kudejova, Lea Canella and Stefan Söllradl working at the PGAA instrument in Munich for their great support in all experimental questions.

... Prof. Jan Jolie and Nigel Warr for their help in the planning and realization of the coincidence measurement.

... Torsten Hehl for all his answers to my questions I had concerning radiation and how to measure it.

... Luciano Pandola for the simulations of the prompt spectra in the GERDA detectors.

... Alexander Hegai for his work with the HPGe detector in our unterground laboratory.

... all members of the AG Jochum, including Michael Bauer, Mikail Bolatekin, Gerhard Deuter, Sebastian Diebold, Dennis Dietrich, Raphael Falkenstein, Daniel Greiner, Marcel Kimmerle, Prof. Tobias Lachenmaier, Bayarto Lubsandorzhiev, Marc Pfeifer, Markus Röhrling, Klemens Rottler, Christof Sailer, Christopher Schmitt, Stefan Scholl, Christian Strandhagen and Igor Usherov.